Universität Hamburg
DER FORSCHUNG | DER LEHRE | DER BILDUNG

Fachbereich
Chemie

Functional 3D printed reactor for continuous oxidation of alcohols to aldehydes

Dissertation

With the Aim of Achieving the Doctoral Degree
at the Faculty of Mathematics, Informatics and Natural Sciences

Department of Chemistry
University of Hamburg

submitted by

Hannah Grotian genannt Klages

Hamburg, 2025

The experimental work described in this thesis was carried out from June 2020 to June 2023 at the Institute of Technical and Macromolecular Chemistry at the University of Hamburg in the working group of Professor Dr. Gerrit A. Luinstra and was financially supported by the Evonik Foundation.

Reviewers of this doctoral thesis:	Prof. Dr. Gerrit. A. Luinstra Dr. Kristina Zentel
Thesis defense committee:	Prof. Dr. Gerrit A. Luinstra Prof. Dr. Volker Abetz Prof. Dr. Michel Steiger
Date of defense:	19.12.2025

Table of contents

List of Abbreviations

ACN	Acetonitrile
AcOBr	Acetyl hypobromite
AcOH	Acetic acid
BAIB	Bis(acetoxy)iodobenzene
BDO	Butanediol
CAD	Computer-aided design
CuAAC	Cu(I)-catalyzed azide-alkyne cycloaddition
DCM	Dichloromethane
DIPEA	N,N-Diisopropylethylamine
DMP	Dess-Martin periodinane
DMSO	Dimethyl sulfoxide
EDX	Energy-dispersive X-ray spectroscopy
FDM	Fused deposition modeling
FFF	Fused filament fabrication
FTIR	Fourier-transform infrared spectroscopy
IBX	2-Iodoxybenzoic acid
NCS	N-Chlorosuccinimide
NMP	N-Methyl-2-pyrrolidone
PEG	Polyethylene glycol
PEK	Polyether ketones
PPM	Post-polymerization modification
PS-TEMPO	Polymer-supported TEMPO
PVC	Polyvinylchloride
RP	Rapid Prototyping
RT	Room temperature
TBAB	Tetrabutylammonium bromide
TEMPO	2,2,6,6-Tetramethylpiperidinyloxyl
TEMPOL	4-Hydroxy-2,2,6,6-tetramethylpiperidinyloxyl
T_g	Glass-transition temperature

1. Abstract

This dissertation covers areas of 3D printing of reactors, development of suitable catalyst materials, and optimization of oxidation reactions. The focus is a functional 3D-printed reactor, designed for the continuous oxidation of alcohols to aldehydes. The selective generation of aldehydes is of some significance as they are reactive compounds, undergoing a set of consecutive reactions under relatively mild conditions. Aldehydes find also direct application in pharmaceuticals and polymer manufacturing. The final results of 3D printed reactors with fixed beds comprising immobilized TEMPO hold a great promise for industrial application.

Common procedures for the conversion of alcohols to aldehydes are not without drawbacks. They may involve hazardous conditions and reagents, also resulting in undesirable byproducts. The catalyst used here, TEMPO (2,2,6,6-tetramethylpiperidin-1-oxyl) is an attractive catalyst for a more environmentally benign approach to the formation of aldehydes.

Advances of applying 3D printing in chemical engineering have made it possible to reliably generate reactors. This technology, in combination with surface functionalization of the reactor wall, enables to build a TEMPO catalytic fixed bed reactor. A continuous reactor was developed that efficiently converts alcohols to aldehydes with a conversion of 95 % over 6 h at 35 °C. using acetonitrile (ACN) as solvent and bisacetoxy iodobenzene (BAIB) as the oxidant and tetrabutyl ammonium bromide (TBAB) as cocatalyst. Vinyl303 (polyvinyl chloride (PVC) filament) from *Fillamentum* was used for printing the reactor and its inserts. A printing temperature of 230 °C and a printing speed of 40 mm/s were adequate to avoid *warping* of the parts and *clogging* of the printer nozzle.

Support material with TEMPO catalyst was prepared by functionalizing the printed PVC using Cu(I)-catalyzed azide-alkyne cycloaddition (CuAAc) and Williamson-ether synthesis. A high surface coverage with TEMPO had to be reached to ensure not only

effective transformations, but also for achieving higher conversions. Functionalization using CuAAc was carried out in several steps, achieving a TEMPO loading of 2 mmol/g. The prepared catalyst-support material was effective in oxidation reactions with alcohol conversions of 67 %. Disadvantageously, activity decreased with time by catalyst leaching and by decomposition.

The efficiency and stability of PVC-TEMPO catalysts were addressed by variation in the anchoring of the TEMPO entity by an ether linkage. Best catalytic action was observed for a TEMPO-functionalized surface obtained using NaH as base, a temperature of 65 °C and a solvent mixture of DMSO/H_2O of 17:3.

The oxidation of benzyl alcohol by the supported TEMPO entity is best performed at 35 °C and using BAIB as oxidant and TBAB as cocatalyst. Temperature was a crucial parameter, a higher temperature accelerated the oxidation, but it led to the decomposition of the catalyst. Various co-oxidants were also tested and were identified as a promising solution to ensure the oxidation of reduced TEMPO. Aromatic alcohols are oxidized at a 1.5 times higher rate than aliphatic derivatives, primary alcohols are oxidized 3 times faster than secondary alcohols.

Functional reactors for oxidation reactions were developed with functionalized PVC pellets in a *packed bed* or a fully printed reactor. The functionalization of the pellets in the former case, using CuAAc showed a conversion of 50 % for the oxidation of benzyl alcohol with loss of activity (weight loss); the catalysts from an anchoring by an ether linkage to TEMPO achieved a conversion of about 63 %. Conversion of 100 % were achieved using a fully printed reactor operated to give a residence time of 15 min. The conversions remained stable at 60 % after 12 weeks of storage. Other alcohols did not show significant differences in performance, and in all cases 100 % conversion was achieved over several hours of continuous operation.

2. Zusammenfassung

Diese Dissertation behandelt die Bereiche des 3D-Drucks von Reaktoren, die Entwicklung geeigneter Katalysatormaterialien und die Optimierung von Oxidationsreaktionen. Der Fokus liegt auf einem funktionsfähigen 3D-gedruckten Reaktor, der für die kontinuierliche Oxidation von Alkoholen zu Aldehyden konzipiert wurde.

Die selektive Erzeugung von Aldehyden ist von Bedeutung, da es sich um reaktive Verbindungen handelt, die unter relativ milden Bedingungen eine Reihe von aufeinanderfolgenden Reaktionen durchlaufen. Aldehyde finden auch direkte Anwendung in der Pharmazie und der Polymerherstellung.

Die Ergebnisse der 3D-gedruckten Reaktoren mit immobilisiertem TEMPO als Festbett, sind vielversprechend für die industrielle Anwendung. Herkömmliche Verfahren zur Oxidation von Alkohol zu Aldehyd weisen Nachteile auf. Sie können gefährliche Bedingungen und Reagenzien beinhalten, die auch unerwünschte Nebenprodukte erzeugen. Der hier verwendete Katalysator, TEMPO (2,2,6,6-Tetramethylpiperidinoxyl), stellt einen attraktiven Katalysator für einen umweltfreundlicheren Ansatz zur Bildung von Aldehyden dar.

Fortschritte bei der Anwendung des 3D-Drucks in der Chemieingenieurswissenschaft haben es ermöglicht, Reaktoren zuverlässig zu drucken. Diese Technologie, kombiniert mit der Funktionalisierung der Reaktorwand, ermöglicht den Aufbau eines TEMPO-katalytischen Festbettreaktors.

Es wurde ein kontinuierlicher Reaktor entwickelt, der Alkohol effizient in Aldehyde umwandelt, mit einem Umsatz von 95 % über 6 h bei 35 °C, unter Verwendung von Acetonitril (ACN) als Lösungsmittel, Bisacetoxyiodobenzol (BAIB) als Oxidationsmittel und Tetrabutylammoniumbromid (TBAB) als Co-Katalysator.

Vinyl303 (Polyvinylchlorid (PVC) Filament) von Fillamentum wurde für den 3D-Druck des Reaktors verwendet. Eine hohe Drucktemperatur von 230 °C und eine langsame Druckgeschwindigkeit von 40 mm/s waren erforderlich, um *Warping* des Materials und *Clogging* der Druckdüse zu vermeiden.

Die TEMPO-Katalysator wurde durch die Funktionalisierung des gedruckten PVC unter Verwendung der Cu(I)-katalysierten Azid-Alkin-Cycloaddition (CuAAc) und der Williamson Ethersynthese hergestellt. Eine hohe TEMPO-Beladung musste erreicht werden, um eine effektive Oxidationsreaktion zu ermöglichen. Die Funktionalisierung mittels CuAAc wurde in mehreren Schritten durchgeführt und erreichte eine TEMPO-Beladung von 2 mmol/g. Das vorbereitete Katalysator-Trägermaterial war in Oxidationsreaktionen wirksam, mit Alkoholumsätzen von 67 %. Nachteilig war, dass die Aktivität im Laufe der Zeit durch Katalysatorleaching und Zersetzung abnahm.

Die Effizienz und Stabilität der PVC-TEMPO-Katalysatoren wurden durch Variationen die direkte Bindung von TEMPO and PVC durch eine Etherbindung adressiert. Die höchste katalytische Aktivität wurde bei einer TEMPO-funktionalisierten Oberfläche beobachtet, die mit NaH als Base, einer Temperatur von 65 °C und einem Lösungsmittelgemisch aus DMSO/H_2O im Verhältnis 17:3 erhalten wurde.

Die Oxidation von Benzylalkohol durch das immobilisierte TEMPO erfolgt bei 35 °C, unter Verwendung von BAIB als Oxidationsmittel und TBAB als Co-Katalysator.

Die Temperatur war ein wichtiger Parameter; eine höhere Temperatur beschleunigte die Oxidation, führte jedoch zur Zersetzung des Katalysators.

Verschiedene Co-Oxidationsmittel wurden ebenfalls getestet und BAIB/TBAB als vielversprechende Mischung identifiziert, um effizient Alkohole zu oxidieren.

Aromatische Alkohole werden 1,5-mal schneller oxidiert als aliphatische Derivate, und primäre Alkohole werden dreimal schneller als sekundäre Alkohole oxidiert.

Funktionsfähige Reaktoren für Oxidationsreaktionen wurden mit funktionalisierten PVC-Pellets in einem Festbett oder in einem vollständig gedruckten Reaktor entwickelt.

Die Funktionalisierung der Pellets im ersten Fall unter Verwendung von CuAAc zeigte einen Umsatz von 50 % für die Oxidation von Benzylalkohol mit Aktivitätsverlust und Gewichtsverlust. Pellets woran TEMPO über eine Etherbindung verankert wurden, erreichten einen Umsatz für die Benzylalkohol-Oxidation von etwa 63 %.

Einen Umsatz von 100 % wurde mit einem vollständig gedruckten Reaktor und einer Verweilzeit von 15 min erreicht. Der Umsatz blieb nach 12 Wochen Lagerung stabil bei 60 %. Die Oxidation anderer Alkohole in dem Reaktor zeigten keine signifikanten Unterschiede, in allen Fällen wurde ein Umsatz von 100 % über mehrere Stunden kontinuierlichen Betriebs erreicht.

3. Introduction

The chemical industry is constantly pursuing innovation, which usually goes along with a higher level of sustainability, thus following the demand for environmentally friendly and efficient processes.

The selective oxidation of alcohols to aldehydes is a standard transformation in industrial chemistry.[1] Aldehydes are essential compounds in various industries with significance turnovers.[2,3] Aldehydes, for instance, are educts for synthesizing a number of drug molecules. They are significant products in the flavor and fragrance industry.[4] Dialdehydes can e.g. be used for polymer synthesis as intermediates.[5,6] This broad scope of applications also motivated the search for an efficient and sustainable approach to aldehyde production. A starting point arises from some of the challenges that come along with conventional methods and catalysts for selective alcohol oxidation.[7] The employment of strong oxidizing reagents frequently leads to selectivity problems and is accompanied by a high environmental impact.[8–10] Catalyst recovery is another point adding to the lower sustainability. Alternatively, TEMPO represents a catalyst (core) that can circumvent many of these issues. It is a homogeneous catalyst which can be immobilized on a support, thus allowing for an easy catalyst recovery.[11]

A further issue is the way 3D printing has the potential of transforming chemical engineering, also in industry. Its integration marks a significant breakthrough in the conception and design of chemical processes and manufacturing of equipment.[12] It enables customization of reactor to a process. This technological innovation has the potential to enhance process intensification in constraints of efficiency, sustainability, and effectivity.

The use of polymers containing functional groups offers the option to immobilize a catalyst through a covalent bond, resulting in the heterogenization of homogeneous catalyst systems.[13] The position of the catalyst matters for efficiency. Minimizing

catalyst leaching is of importance for rates and turnover number (TON) and reduces environmental impact.

3.1 Motivation

This thesis aims to use the combination of 3D printing based reactor design options and immobilized TEMPO-based catalyst for the selective oxidation of alcohols. The development of a functional 3D printed reactor targets a solution for the oxidation of alcohols to aldehydes with a higher efficiency and effectivity, safety, and environmental impact. The project is divided into three areas: 3D printing of reactor, the development of suitable immobilized TEMPO catalysts, and the oxidation of alcohols in batch and continuous operation (Figure 1).

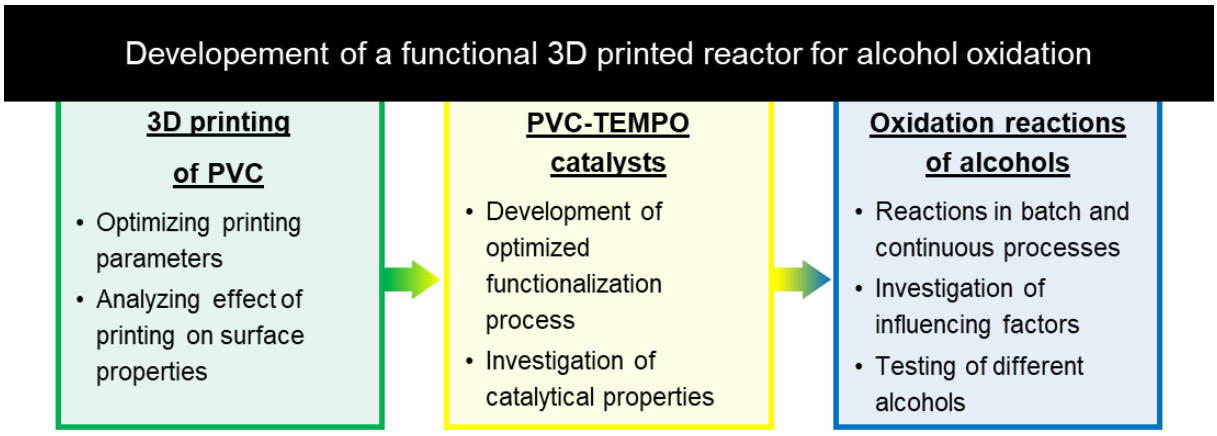

Figure 1. Tasks for target approach.

The research targets the viability of using polyvinyl chloride (PVC) as a printing material, aiming to determine the best printing parameters for the production of high-resolution prints. It was found necessary to investigate how the properties of PVC are changed in the printing process, by the conditions of the surface functionalization and by the oxidation reactions. The potential for functionalizing PVC to optimize the catalyst immobilization is addressed. PVC pellets are printed and functionalized with TEMPO using click chemistry or by a Williamson ether reaction in an orientating study. The catalyst's stability in oxidation reactions is evaluated using batch oxidations in a series of consecutive reactions. Main factors affecting the oxidation reactions of PVC-TEMPO catalysts are determined in batch experiments. The catalytic activity in the oxidation of various alcohols (aromatic, aliphatic and diolic alcohols) is mapped.

A fixed-bed reactor will be employed in this screening phase. The stability of operating continuous fully 3D printed catalytic reactors will be evaluated. The reactor is being investigated for the oxidation of different alcohols

4. State of the Art

4.1 Oxidation of alcohol to aldehydes by nitroxyl radicals

Aldehydes are key components in industrial chemistry transformations, as exemplified above.[2,3] Of particular interest is the application of dialdehydes in the TISHCHENKO reaction for the synthesis of linear polyesters using renewable raw materials in the atom-efficient coupling process.[6]

Standard oxidation reactions have some issues. Aggressive and hazardous oxidants, such as chromium(VI)[14], dipyridinechromium(VI)[15,16], pyridinium chlorochromate[17], and pyridium dichromate[18], manganese(IV)[19], and ruthenium salts[20] are commonly employed in industry. These oxidants are used under harsh conditions.[8] The catalysts or reagents used under milder conditions, such as Dess-Martin periodinan[21], dimethyl sulfoxide (DMSO) [22] or 2-iodoxybenzoic acid (IBX) are limited to laboratory scale.[9,10] Overoxidation to carboxylic acids can take place.[3,10,23] The development of oxidation reagent should prioritize chemical selectivity, the capacity to be employed under mild conditions and the ability to prevent side reactions. Higher yields should be achieved and reaction times should be shortened. Oxidizing agents that are non-toxic, regenerable, and scalable should be used. Nitroxyl radicals, such as TEMPO fulfil the necessary criteria and are appropriate for catalytic oxidation reaction in both laboratory and industrial scales.

4.1.1 Nitroxyl radicals

Conjugated organic nitroxyl radicals were first identified in 1901.[24] TEMPO is the best known compound in this group.[11,25–28] A large variety of conjugated nitroxyl radicals have been synthesized since then.[29–31] No dimerization or decomposition of TEMPO occurs, even over extended periods.[27,32] The absence of protons on the α-carbon atoms in TEMPO is crucial for its stability.[33]

TEMPO shows useful redox behavior:[34] It can be reduced to hydroxylamine using mild reducing agents, such as hydrazine or ascorbic acid.[29,35,36] Oxidation of nitroxyl

radicals to oxoammonium salts occurs with oxidants like bromine or through acid-catalyzed disproportionation.[37]

TEMPO is non-toxic. It is widely used as a reagent or catalyst in laboratory and industrial applications.[11] TEMPO is also used as a spin label[30] or spin trapping agent[38]. In macromolecular chemistry, TEMPO is used to synthesize narrow distributed polymers in a living polymerization, which is referred as NMP: nitroxide-mediated radical polymerizations.[11,39,40]

TEMPO facilitates various reactions, including C-C or C-N linkage transformations.[11,39] Its use as a catalyst in the selective oxidation of alcohols to aldehydes is particularly relevant to this work.[41,42,43]

4.1.2 Mechanism of TEMPO mediated oxidation reactions

TEMPO-mediated oxidation reactions can be fast reactions, have high conversions and a good selectivity.[11] This reaction has become an important method in organic synthesis. The first reported TEMPO-mediated oxidation reaction was on the oxidation of methanol to methanal and isopropanol to acetone.[44]

The oxidation of alcohols to aldehydes proceeds through the intermediate oxoammonium salt. This is a two-electron reaction. Nitroxyl radicals can also act as oxidants, but oxoammonium salts are stronger oxidizing agents.[43,45] A disproportionation reaction converts nitroxyl radicals into oxoammonium salts and hydroxyl amines (**Figure 2**).

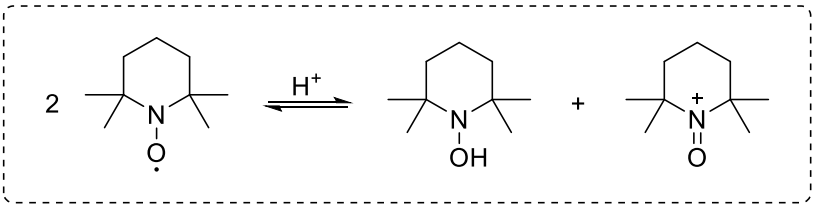

Figure 2. Acid-catalyzed disproportionation of TEMPO to hydroxyl amine and oxoammonium salt.

The pH should be lower than two to achieve a significant product quantity in the equilibrium of disproportionation (Figure 2).[46] Agents such as *p*-toluene sulfonic acid

are effective. [47,48][49] The rate of oxidation of alcohols decreases in the order of isoprop > EtOH > MeOH. This is associated to the increasing dissociation energy of the α-CH bond.[50] Limitations of TEMPO mediated oxidation of alcohols exist too, as overoxidation, Baeyer-Villiger reactions, and epoxidation of double bonds can take place. These reactions require TEMPO in stoichiometric amounts. The TEMPO mediated oxidation reaction shows high selectivity for primary alcohols. Secondary alcohols have significantly lower rates.

A primary oxidant is necessary to use TEMPO in catalytic amounts. The primary oxidant regenerates the oxoammonium salt continuously in a one-electron process under milder reaction conditions (pH > 3). The first primary oxidant used was Cu(II)/O_2.[51,52] Other primary oxidants, such as hypochlorite can be used. Single oxygen donors, including 2-chloroperbenzoic acid sodium bromite[53], sodium chlorite[54], persulfate/oxone[55], or periodic acid[56] will transform TEMPO to its oxoammonium salt.

The oxidation pathway depends on the reaction conditions, which can be basic or acidic. The mechanism remains incompletely understood in both cases. The hydroxylamine formed during the oxidation under basic conditions reacts with another oxoammonium salt. This reaction leads to a comproportionation, the reverse of acid-catalyzed disproportionation of Figure 2, and forms the nitroxyl radical.[41,46] Oxidation of the nitroxyl radical with a primary oxidant recovers the oxoammonium salt (**Figure 3**).

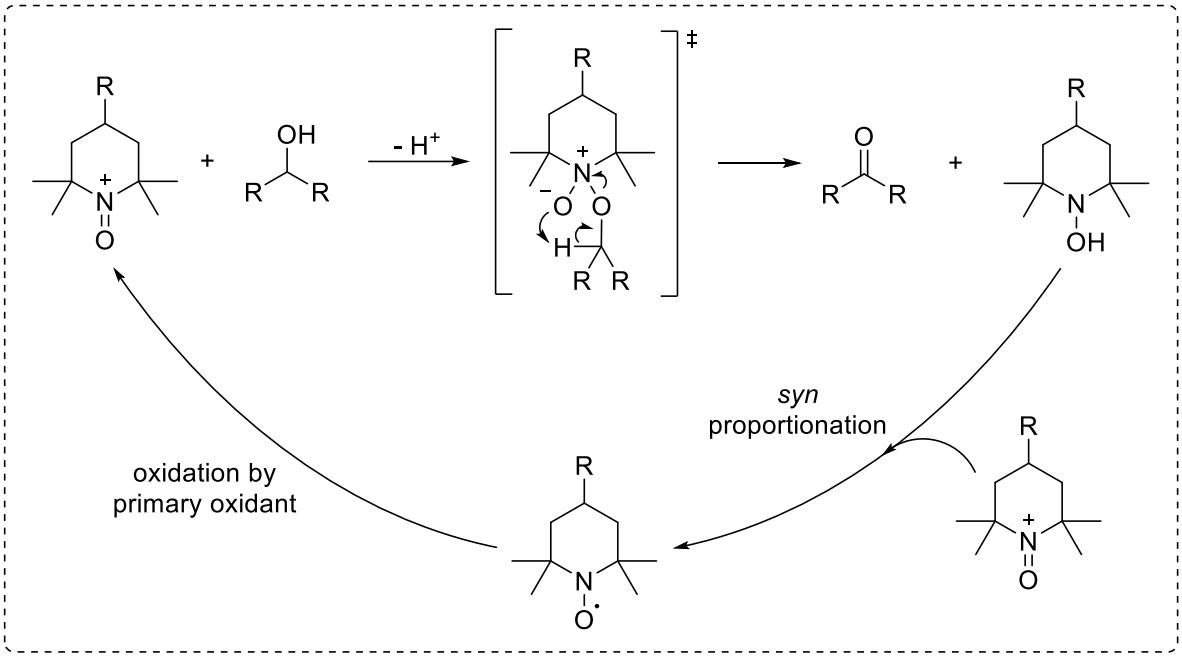

Figure 3. Reaction mechanism of the oxidation reaction of alcohol to carbonyl under basic conditions.

The addition of alcohol to the oxoammonium salt leads to the formation of the adduct. Through a Cope-like elimination in the adduct, the aldehyde and hydroxylamine are formed.[47,57] The formation of the adduct is rate-determining. Steric effects are significant for the formation of the adduct under basic conditions. Secondary alcohols react more slowly than primary alcohols.[58]

Under acid conditions, intermediate hydroxylamine will react with the primary oxidant and form the hydroxyl radical (**Figure 4**).[59] The radical disproportionates in an acid-catalyzed reaction to the oxoammonium salt and hydroxylamine (**Figure 2**).

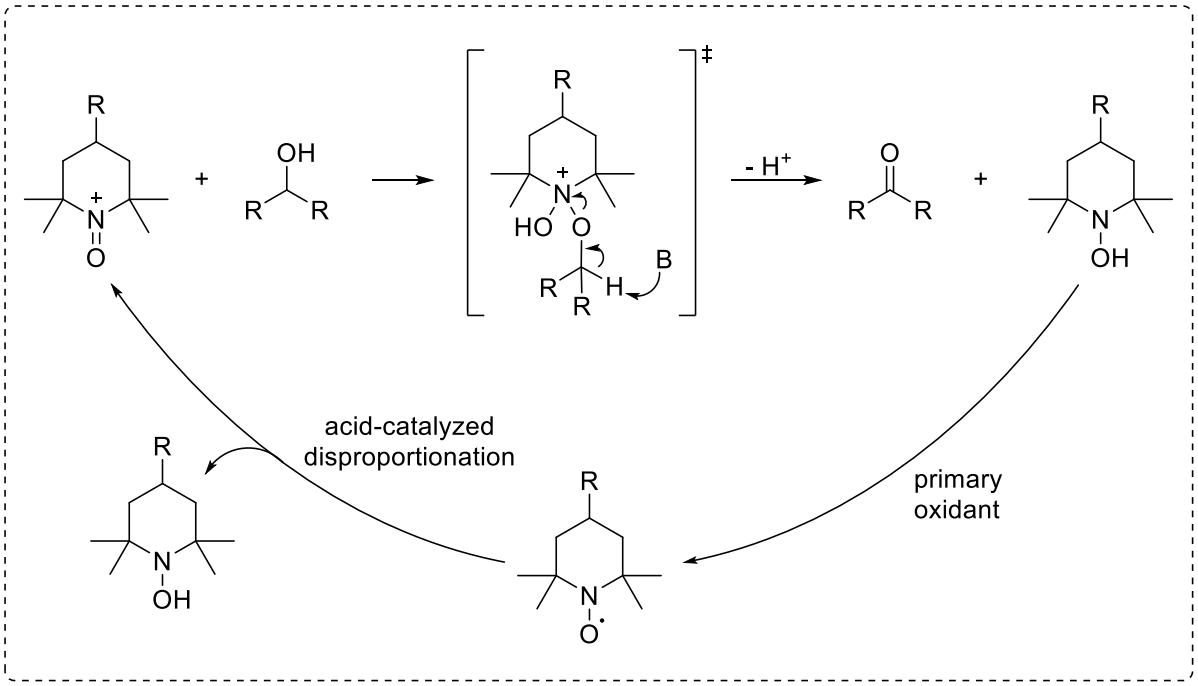

Figure 4. Reaction mechanism of the oxidation reaction of alcohol to carbonyl under acid conditions.

Different primary oxidants are used in dependence of the pH value. Under alkaline conditions, Cu-salt/O_2[52,60], hypohalite[61], $NaBrO_2$[36], $NaClO_2$/NaOCl[54], NaOCl/NaBr[59,62] and NCS[63] have been applied. The most common method under basic conditions uses TEMPO with hypochlorite in DCM/H_2O medium. NaBr is added as co-catalyst.[41,45][62,64]

m-Chloroperbenzoic acid[48] can be used under acid conditions. Pentavalent iodine reagents are effective too. These reagents are mild and produce high yields of aldehyde from alcohols.[65] Iodine(III) species like BAIB[66], combined with Br^- are also suitable.[67,68] Combining TBAB with BAIB accelerates TEMPO mediated oxidation. This combination regenerates oxoammonium from hydroxylamine and nitroxyl radicals.[69][70] The action of the bromide ion is crucial in that regard. The solubility of TBAB allows the oxidation to perform at high rates in organic, water free solvents, making the bromide available. The absence of water in this TBAB reaction is also beneficial for preventing overoxidation of the aldehyde product to carboxylic acids.

The counterion of the oxoammonium salt influences the reaction rate and the selectivity under acidic and basic conditions.[45,71] The reaction rate decreases in the

following order: ClO_4 > NO_3 > Br > Cl > OAc.[68,72] The substituent on TEMPO in *para* position has a minor effect on reactivity and selectivity [73]

4.1.3 Immobilization of TEMPO

Recovery and reuse of a catalyst are important for sustainable and economical technologies.[74] Homogeneous catalysts are less suitable for this purpose. They are difficult to recover and reuse. This is why less than 20% of industrial processes use homogeneous catalysts, despite their high activity.[75]

Heterogeneous catalysts are in a different phase than the reactants. This simplifies the isolation of the product.[76] They also enable better process control and continuous operation. Catalytic rates go along with the catalyst surface area.[77]

Homogeneous catalyst can be heterogenized by immobilizing the molecules on solid support. [11,25–28,78] Inorganic supports, such as mesoporous silica particles or carbon nanotubes, and also ionic liquids are commonly used.[79] TEMPO supported on silica was thus used as a catalyst for continuous oxidation of alcohols. Stable conversions of 60 % for up to 6 h were achieved in a reactor operated with residence time of 14 min. ACN was used as solvent and BAIB as co-oxidant.[80]

Organic supports for TEMPO immobilization include polystyrene[81], polyurethanes[82], polyacrylates[83], polyetherketones[84], and polyamine[85]. TEMPO loadings range from 0.2 to 3.6 mmol/g. Oxidation reactions with such supported TEMPO entities achieve moderate to excellent conversions, ranging from 37 % to over 99 %. Catalysts maintained their activity for up to eight cycles of reuse.

4.2 Post-polymerization modification

Functional polymers exhibit per definition some physical or chemical activities, and thereunder are also catalytic properties.[86] They can be prepared by direct polymerization of functional monomers or by post-polymerization modification (PPM). Direct polymerization of (catalytical active) monomers is limited in terms of

choice of functional groups as these groups need to be compatible with the polymerization reaction. PPM is the functionalization after polymerization.[87,88] Polymeric compounds are functionalized without changing their degree of polymerization.[89] PPM requires specific reactive groups in the repeating units of the polymer.[88] These groups, such as chlorine, can then act as reaction sites for subsequent modifications (**Figure 5**). Elimination, addition and substitution reactions are used in PPM. Substitution reactions are the most common.[87]

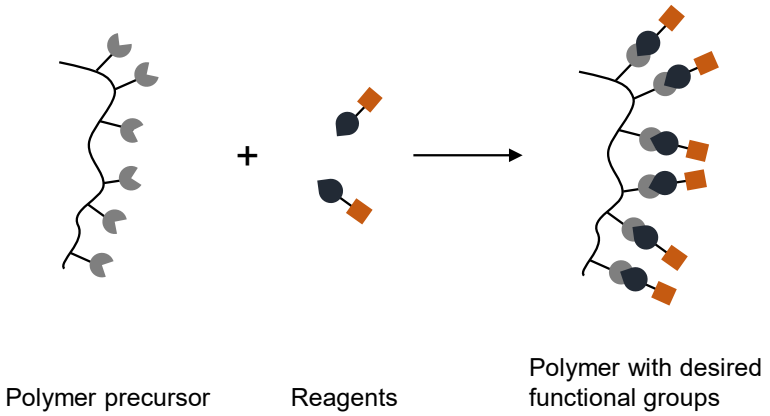

Figure 5. PPM using a polymer precursor and a reagent that contains a desired functionality.

Maintaining the catalytic efficiency of TEMPO is an essential prerequisite for its controlled surface anchoring. This is not achievable by a direct radical polymerization of TEMPO based monomers. TEMPO would be incorporated into the polymer at then chain end in the created NMP process and would show no catalytic activity in the sense of the above-mentioned oxidation processes. Also, if TEMPO were incorporated into a polymer for FFF 3D printing, it might (partly) decompose at the process temperatures. Post-printing functionalization therefore seems to way to a reactor for oxidation with catalytically active TEMPO sites.

4.3 Functionalization of PVC

PVC carries labile chlorine atoms, mostly allyl or tertiary chlorides.[90] These atoms are easily substitutable in PPM.[91] Modified PVC materials are suitable for use as electron materials, membrane sensors or ion-exchange columns.[92] Nucleophilic substitution is

the most studied method. Elimination competes with substitution in PVC. Elimination is favored when the basicity of the nucleophile exceeds its nucleophilicity.[93]

Etherification of PVC is possible using alkylate anion or alcohol/alkali metal systems. Substitution reached 20 % with an OH-/Cl ratio of 4 at 190 °C, but elimination was preferred.[94] Montmorillonite can enhance etherification reaction, increasing the substitution degree up to 83 % without dechlorination.[95,96]

Azidation of PVC replaces chlorine atoms with azide groups. Azidation enables click chemistry reactions.[97]

4.3.1 Click reaction

The Cu(I) catalyzed azide/alkyne cycloaddition (CuAAC) links azide with alkyne moieties.[98,99] The alkyne reacts with the copper catalyst to form a Cu(I) acetylide in a first step. The Cu(I) acetylide then reacts with the azide to form a heterocyclic five-membered ring.[100] Cleavage of the copper(I) complex liberates the product (**Figure 6**).

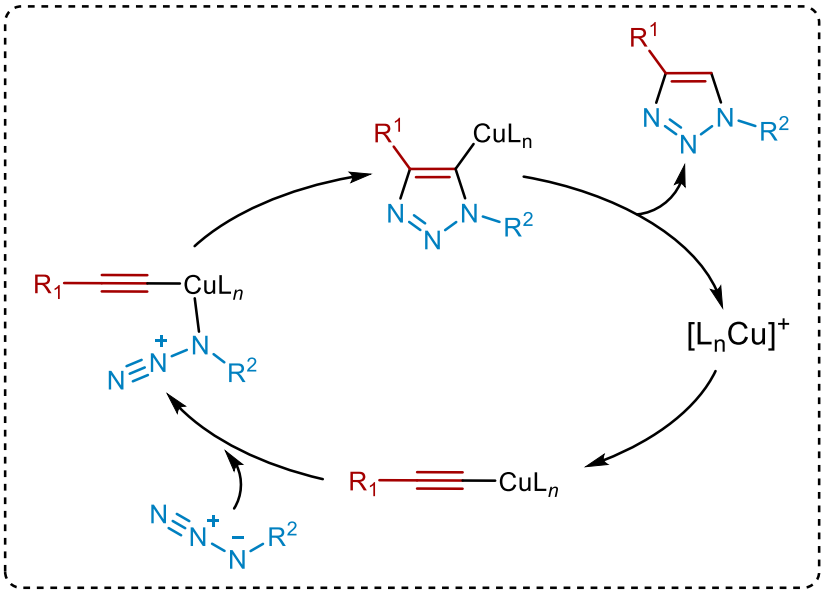

Figure 6. Reaction mechanism for CuAAC with alkyne and azide using Cu(I) catalyst. [98]

CuAAC can also be used for PPM.[97] PVC could be modified with sodium azide, then reacted with CuBr and triethyl citrate. PVC can also be modified with phthalate

plasticizers through a copper-free click reaction.[101] DMF is a common solvent for the CuAAC of PVC. The reactions proceed at temperatures between 30 °C and 62 °C.

4.3.2 Williamson ether synthesis

The Williamson ether synthesis is the primary reaction for preparing ether linkages,[102,103] and can be used in PPM. It reportedly allows an easy post-polymerization of narrowly distributed polymers.[104] This method enables grafting of organic compounds onto inorganic nanoparticles, such as silica.[105]

The Williamson ether synthesis is a one-step process. An organic alcohol reacts with a halogen group (**Figure 7**) to give an ether functionality.[103] The reaction rate can be increase by prior convertion of the alcohol to an alkoxide nucleophile, e.g. by using sodium hydride (NaH) or other strong bases. The Williamson ether synthesis with primary alkyl halides often lead to elimination reactions (alkene formation). In addition, sterically more congested alkoxides also tend to induce halogen acid elimination from haloalkanes and lead to alkenes.[106] Polar aprotic solvents like DMSO are favorable for ether formation (reduces elimination as side reaction). Bromide is a better leaving group than chloride, which leads to a higher reactivity and faster reaction rate.[102]

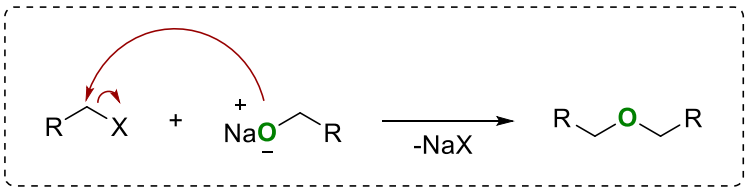

Figure 7. Reaction mechanism of Williamson ether synthesis from a haloalkane and an alcoholate

4.4 Reactor types

Reactions can be carried out in discontinuous or continuous processes and various reactors have been developed over time to accommodate these.[107]. Reactants are added and mixed initially in batch processes. The reaction ends when the desired processing state is reached. A batch process offers high flexibility. It fits reactions with long reaction times. Product quality is variable, space-time yield is low, and relatively

long idle times need to be considered for economics.[108,109] Continuous operated reactors involve a steady inflow and outflow of materials. This leads to more constant product qualities when steady state operations can be reached. Space-time yield is high. Processes with long reaction times are less suited for continuous operated reactors.[108,109]

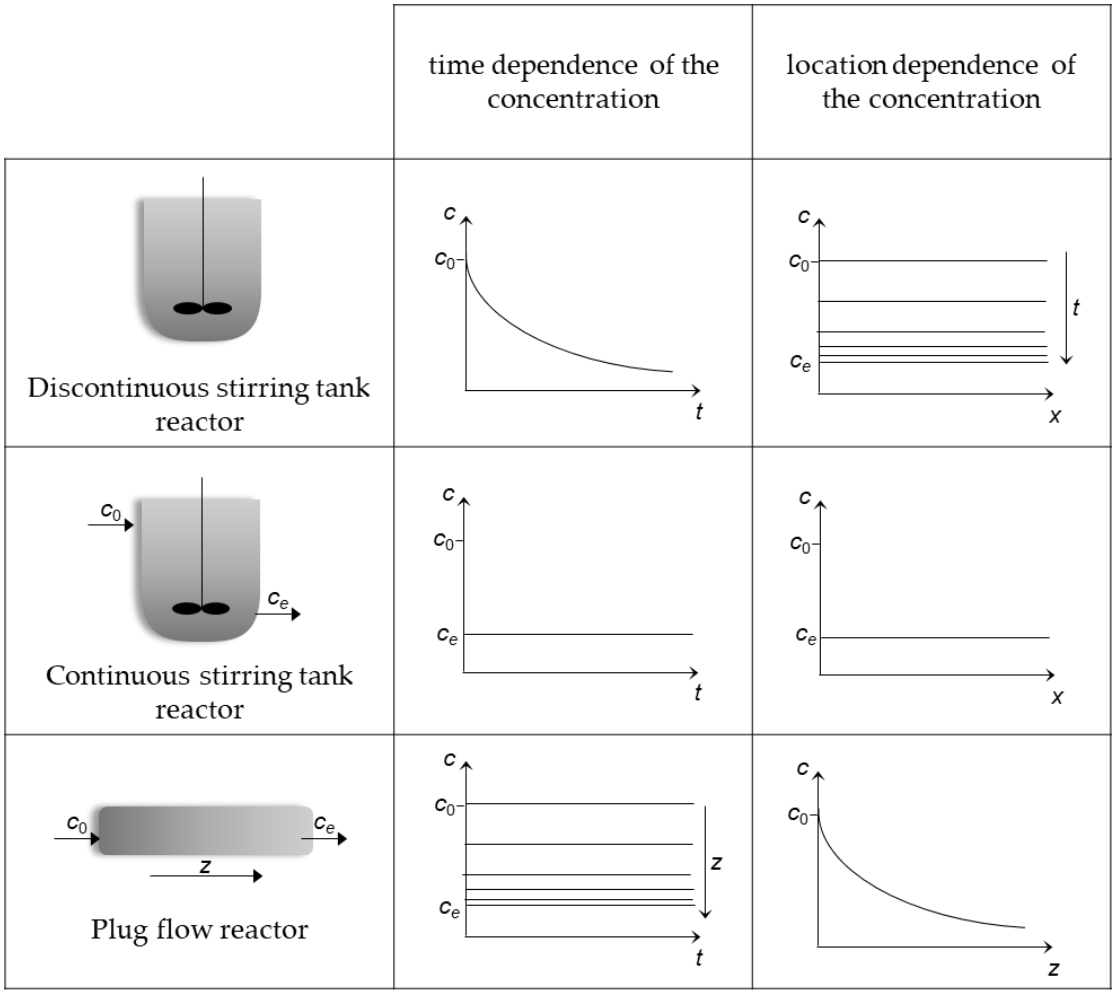

Figure 8. Concentration profiles of ideal reactors as a function of location and time.[108]

The main types of ideal reactors are batch (DSTR), continuous stirred-tank (CSTR), and the plug-flow reactors (PFR; **Figure 8**).[108,109] Reactants are added to the tank at the beginning of a process in a closed DSTR reactor. The concentration of the reactants decreases over time. Product concentration increases. This progression depends on reaction time.[108,109] Reactants are continuously added and products are removed in a CSTR. Concentrations are homogeneous spatially because of constant mixing. The

conversion depends on the flow rate.[108,109] Plug-flow reactors have constant reactants flow through the reactor without much mixing. Reactants concentrations decrease and product concentrations increase along the position in the pipe. The concentration profile depends on reaction and flow rate.[108,109]

A packed bed reactor (PBR), a special case of a PFR can be used for a reaction that proceeds under heterogeneous catalysis. It contains catalysts particles arranged in a packed bed. These particles have a reactive surface that mediate the reaction. Diffusion to and from the particles, and non-ideal flow patterns in the bed can broaden residence time distributions and negatively influence selectivity and conversion.[110]

4.5 Combining 3D printing and flow chemistry

Catalytic oxidation with polymer-supported (PS)-TEMPO was reported in batch reactors at the mL scale.[82] But batch processes are not so suitable for industrial-scale alcohol oxidation because of the exothermic nature of the reaction[9] A continuous process would be desirable. Continuous setups provide higher space-time yield, easy automation, and simpler scale-up.[111] Batch operation can help to determine suitable reaction conditions.[112] Parameter such as flow rates, concentrations, reactor size and conditions can be estimated.

Transferring a batch to a continuous process has gained some attention in organic chemistry.[16,113] Controlled mixing and heat transfer are ensured with high surface area mixing elements.[114] A catalytic process in a PBR profits from the option of fixating the catalyst on a solid in the reactor.[115] Solid-liquid phase interaction is more intense. Separation of the catalyst is not required, making the process efficient and sustainable.[116] Catalyst leaching must be minimized. It not only causes a loss of catalysts but also an uneven distribution of the catalysts in the bed can arise. [117][118]

Rapid prototyping (RP) can be used to design and build a reactor for flow chemistry comprising an immobilized catalyst.[119,120] Fused deposition modeling (FDM) is a

common RP processes.[121] Prototypes are designed with computer-aided design (CAD) and converted into a 3D geometry by printing.

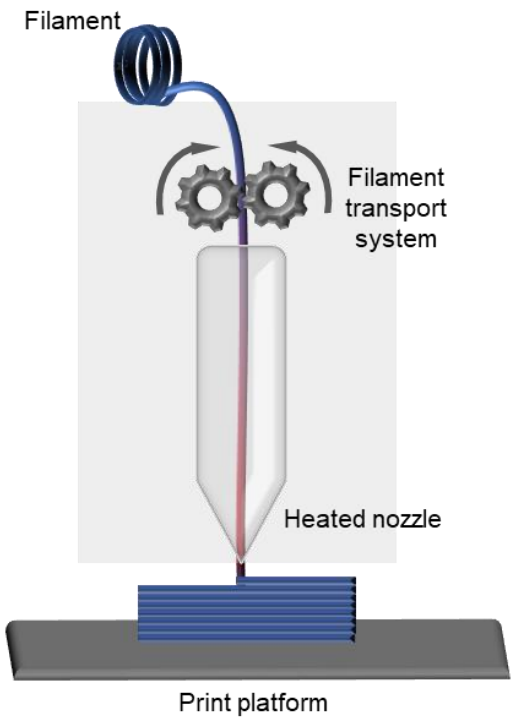

Figure 9. Schematic illustration of the FDM process.

The thermoplastic filament is melted, extruded and applied layer by layer.[122,123][123] FDM is easy to handle, costs-efficient, and can produce complex geometries.[122,124] The design of freedom ranges from mixing elements to manufacture of reactors.[125,126] 3D printing is also used in micro- and millifluidics, enabling embedding of catalytically active materials and expanding heterogeneous catalysis.[126–129][119,130]

Printing materials are thermoplastic polymers.[131] Common polymers for catalytic flow reactors include are nylon, HIPS (high impact PS) or PLA. PVC is not widely used, but offers a possibility of bonding the catalysts because of the high chlorine content.[132] Challenges in printing PVC involves its thermal decomposition and crystallization.[133][134] A catalytically active material can be introduced into a 3D printed continuous reactor in at least three ways.[135–138] The first option is to modify the material before printing.[138,139] The second option is direct printing of a catalytically active material, for example by inject printing.[126–129,140] The third option is

functionalizing printed surfaces using PPM.[119,137,141] PPM ensures that the catalyst is only present on the relevant surface. Surface enlargement can be achieved by enlarging the reactor or printing static mixers or grid-like structures.[136,142]

5. Results and discussion

5.1 Printing and characterization PVC

Two factors ar at least to be considered for the objective of reaching a 3D printed reactor functionalized with TEMPO as catalyst: The filament needs a functional group for covalent bonding with the catalyst, and it must also resist reaction conditions and solvents to prevent damage. PVC is a suitable material. It contains substitutable chlorine atoms and is available from *Fillamentum* as *Vinyl 303* (1.75 mm diameter). PVC resists solvents and reaction conditions.

The filament printer *Creality ender cr10* is used (**Figure 10**, left) for printing PVC parts. A layer height of 0.15 mm is set. The bed temperature is 80 °C, and line width is 0.60 mm. Material flow is set to 120 %. A 0.6 mm brass nozzle is used to prevent clogging. Nozzle temperature is set to 230 °C, and print speed is 40 mm/s. The fan is set to 50 % to print overhangs. These settings prevent wavy or rough edges (**Figure 10**, right top). A stronger fan causes warping (**Figure 10**, right bottom). Warping is also resulting when the bed temperature is too low.

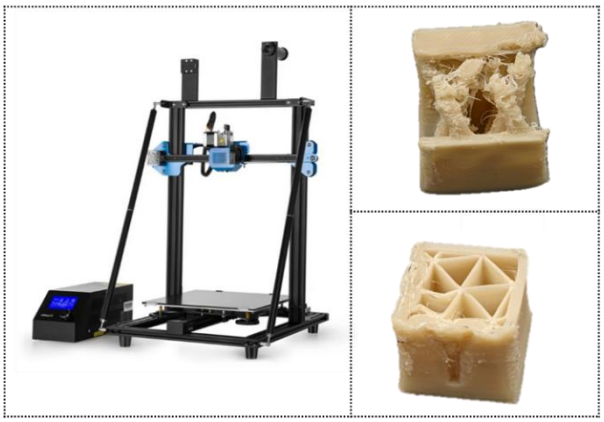

Figure 10. Left: 3D printer used *creality enders cr10* and right: misprints with rough endges (top) or warping (bottom) caused improper printing settings.

No dechlorination occurs during the 3D printing process. The FTIR curves before and after printing overlap. Typical C-Cl stretching vibration appear at a wavelength of

623 cm^{-1}.[94,143] No substantial double bonds are formed as the result of a dehydrohalogenation as no absorbances at ≈ 1564 cm^{-1} arise (**Figure 11**).[94,143]

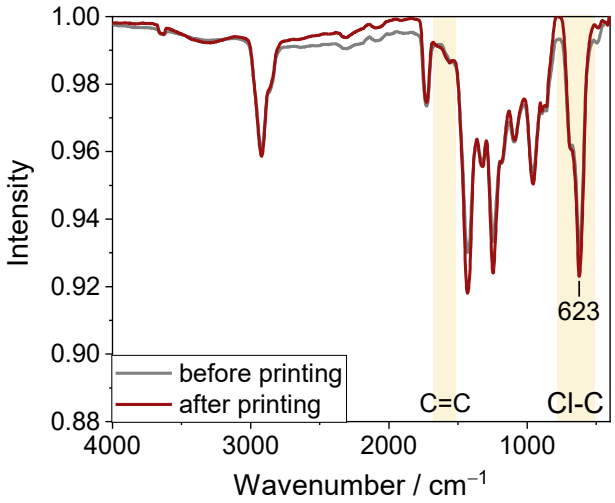

Figure 11. FTIR spectra of filament before printing (grey) and after printing (red).

The chlorine amount on the surface is high. The chlorine content after printing is 14 *atom*% and the carbon content is 78 *atom*% by EDX mapping (**Figure 12**). The expected ratio for PVC is 2:1 C/Cl. The measured ratio of C/Cl is about 5:1 C/Cl. This could indicate a chlorine release, but EDX is a surface method and therefore the result does not always reflect the elemental composition. Additives like plasticizers or heat stabilizers could also affect the chlorine content.

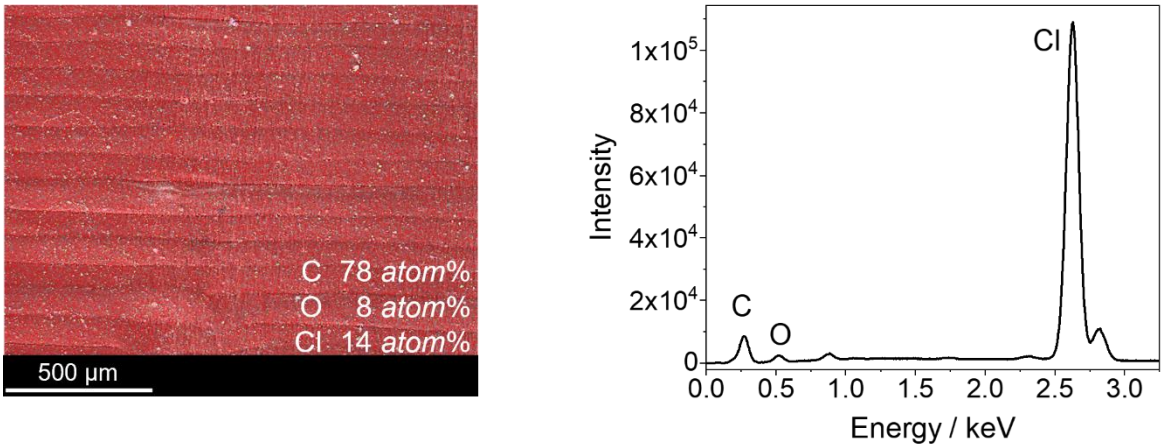

Figure 12. EDX mapping overlap of printed PVC (left) and resulting EDX spectrum (right).

5.2 Post functionalization of printed PVC

5.2.1 Click-Chemistry

PVC-Click-TEMPO can be synthesized in a 3-step synthesis. The first step is functionalization of PVC with sodium azide to PVC-N_3. The second step is the conversion of TEMPOL to propargyl-TEMPO using propargyl bromide as source for the alkyne entity. PVC-click-TEMPO was synthesized by 1,3-cycloaddition (**Figure 13**) using copper(I)iodid as catalyst and *N,N*-diisopropylethylamine (DIPEA) as phase transfer agent.

Printed PVC pellets measuring 8 mm in diameter, with a wall thickness of 0.8 mm and a height of 10 mm, were utilized as substrate.

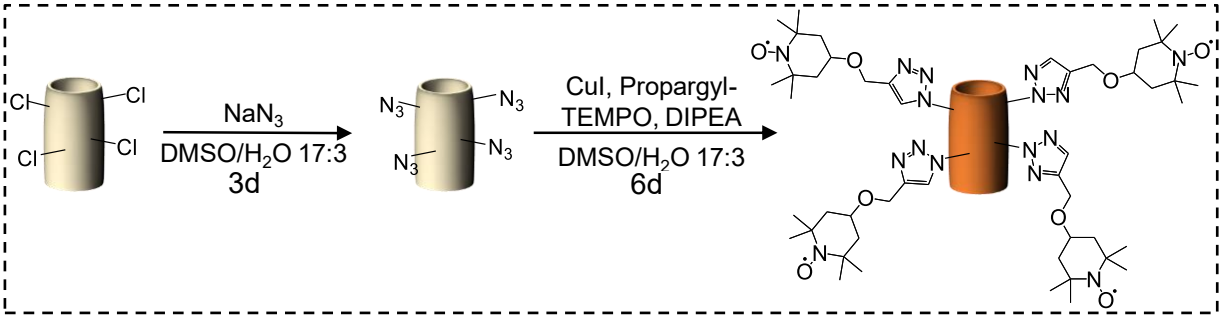

Figure 13. Functionalization pathway of PVC with propargyl-TEMPO in a 1,3-cycloaddition using copper(I)iodid as catalyst.

Propargyl-TEMPO is synthesized by stirring the sodium salt of TEMPOL with propargyl bromide for 4 h at RT. The product is isolated using column filtration. The FTIR spectrum of propargyl-TEMPO shows bands at 3230 cm^{-1}, 2112 cm^{-1} and 1082 cm^{-1} (**Figure 14**). The first two bands are indicative of the vibrations of ≡C-H and C≡C motives.[144] The last band is expected for bend mode of C-O-C moieties in aliphatic and alicyclic ethers.[144] These findings confirm the etherification of TEMPOL with propargyl bromide. The yield is 65 %. The presence of an unpaired electron was incompatible with NMR analysis.

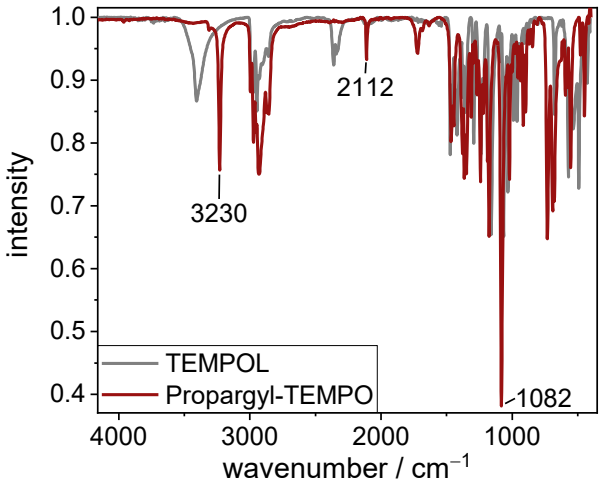

Figure 14. FTIR spectra of TEMPOL (grey) and propargyl-TEMPO (red).

The second step is the introduction of an azide functionality on PVC. Therefore, sodium azide is dissolved in DMSO/H_2O mixture (17:3 *v*/*v*) and PVC pellets are added to the solution. The reaction mixture is stirred at 65 °C for 3 d after which some (surface) chlorine atoms are substituted for azide groups. The PVC pellets undergo a visible color shift to orange. The printed pellet structure remains intact (**Figure 15**). The print layers expand slightly during functionalization. The thickness increases from 0.09 mm to 0.16 mm. This swelling occurs without holes or cracks forming.

The reaction is easily monitored by FTIR spectroscopy (**Figure 15**, left) as the characteristic vibration band of N_3 appears at 2104 cm^{-1}. This band increases over time and is found at higher wavenumbers than in NaN_3 (2019 cm^{-1}), indicating covalent bonding of N_3 groups to PVC. Elemental analysis on the pellets also indicates the presence of azide entities (**Figure 15**, right). The azide loading X_{azide} was calculated by the ratio of nitrogen content of EA (%N) to the number of nitrogen atoms in PVC (N(N) = 3) and the molar mass of nitrogen M(N):[80]

$$X_{azide} = \frac{\%N}{N(N)M(N)} \quad (1)$$

Reaction is more or less finished after 48 h.

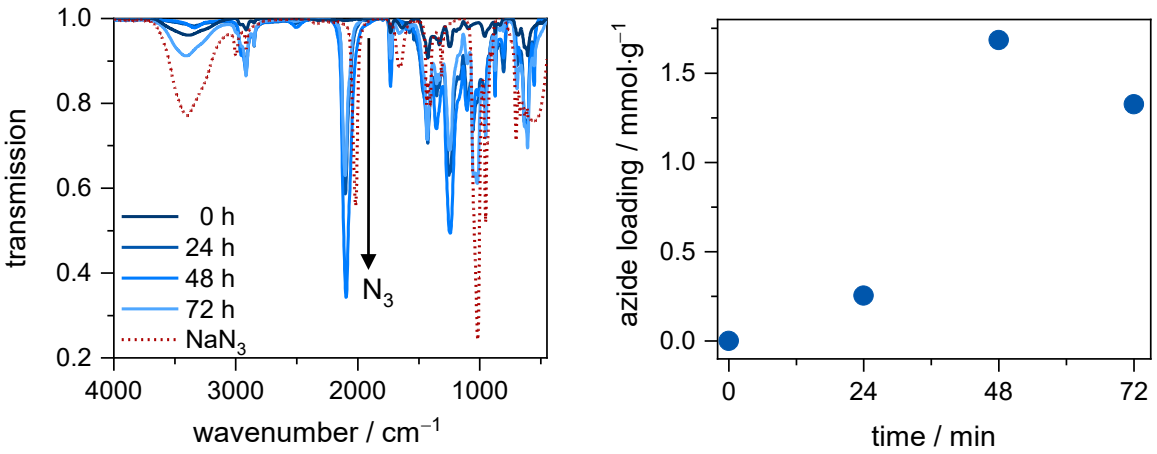

Figure 15. Left: FTIR spectra of azide-treated PVC after 0 h, 24 h, 48 h and 72 h of reaction time. Right: Calculated azide loading by EA.

The presence of nitrogen and thus azide entities at the PVC surface is also found in SEM-EDX measurements (**Figure 16**). The chlorine content of the surface consistently decreases with reaction time and the nitrogen content increases **Table 1**).

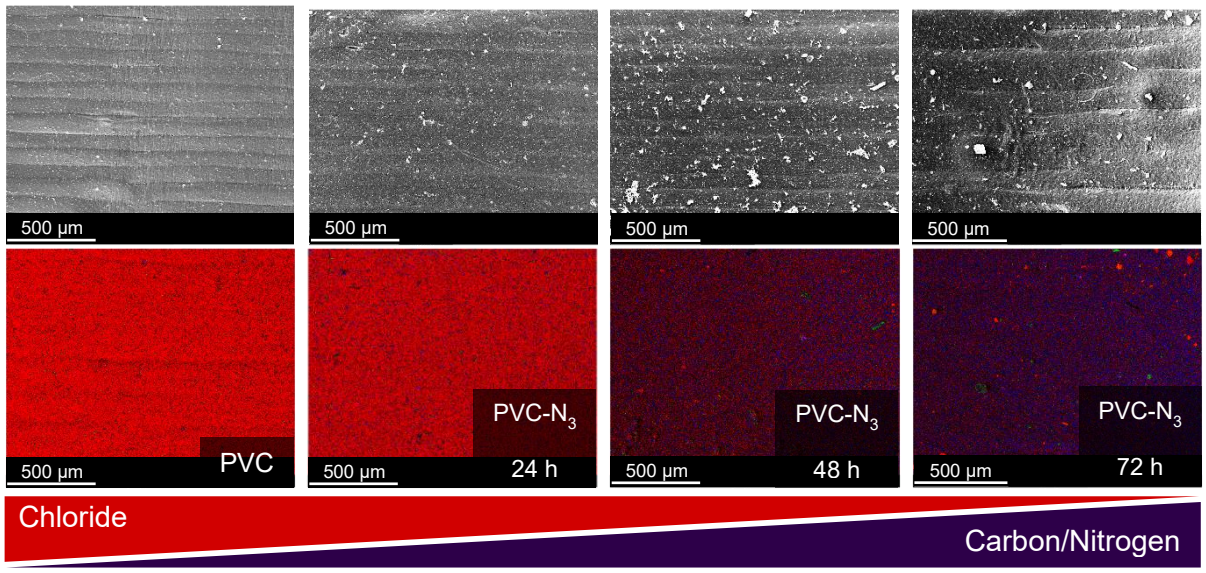

Figure 16. SEM images (top) and EDX mapping images (bottom) of PVC and PVC after 24 h, 48 h and 72 h of treatment with sodium azide, giving PVC-N3.

Table 1. Atomic ratios of carbon, chlorine, and nitrogen by EDX analysis of PVC and PVC-N_3 after 24 h, 48 h and 72 h.

Sample	C%	Cl%	N%
PVC	78	14	8
PVC-N_3 24 h	66	9	15
PVC-N_3 48 h	53	4	32
PVC-N_3 72 h	50	2	36

The final coupling of PVC-N_3 and propargyl-TEMPO was effectively catalyzed by a mixture of CuI and DIPEA. The CuAAC click reaction leads to PVC-click-TEMPO pellets at 45 °C, but conversion was unsatisfactory even after 6 d. Increased temperature results in 4.5 times higher TEMPO fixation on the PVC surface in less time.

Again, the progress of the reaction is readily monitored by FT IR spectroscopy: The N_3 vibration band at approximately 2104 cm^{-1} decreases which is taken as an indication of its transformation to a triazole ring (**Fehler! Verweisquelle konnte nicht gefunden werden.**). TEMPO loadings determined by EA (right) reaches 0.45 $mmol \cdot g^{-1}$ after 144 h. A change in color of the PVC pellets from white/yellowish to brown is also observed. No N_3 vibration band is detected at the PVC after 24 h at 65 °C. TEMPO loading reaches 2 $mmol \cdot g^{-1}$.

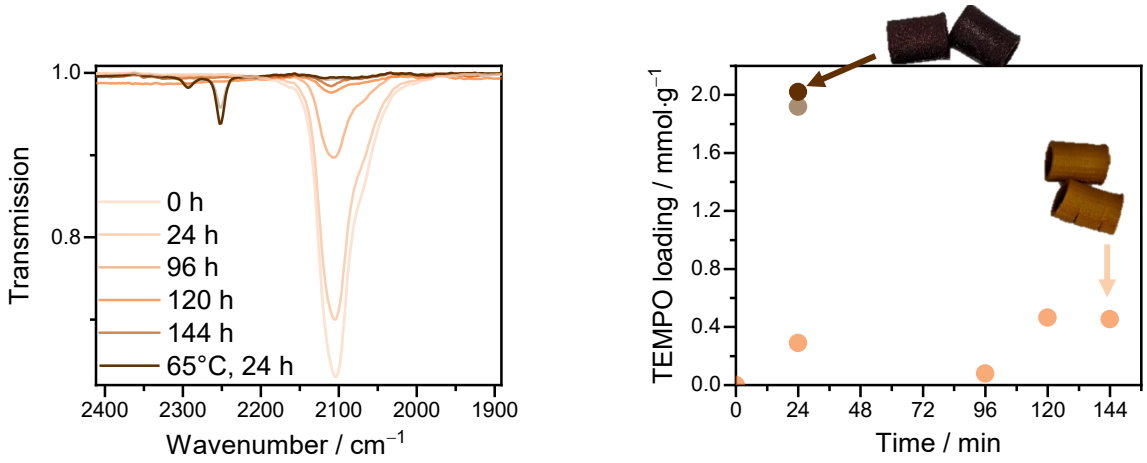

Figure 17. Reaction monitoring by FTIR (left) and calculated TEMPO loadings by EA (right) of click reactions at 45 °C (orange) and 65 °C (brown)

The high reaction temperatures in click reaction cause a structural change of the pellet surface (**Figure 18**). The surface appears cluster-shaped instead of layered. The reaction temperature is slightly below T_g of PVC (78 °C, section 6.2.5). The surface is partially melted and dissolved. Cooling and drying result in material contraction. This process partly restores the surface.

EDX mapping is consistent with the success of the click reaction (**Figure 18**, **Table 2**). The carbon and oxygen content increase, and the nitrogen to oxygen ratio of 2:1 confirms propargyl-TEMPO bonding to PVC-N_3.

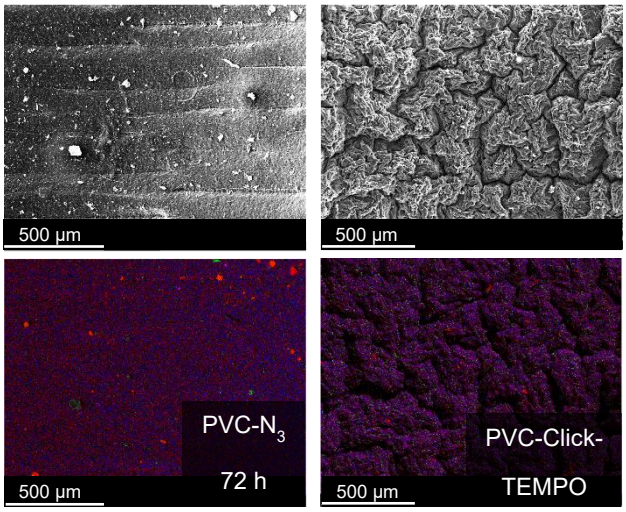

Figure 18. SEM images (top) and EDX mapping images (bottom) of PVC-N3 after 72 h (left) and PVC-Click TEMPO after 24 h at 65 °C (right).

Table 2. Atomic proportion of carbon, chlorine, oxygen, and nitrogen by EDX analysis of PVC, PVC-N_3 and PVC-Click-TEMPO.

Sample	C%	Cl%	O%	N%
PVC	78	14	8	-
PVC-N_3 72 h	50	2	10	36
PVC-Click-TEMPO	62	1	14	22

Orientating activity study of PVC-click-TEMPO in the oxidation of benzyl alcohol

Prepared PVC-click-TEMPO catalysts with BAIB as a co-catalyst convert benzyl alcohol at a moderately rate. Samples are taken for ^{1}H-NMR measurements to determine conversions (**Figure 20**). The conversion was 67 % after reaction time of 30 min. The catalytic pellets were subsequently washed with water and acetonitrile and reused in a next cycle. This was repeated one more time afterwards. It is found that the activity decreases with each cycle, conversion was only 43 % in the 3rd one. Leaching or deactivation of TEMPO is thought to cause this.

The reactivation of the pellets with BAIB produces acetic acid. AcOH can protonate the hydroxylamine (TEMPOH). TEMPOH-H+ is formed.[145] The formation of TEMPOH-H+ is irreversible. The regeneration to oxoammonium salt is no longer possible.

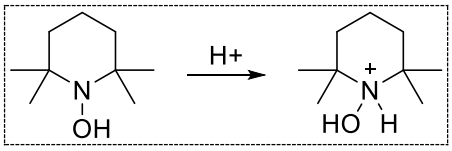

Figure 19. Protonation of hydroxyl-TEMPO to TEMPOH-H+

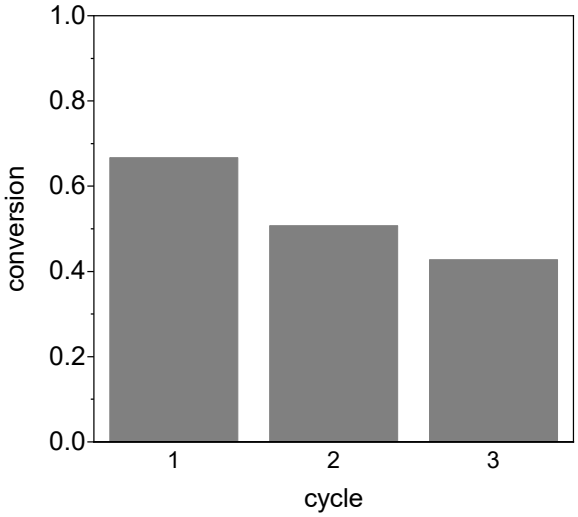

Figure 20. Conversions of benzyl alcohol oxidation in three consecutive cycles with PVC-click-TEMPO.

5.2.2 Substitution of PVC by etherification

The functionalization of PVC with TEMPO using the CuAAC has some drawbacks with respect to long time of synthesis procedures and stability in the oxidation catalysis. The Williamson ether synthesis for TEMPO surface functionalization was therefore addressed as a possible alternative. The substitution can be carried out under various reaction conditions, some are in a preliminary approach.

The first reaction conditions considered for the substitution reaction uses DMSO/H_2O (**Figure 21**, green) as solvent. TEMPOL is activated for nucleophilic attack by forming the alkoxide TEMPOL salt with sodium hydride (NaH) in DMSO. Water is added after full conversion of TEMPOL and no remaining NaH to prevent reaction between NaH and water. An extended choice is the same Williamson ether synthesis protocol in combination with Maghnite K^+ as catalyst (**Figure 21**, red). It has been reported that Maghnite K+ is a suitable auxiliary for modifying PVC with alcohols.[95,96] Maghnite K+ is an inorganic clay, which here is loaded with intercalated potassium ions. 63 % of the chlorine in PVC could be substituted for alcohols. The third option is like the first one, but rather using toluene (**Figure 21**, blue). The last functionalization reaction alternative uses silver oxide as base and toluene as solvent. This approach is expected

to prevent dehydrochlorination of PVC (**Figure 21**, orange). All reactions are carried out at a temperature between 20 °C and 65 °C and reaction times of 48 h.

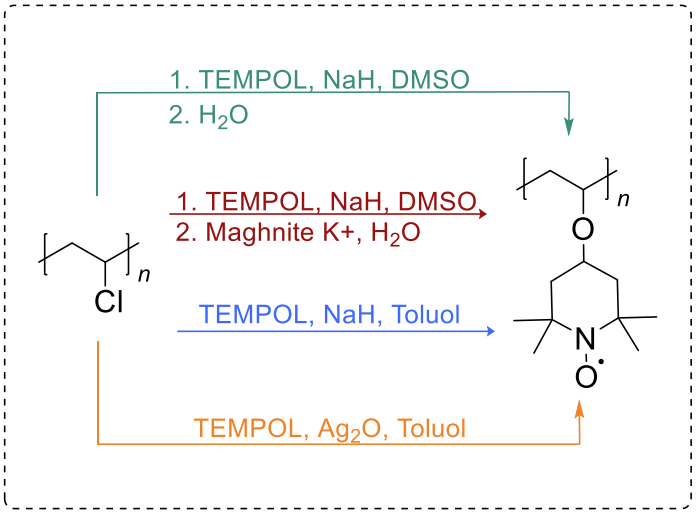

Figure 21. PVC-TEMPO preparation via Williamson ether synthesis (green), Williamson ether synthesis with maghnite K+ as supplement (red), Williamson ether synthesis in toluol (blue) and Williamson ether synthesis as solvent and Ag_2O (orange).

PVC-TEMPO-functionalization occurs under all reaction conditions. Chlorine content decreases, and oxygen content increases Nitrogen is measured in all samples, confirming the substitution. Low nitrogen mass can cause measurement errors. The analysis of nitrogen at the surface is only qualitative.

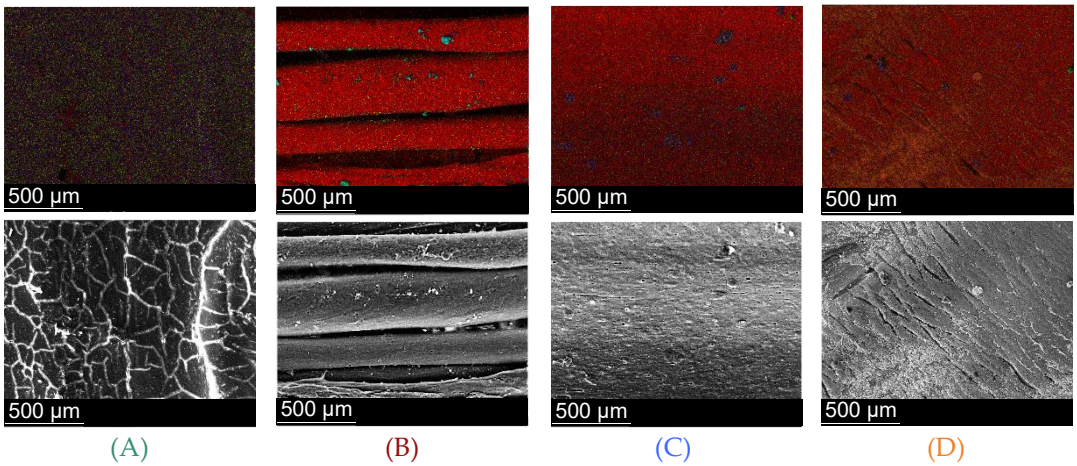

Figure 22. SEM images (bottom) and EDX mapping images (top) of PVC-TEMPO by (A) classic Williamson ether synthesis (green route, figure 22) (B) with Maghnite K^+ (red rote, figure 22) both in DMSO/H_2O and (C) classic Williamson ether synthesis in toluol (blue route, figure 22) and (D) with Ag_2O (orange route, figure 22).

The most suitable method for producing the PVC-TEMPO catalyst is Williamson ether synthesis in DMSO/H2O (**Figure 21**, green route). This method achieves the highest functionalization, as indicated by the high proportion of oxygen (22 %) and the lowest chlorine content (0.4 %) (**Figure 22**, A and **Table 3**). No structural changes in the pellets were observed after functionalization. No swelling is observed in this reaction. The SEM image shows a smooth surface. The printing structure is no longer visible.

Sample C (**Figure 21**, blue route) follows with 6 % chlorine. But the reactions in toluene (**Figure 21**, blue route and orange route) resulted in swollen pellets, causing the print structure to disappear in the SEM images (**Figure 22**, C and D).

By using Maghnite K+ (**Figure 21**, red route), the print structure is retained. Swollen layers of up to 0.28 mm and 0.42 mm form (**Figure 22**, B).

Table 3. Atomic fraction of C, N, O and Cl by EDX mapping in samples A, B, C, D and PVC

Sample	C%	Cl%	O%	N%
PVC	78	14	8	-
A	67	0.4	22	8
B	73	12	12	3
C	70	6	15	7
D	71	10	11	4

Orientating activity study of PVC-TEMPO in the oxidation of benzyl alcohol

Again, a short assessment of the performance of the TEMPO containing PVC from a Williamson functionalization in the oxidation of benzyl alcohol is carried out. The catalysts is applied again in three consecutive cycles and are washed with water and ACN between cycles (**Figure 23**). All pellets show catalytic activity, conversions of benzyl alcohol range from 76 % to 94 %. The catalytic action is always lower in the

second and even more in the third cycle. The drop in activity is related to loss of TEMPOL: unbound TEMPOL diffuses out of the pellets in the first cycle. The chemical coupling of TEMPOL and PVC was incomplete. The best results in the oxidation reactions are obtained from PVC functionalization in DMSO/H_2O . Catalytic pellets from Williamson ether synthesis in DMSO/H_2O (green route) maintain higher activity over multiple cycles, and they show the smallest decrease between the first and the second cycle.

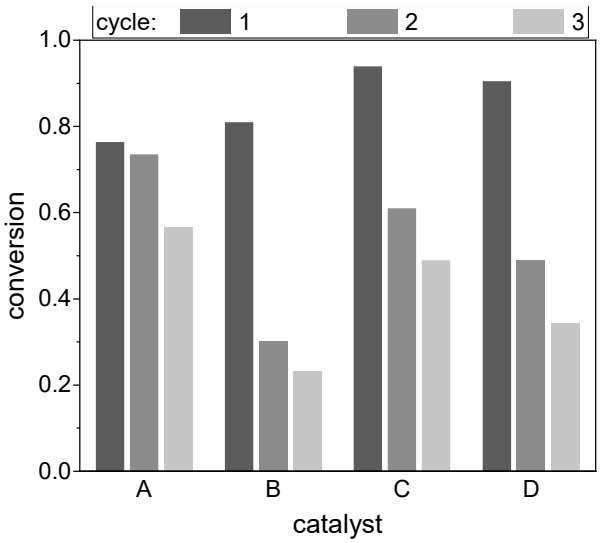

Figure 23. Conversions of benzyl alcohol oxidation in three cycles with pellets from green route, red route, blure route and orange route (**Figure 21**).

Influence of temperature on Williamson ether synthesis

The initial results indicate that a PVC pellet functionalization is most effective in DMSO using NaH as base. Further efforts allowed to reach a higher conversion, the main insight is to increase the reaction temperature, which was first at 35 °C and later at 50 °C. The progress of the substitution reaction can be assessed from IR spectra of the pellets (**Figure 24**). Characteristic bands are ether bend vibrations at 1050 cm^{-1}, chlorine carbon starch around 609 cm^{-1} and the nitroxyl band at 2350 cm^{-1}, next to the valence vibration of carbon double bonds around 1630 cm^{-1}. Latter results from dehydrohalogenation. The integrals of these bands are referenced to the integral of the

absorption of the CH backbone at 2800 cm^{-1}. Its constant intensity during reaction is assumed.

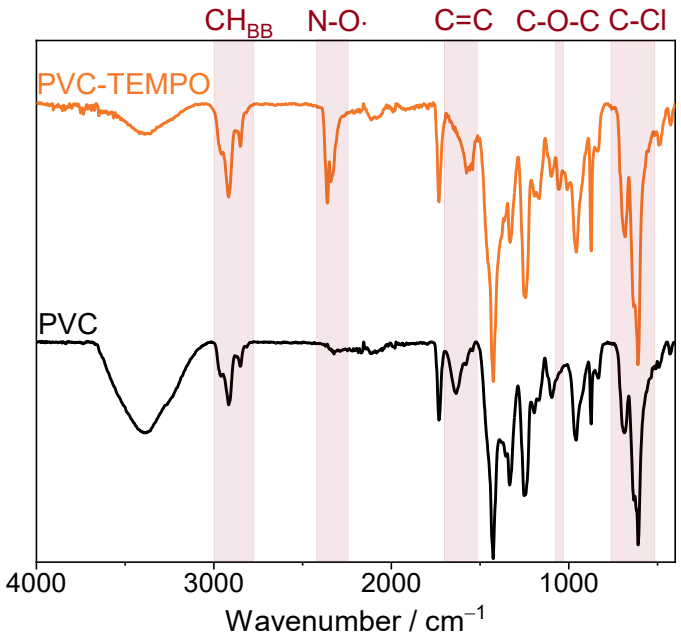

Figure 24. FTIR spectra of a functionalized PVC-TEMPO (orange) and printed PVC (black).

Increasing the temperature accelerates the reaction, and also side reactions become faster (**Figure 25**). The chlorine content on surface decreases with time the fastest at 35 °C and reaches like for all reaction temperatures a plateau after 24 h. The concomitant intensity of the C-O-C also shows a plateau formation after 24 h at 20 °C and 35 °C, but not for 50 °C reaction temperature. The plateau after 24 h indicates that the maximum number of exchangeable chlorine atoms with TEMPOL was reached. This means that either no further chloride entities are reactive, or that the base, necessary for the activation of TEMPOL has been consumed in side reactions. HCl-elimination is observed as dominant side reaction. The content of double bond increase with reaction time by consuming the base, the highest content is also reached at 35 °C reaction temperature, the lowest at 50 °C. The competition between chloride substitution and HCl elimination and their temperature dependence may underly the complexity of the behavior. The intensity of the N-O vibrations in the pellets increase in the first hours, but show a rather erratic course of the intensity. This may be caused

by the physisorption of TEMPOL in the PVC, which is not easily reversed, i.e. although the pellets were cleaned (by H_2O and ACN) before IR analysis, an arbitrary amount may have remained.

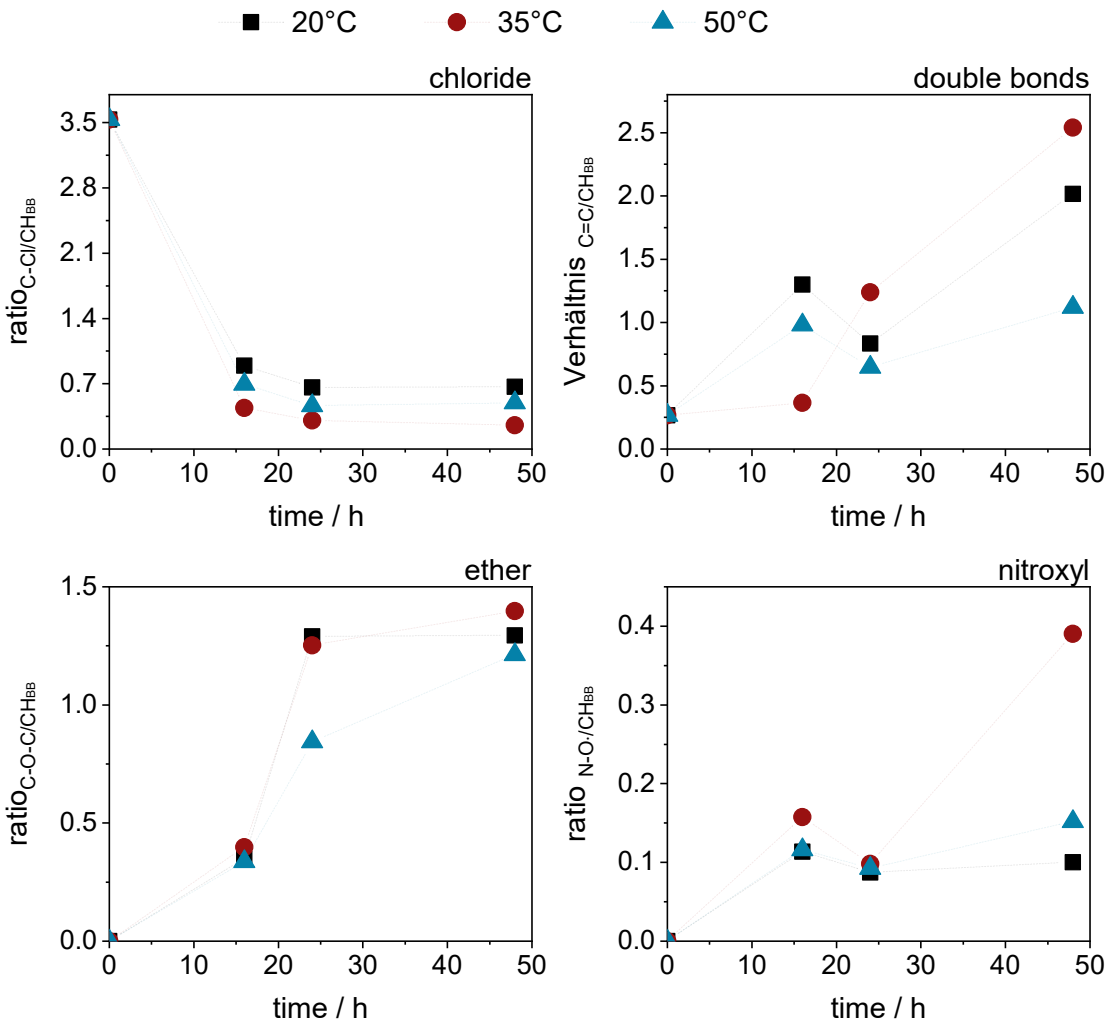

Figure 25. Ratios of chlorine band (top left), double bonds (top right), ether band (bottom left), and those of nitroxyl bond (bottom right) to the CH backbone of the reactions at 25 °C (black), 35 °C (red), and 50 °C (blue).

Activity of the respective PVC-TEMPO catalysts (48 h) in the oxidation of benzyl alcohol

The catalytic activity of the pellets from the synthesis after 48 h were evaluated like described above, i.e. three cycles with intermediate washing. The three types of catalyst pellets showed good benzyl alcohol conversion in the first cycle, ranging from 74 % (20 °C) to 92 % (35 °C; **Figure 26**). The conversion decreases to about half the values in the third run for the pellets functionalized at 20 °C and 35 °C. The oxidation

reactions with the catalysts prepared at 50 °C show a smaller drop of about a third of the activity. This seems to indicate that pellet functionalization at 50 °C is more effective for the catalytic properties, although an optimum of TEMPOL substitution at the pellet surface as detected by IR is not at a maximum: the amount of ether linkages as detected appear lower and the chloride content higher at a reaction temperature of 35 °C. The general scattering in the IR analysis may be factor in this, and a functionalization away from the surface may also be factor. PVC swells and expands in DMSO, but not so much in benzyl alcohol. Thus, TEMPOL bound more in the bulk of the pellets may not participate in the catalysis.

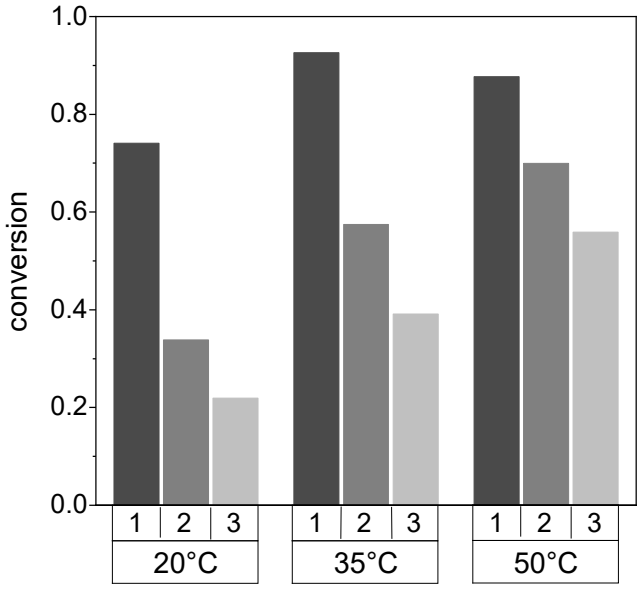

Figure 26. Conversions of the oxidation of benzyl alcohol to benzaldehyde mediated by the PVC pellets after a functionalization time of 48 h (c.f. **Figure 25**).

Influence of water in the pellet Williamson ether functionalization in DMSO

The swelling of PVC in DMSO may come, as pointed out above, with disadvantages for the effective amount of TEMPO available for the catalysis, but also if a reactor wall is functionalized, leakage could result in less available catalyst amount. The quality of the DMSO solvent for swelling of PVC can be diminished by the addition of non-solvent water.

Four functionalization reactions of PVC pellets with TEMPOL/NaH are performed using different DMSO/H_2O ratios (3:1, 1:1, 1:3, and 17:3 (*v*/*v*)) at 50 °C, IR spectroscopy on the pellet surface again was used to assess the progress of reaction. It is generally found that the presence of water tends to lead to lower conversions, possibly by the smaller extent of swelling, making less chlorine entities accessible (**Figure 27**). A high content of DMSO is thus a prerequisite. A solvent ratio of DMSO/H_2O of 17:3 (*v*/*v*) shows a good balance between etherification and elimination. When pure DMSO is used, the pellets swell, causing their size to approximately double after functionalization. A low proportion of water is advantageous to prevent the formation of double bonds and swelling of the pellets.

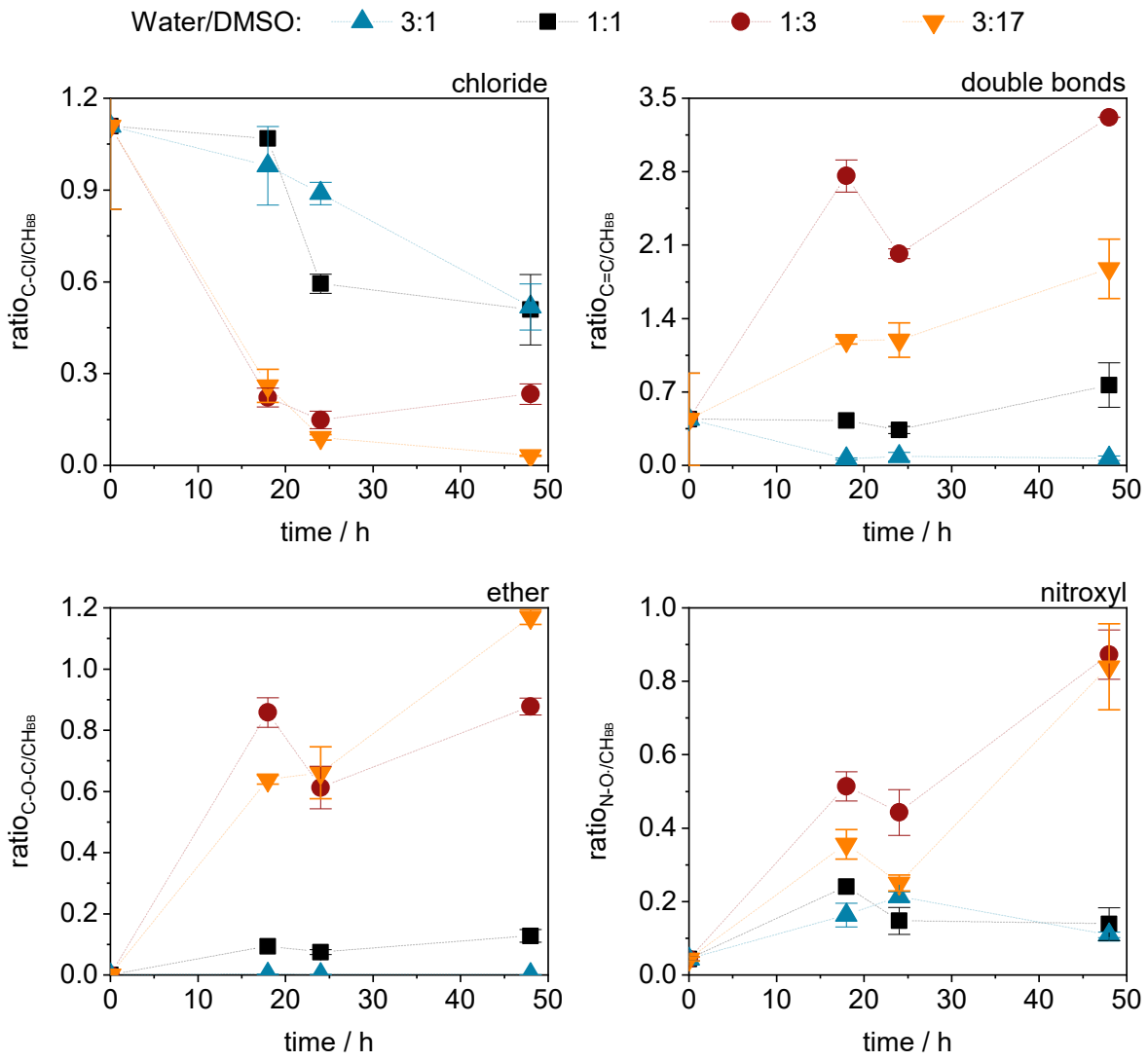

Figure 27. Ratios of chlorine band (top left), double bonds (top right), ether band (bottom left), and of nitroxyl bond (bottom right) to the CH backbone of the PVC TEMPOL functionalization in H_2O/DMSO 3:1 (blue), 1:1 (black), 1:3 (red), and 3:17 (orange).

Activity of the respective PVC-TEMPO catalysts (48 h) in the oxidation of benzyl alcohol

The pellets isolated after 48 h of functionalization conditions were again standardly (three cycles with intermediate washing) tested in benzyl alcohol oxidation reactions to benzaldehyde. The catalytic activity of the pellets prepared with an excess of DMSO/H_2O ratios of 1:3 and 1:1 fall behind of those prepared in a medium with a higher DMSO content (**Figure 28**). This is consistent with the FTIR analysis on the degree of PVC substitution. In addition, a low amount of TEMPO is immobilized on the surface, the rest appears mobile. A sharp drop of benzyl alcohol conversion is

found to the second and third cycle. PVC pellets functionalized in a medium with a higher DMSO to water ratio achieve good catalytic activity and the loss of activity in the second resp. third cycle is less.

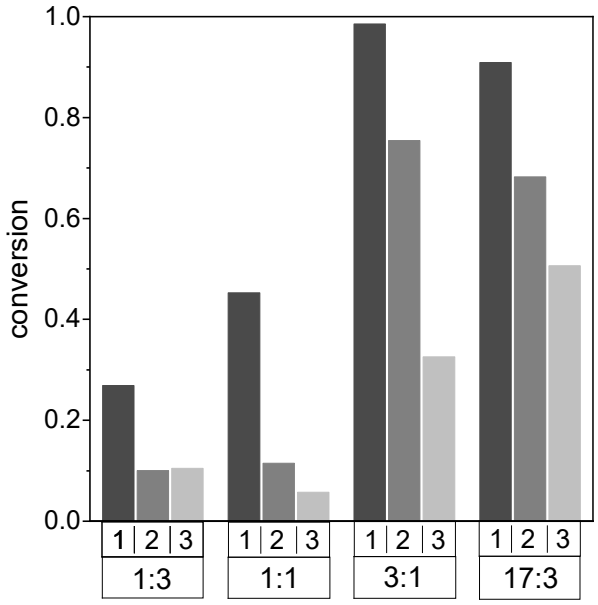

Figure 28. Conversions of the oxidation of benzyl alcohol to benzaldehyde with the catalyst pellets obtained after 48 h from the functionalization using DMSO/H_2O 3:1, 1:1, 1:3, and 17:3 mixtures in three consecutive cycles.

Presence of Maghnithe K+ during the pellet functionalization in DMSO

The catalysis described in literature results in fewer double bond:[95,96] Maghnite K+ is therefore also evaluated in detail as aid in the PVC functionalization with TEMPOL, using a medium with a DMSO/H_2O ratio of 3:1. The temperature is 50 °C, the reaction time is 48 h. Three variants were exploited in form of using only Maghnite K+ as base catalyst and mixtures of Maghnite K+ and NaH in ratios of 3:1 and 1:3. Chemical changes at the surface of the pellets were again assessed through IR spectroscopic analysis (**Figure 29**).

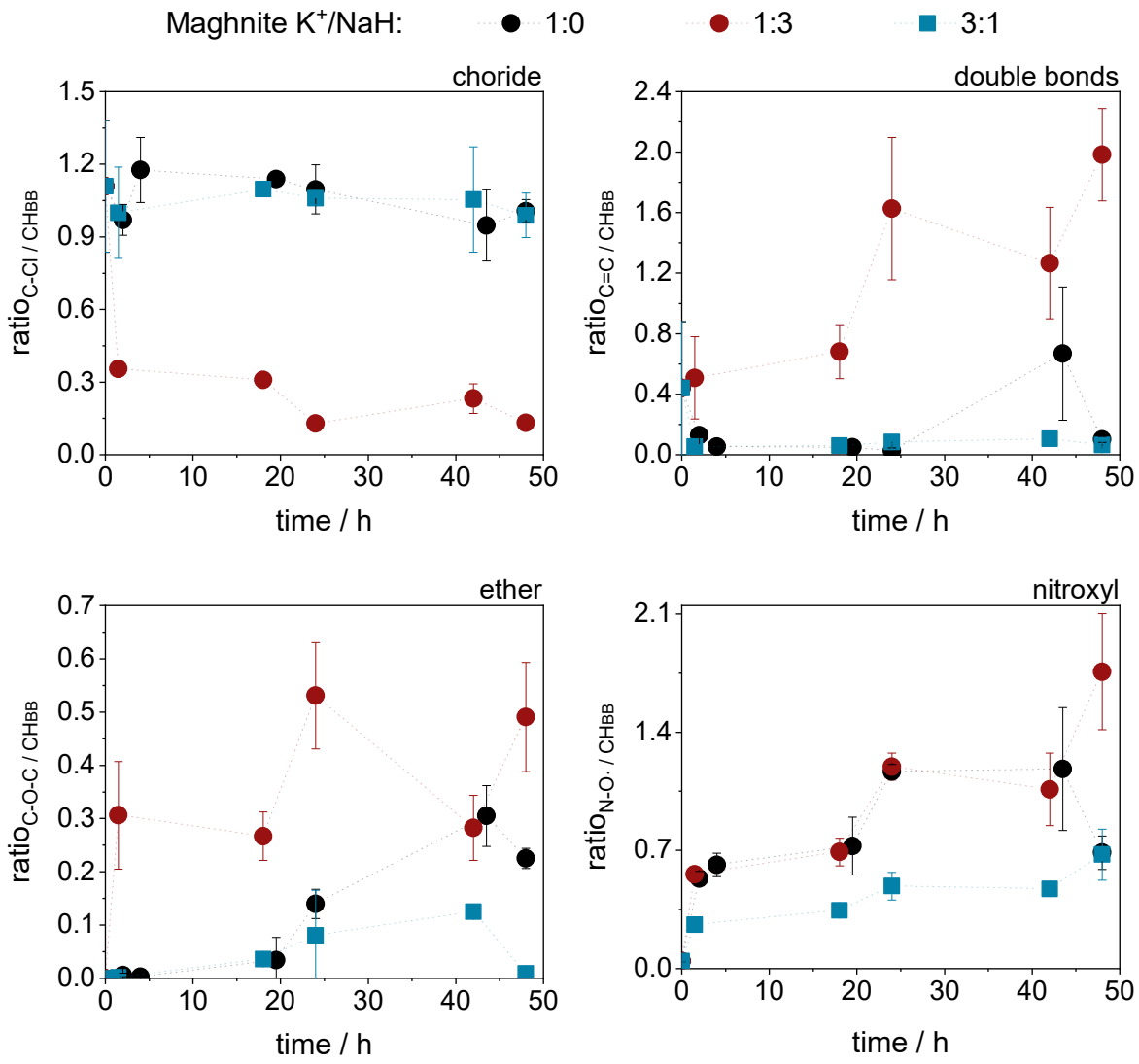

Figure 29. Ratios of chlorine band (top left), double bonds (top right), ether band (bottom left), and those of nitroxyl bond (bottom right) to the CH backbone of the reactions with DMSO/H_2O 3:1 with Maghnite K+ (black) Maghnite K+/NaH 1:3 (red) and Maghnite K+/NaH 3:1 (blue)

Etherifying PVC with TEMPOL mediated only by Maghnite K+ proceeds without dehydrochlorination. This method is less effective and the reaction is slower than using NaH as a base. Chlorine substitution remains at a low level after 48 h, the clay is not very basic and only weak nucleophiles are present to react with electrophilic center in PVC. The additional presence of NaH leads to more substitution and also more double bonds are formed, increasing with the amount of NaH used. This result indicates that the clay is not participating in the reaction. EDX mapping analysis confirms the result. With excess Maghnite K+, the chlorine content remains permanently above 10 at% while the chlorine content of NaH:Maghnite K+ 3:1

decreases after only 5 hours and is around 0 at% after 48 hours. This can be seen visually in the red color in the EDX mapping images (**Figure 30**). The surfaces in both reactions with additional NaH do not change. The layer structure of the print remains visible after 48 hours.

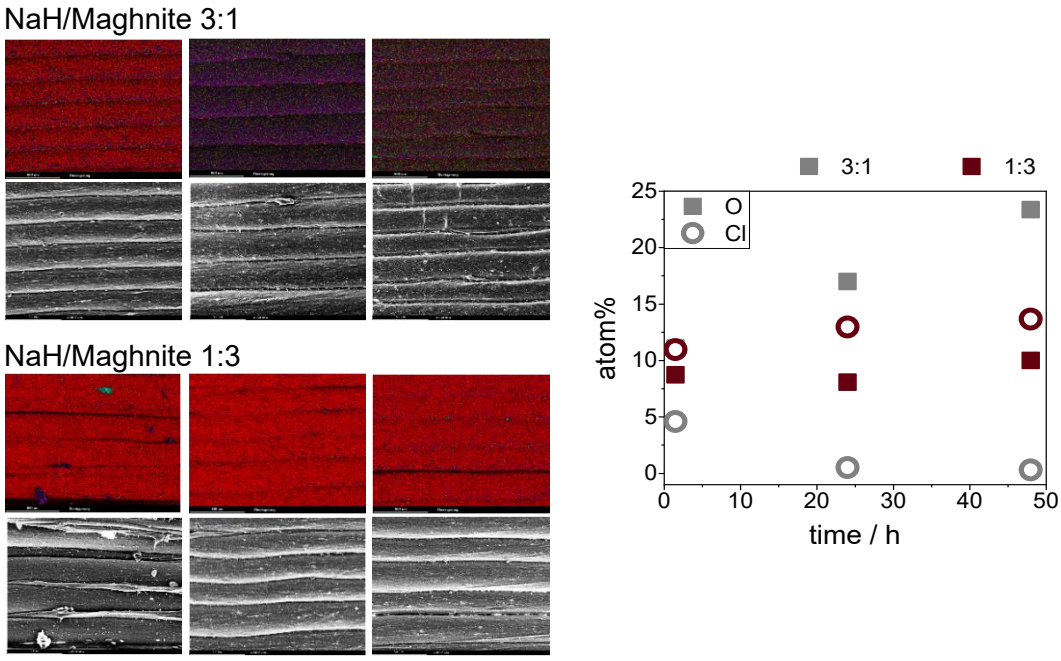

Figure 30. Left: SEM images (top) and EDX mapping images (bottom) of PVC-TEMPO in the functionalization reaction using NaH/Maghnite 3:1 (grey) and NaH/Maghnite 1:3 (red) at 5 h, 24 h and 48 h.

Activity of the PVC-TEMPO catalysts (Maghnite K+; 48h) in the oxidation of benzyl alcohol

Good conversions ranging from 70% to 81% in all initial runs were achieved, which is contrary to expectations. The hypothesis was that functionalization of catalysts using Maghnite K+/NaH 3:1 would result in poor performance since the FTIR and EDX analyses indicated only a small amount of covalently immobilized TEMPOL. This amount, along with an unbound amount of TEMPOL, appears to be sufficent for oxidizing benzyl alcohol to a adequate degree.

There was a substantial decrease in conversion in both the second and third runs of the oxidation reactions. The catalysts obtained with Maghnite K+/NaH 3:1 were found to be the most unstable, which aligns with previous findings that low levels of

functionalization lead to poor stability. The catalysts with only Maghnite K+ and Maghnite K+/NaH 1:3 are comparable in stability, although the ones with only Maghnite K+ exhibit slightly higher stability. Overall, the results confirm Belbachier's conclusions. Substituting chlorine with TEMPOL in PVC is feasible. Fewer double bonds are produced, but they are not completely inhibited.

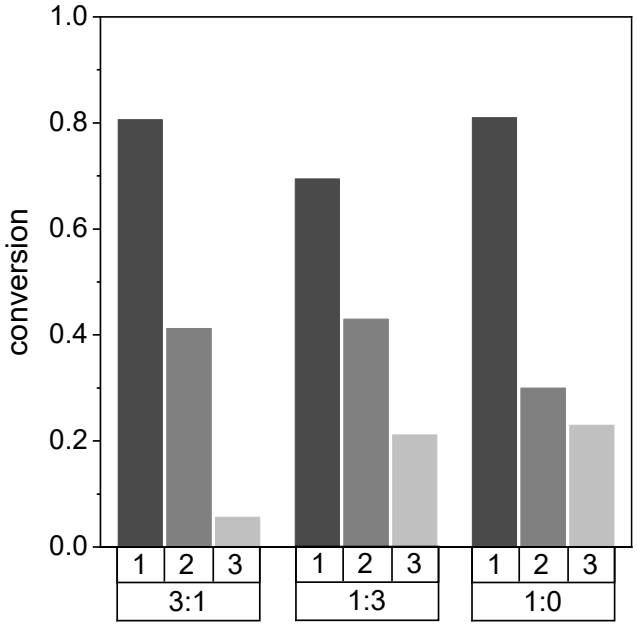

Figure 31. Conversions of the oxidation reactions of benzyl alcohol to benzaldehyde with the catalysts after 48 h from the functionalization reactions with Maghnite K+ (1:0) Maghnite K+/NaH 1:3, and 3:1. The reactions were repeated in three cycles.

5.3 PVC-TEMPO as heterogeneous catalysts in batch experiments

The immobilization of TEMPOL on PVC surfaces by a Williamson ether synthesis seems an effective procedure to reach a heterogenized catalyst system for an alcohol oxidation. The best temperature identified for functionalization is 50 °C in medium of DMSO/H_2O of 17:3 (*v*/*v*) and using NaH as base, like described above. These pellets were subsequently used to map their catalytic activity as function of the oxidation reaction conditions. The oxidation of 1.0 mmol benzyl alcohol with 1.1 mmol BAIB as oxidizer was carried out with 736 mm^3 of PVC-TEMPO catalyst. Two consecutive cycles are carried out, the pellets are washed with water and ACN after the first cycle.

5.3.1 Temperature

Oxidations carried out at 50 °C proceed to a higher extent than those at 35 °C (**Figure 32**). The conversion increases with time in all cases. Maximum conversion is not achieved after 60 min. Oxidation at room temperature is appreciably slower.

High temperatures deactivate the catalysts. No conversion occurs during the second run with the catalyst at 50 °C. Benzyl alcohol uncatalyzed oxidation by BAIB explains the 16% conversion. The most effective oxidation reaction is achieved at 35 °C.

TEMPO-mediated oxidations with NaOCl in DCM/H_2O work best at 10 °C to 15 °C.[28] PVC-TEMPO and BAIB require higher temperatures. The best temperature is 35 °C.

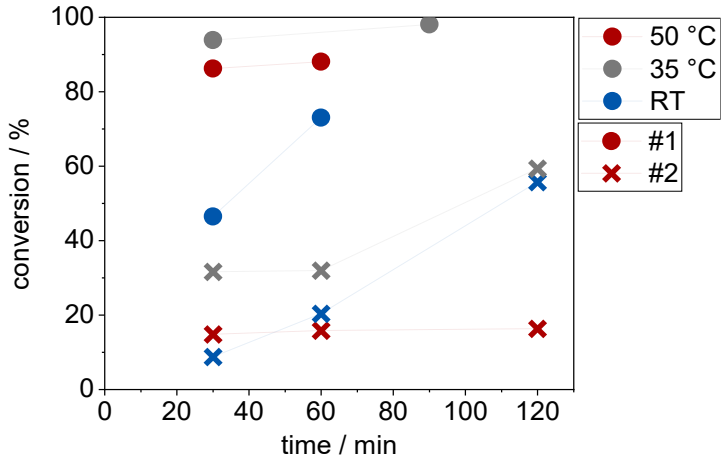

Figure 32. Obtained conversions in benzyl alcohol oxidations at 50 °C (red), 35 °C (grey) and RT (blue) in the first reaction (dots) and in the second reaction (cross).

5.3.2 TEMPO activation

The oxo-ammonium salt form of TEMPO presumably is the active species responsible for inflicting the oxidation reaction. NCS can produce it during or prior to the oxidation reaction (**Figure 33**). Thus, the pellets were treated with NCS to produce the active form. Again, two cycles were carried out at RT and at 50 °C, now using 1 mmol benzyl alcohol, 1.1 mmol BAIB and five catalyst pellets with a total surface area of 670 mm^2.

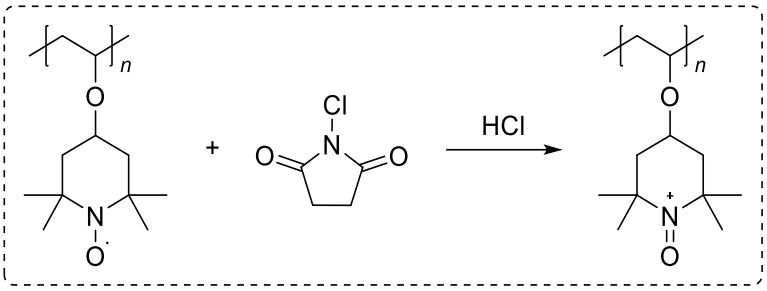

Figure 33. Activation reaction of TEMPOL with NCS and HCl.[80]

TEMPO oxidation as activation steps of the catalysis is essential at low reaction temperatures (**Figure 34**), the preformation of the oxoammonium salt yields benzaldehyde at a much higher concentration. The TEMPO oxidation by BAIB is part of the rate-determining step. Conversion increases slowly in the reaction with non-activated catalysts, reaching 48 % after 60 min. Activation makes no difference at 50 °C. Activated catalysts achieve 58 % conversion after 30 min. Non-activated catalysts achieve 62 % conversion. A complete conversion of benzyl alcohol was achieved after 60 min at 50 °C.

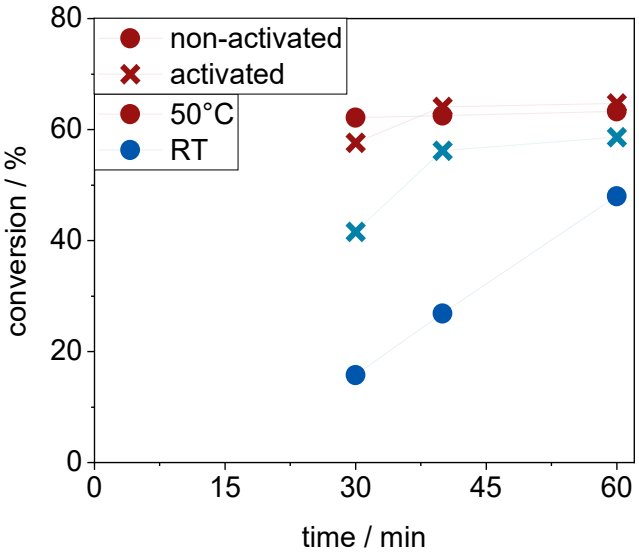

Figure 34. Conversions of benzyl alcohol n oxidation reactions with preactivated (cross) and non-activated (dots) catalyst pellets.

5.3.3 Oxidizing agents

NCS and combinations of BAIB and TBAB were screened as activation agents in detail for converting TEMPO in oxoammonium salt since these are well known in literature. Reactions were carried out in ACN.

As mentioned above, NCS can serve as oxidant in various oxidation reactions involving TEMPO (5.3.2) and is used for activating TEMPO. The TEMPO functionalized pellets were used to catalyze the oxidation of benzyl alcohol (1 mmol) and NCS for activating TEMPO in five consecutive cycles at 35 °C for 30 min. The pellets are washed with water and acetonitrile between each run.

NCS oxidizes benzyl alcohol to conversions of about 68 %, independent of the cycle number (**Figure 35**), suggesting no leaching and successful activation of TEMPOL. However, further analysis shows that 1 eq NCS without a catalyst also achieves conversions of about 67 %. The conversion increases linearly with NCS content, indicating that NCS converts the alcohol to the aldehyde without the necessity of catalyst. This result was somewhat surprising, inconsistent with existing literature.[63]

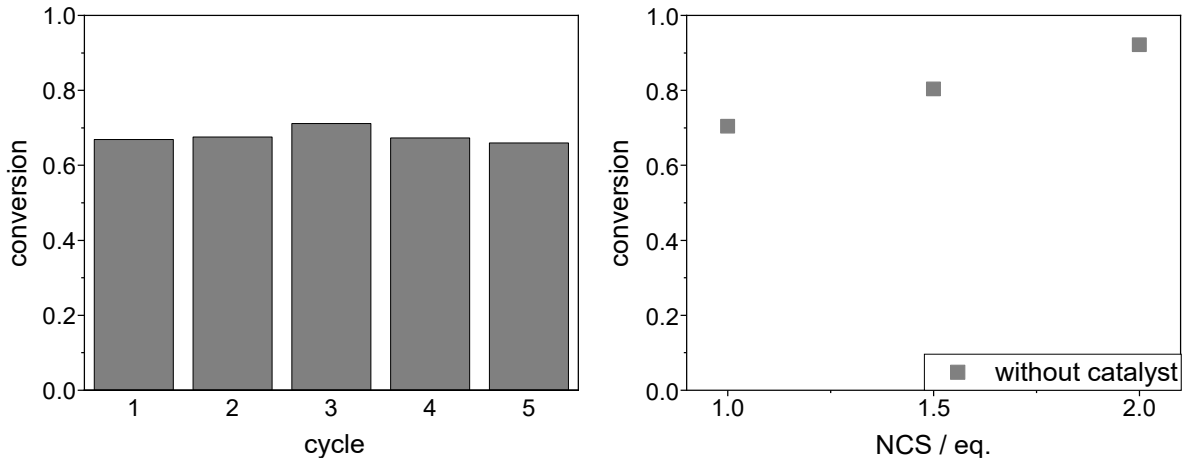

Figure 35. Conversions obtained in five consecutive benzyl alcohol oxidation cycles with 1 eq NCS and PVC-TEMPO (left) and conversions obtained in benzyl alcohol oxidations without catalyst with 1.0, 1.5, and 2.0 eq NCS (right).

5.3.3.1 BAIB

BAIB is an ACN soluble oxidator, it reacts with the reduced form of TEMPO, transforming the hydroxylamine to the radical, splitting off AcOH. AcOH induces the

formation of the oxoammonium salt by the acid-catalyzed disproportionation. The oxidation reactions seen previously are based on BAIB as a co-catalyst. For a detailed analysis of BAIB as a co-catalyst, further reactions were carried out under identical conditions as for the NCS-catalyzed oxidation reactions. As already seen, TEMPO in combination with BAIB is efficient, resulting in a high conversion of benzyl alcohol (88 % in the first cycle; **Figure 36**). Benzyl alcohol is also oxidized effectively in the second and third cycle be it at a lower rate. This is a usual feature of the pellets (vide supra).

To verify whether BAIB, like NCS, is capable of oxidizing benzyl alcohol without TEMPO catalysts, reactions with BAIB and benzyl alcohol were carried out without TEMPO catalysts. The amount of BAIB was varied from 1 to 3 equivalents relative to alcohol. Unlike NCS, BAIB without TEMPO catalysts only reaches conversions of < 20 %, thus is not capable of oxidizing benzyl alcohol by itself.

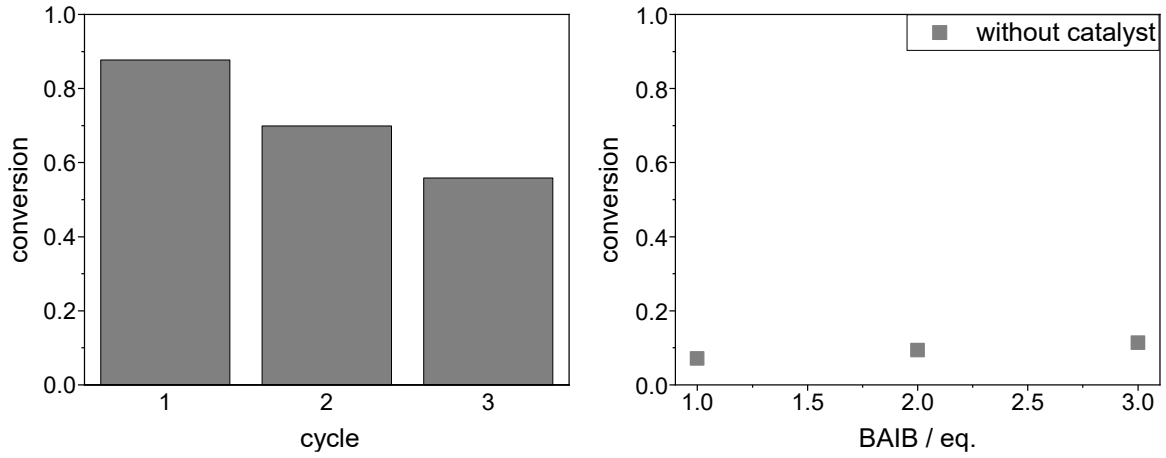

Figure 36. Conversions obtained in three consecutive benzyl alcohol oxidations with 1.1 eq BAIB (left) and conversions obtained using 1.0, 2.0 and 3.0 eq. BAIB without TEMPO catalysts (right).

5.3.3.2 BAIB/TBAB mixtures

A further set of tests was carried out using BAIB in combination with various amounts of TBAB (1 mol%, 2.5 mol% and 5 mol% with respect to benzyl alcohol. The reactions are carried out in ACN as solvent and with around 0.55 g pellets at 35 °C for 30 min. TBAB improved the effectivity of the catalytic oxidation benzyl alcohol with BAIB.

The catalytic oxidation of benzyl alcohol is enhanced by the addition of up to 2.5 *mol*% TBAB (**Figure 37**). Complete conversion is achieved in 20 min. Lower conversions are observed in the oxidation of butanol, as expected on account of the lower reactivity of alcohols.[146] Higher amounts of 5 *mol*% of TBAB accelerate oxidation reaction even more, a conversion of 68 % is reached after 20 min. Although the reaction appears to subside at that moment in time, overoxidation of the alcohols to the respective carbon acid does not occur.

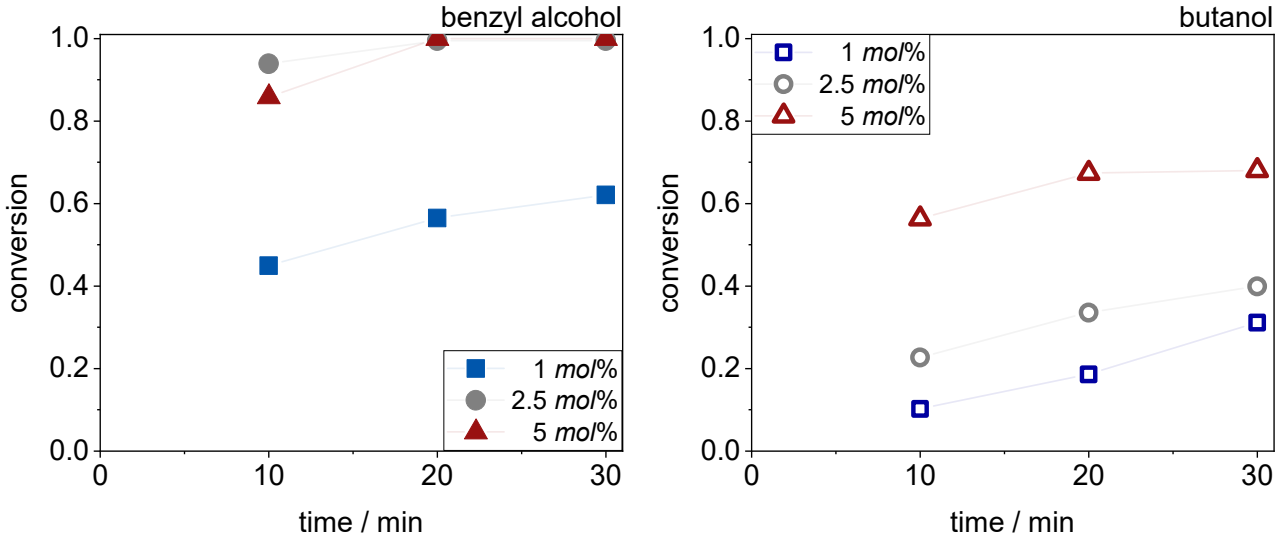

Figure 37. Conversions in oxidation of benzyl alcohol (left) and butanol (right) with BAIB/TBAB.

The mixture of BAIB/TBAB is an effective oxidizer in combination with TEMPO. The amount of 5 *mol*% TBAB was chosen in the next set of five consecutive cycles of oxidation of benzyl alcohol (t = 30 min, T = 35°C, ACN as solvent, ~ 0.55 g pellets). The catalysts are washed with H_2O and ACN after each cycle. Complete conversions are achieved in all five runs (**Figure 38**). A benzyl alcohol conversion of only 19 % is achieved with the BAIB/TBAB mixture in the absence of PVC-TEMPO catalysts. No conversion of benzyl alcohol is found using only TBAB under the given conditions.

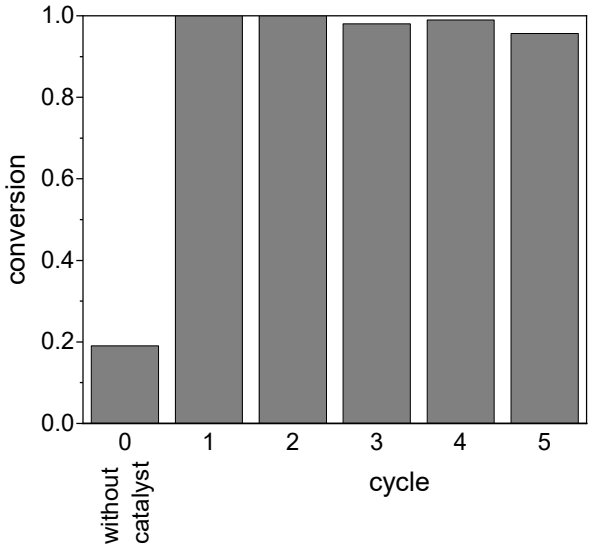

Figure 38. Conversions in five consecutive benzyl alcohol oxidations with BAIB/TBAB.

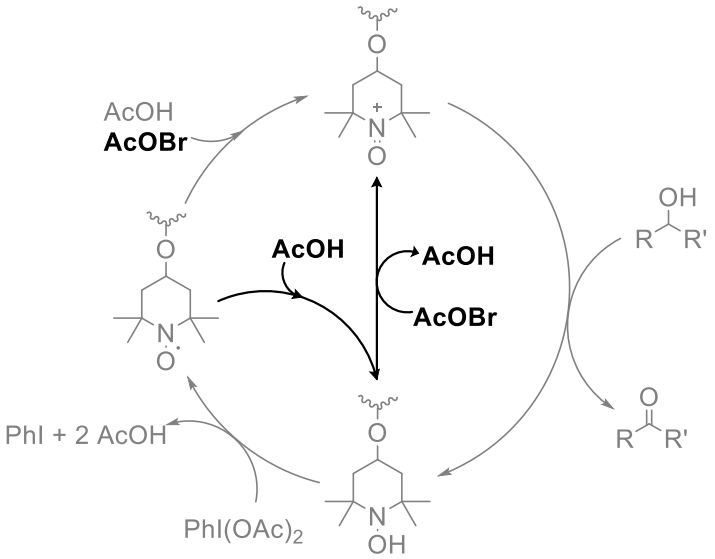

Figure 39. Pathways in the TEMPO-mediated alcohol oxidation by BAIB/bromide mixture.

The importance of the counterion of the oxo-ammonium salt was explained in section 4.1.2. Chloride is the corresponding counterion when activating the catalysts with NCS. Introducing TBAB results in the exchange of chloride ions with bromide ions. The bromide ion is an important mediator in the catalytic cyclic (**Figure 39**).[70,147] Although basicity decreases, nucleophilicity increases upon addition. Bromide is larger and has a positive influence on the electronic effects. This leads to an acceleration of the reaction. The bromide ion reacts with BAIB to give intermediate bis(acyloxy)bromate(I), which decomposes to acetyl hypobromite. Acetyl

hypobromite can regenerate the oxoammonium salt directly. The regeneration is more efficient than protonation of hydroxylamine and disproportionation.[148]

5.3.4 Solvent choice

Benzyl alcohol oxidations are performed with PVC-TEMPO, BAIB and TBAB in ACN, NMP, H_2O or DMSO. Also, an experiment in bulk benzyl alcohol was carried out. ACN is the best suited solvent for the oxidation reaction (**Table 4**). Benzyl alcohol is also suitable, a conversion of 93% is reached. The conversion is limited to the presence of 1 mmol BAIB. The use of benzyl alcohol facilitates purification of the aldehyde.

The benzyl alcohol oxidation is not progressing to a large extent in NMP, DMSO or water. PVC-TEMPO swells in NMP and DMSO. This swelling is considered unfavorable, it could potential damage a 3D printed PVC-reactor. The swelling also reduces the surface of the pellets, decreasing the accessibility of TEMPO entities. ACN does not cause swelling of PVC-TEMPO. Water is not suitable: BAIB and benzyl alcohol are not very soluble in water. No overoxidation to benzoic acid is observed.

Table 4. Conversions of benzyl alcohol of oxidation by BAIB/TBAB mediated by PVC-TEMPO pellets.

Solvent	Conversion
ACN	99%
Benzyl alcohol	93%
NMP*	32%
Water	23%
DMSO*	8%

*Structure of the catalyst pellets decomposed in the used solvent.

5.3.5 General alcohol oxidation with the catalytic pellets

The general catalytic action of the pellets (0.55 g grid-pellets) was assessed using a set of benzylic (aromatic) and aliphatic alcohols (**Table 5**). The study shows that the heterogenized TEMPO catalysts are able to oxidize various of alcohols. The usual trends in rates are followed.[146,147]

Benzylic alcohols are oxidized at the highest rate, within a time frame of 10 min, conversion is complete. The oxidation of dimethoxybenzyl alcohol is clearly slower reaction. The aromatic ring is more electron rich, which should inductively decrease the acidity of the CH_2 protons.[147] A conversion of 32 % is observed in the oxidation reaction of phenethyl alcohol. Phenethyl alcohol reacts like aliphatic alcohols.

Aliphatic and secondary alcohols exhibit low reactivity under acidic reaction conditions. The oxidation of butanol results in 68 % butanal after 30 min. The oxidation of isopropanol yields only 17 % conversion after 60 min. This conversion is only a quarter of the conversion of propanol in double of the time.

Table 5. Conversions of different alcohols with BAIB/TBAB mixtures using PVC-TEMPO pellets.

Alcohol	Product	Time	Conversion
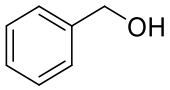	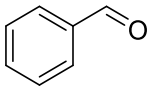	10	100 %
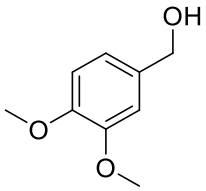	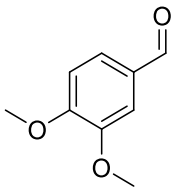	90	85 %
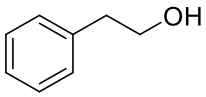	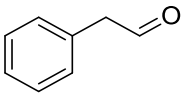	135	32 %
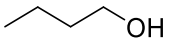	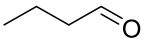	30	68 %
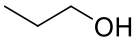	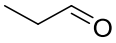	30	47 %
		60	17 %
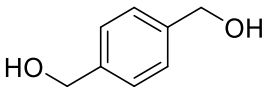	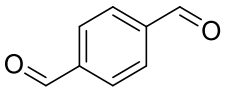	30	91 % 2 %
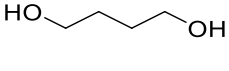	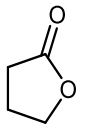 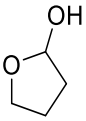 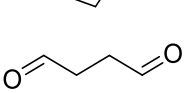	30	19 % 39 % 4 %

Conditions: 1 mmol alcohol, 5 *mol*% TBAB (based on alcohol) and 1 mmol BAIB in 4 mL ACN at $T = 35°C$.

Dialdehydes can be obtained with 5 *mol*% TBAB in this process. 91 % of dialdehyde and only 2 % of monoaldehyde are formed after 30 min in the oxidation of 1,4-benzene

dimethanol. The presence of less TBAB results in a slower oxidation and the intermediate monoaldehyde is easily detected (section 6.8.7).

The oxidation of BDO proceeds along a tautomerization of the intermediate 4-hydroxybutanal (**Figure 40**). A furan species is predominantly formed after 30 min. The equilibrium favors the formation of tetrahydrofuran-2-ol. Only 4 % of the dialdehyde is produced. The secondary alcohol formed by the tautomerization of 4-hydroxybutanal is further oxidized. The total conversion of BDO was 62 %, the conversion to the lactone species reaches 19 %.

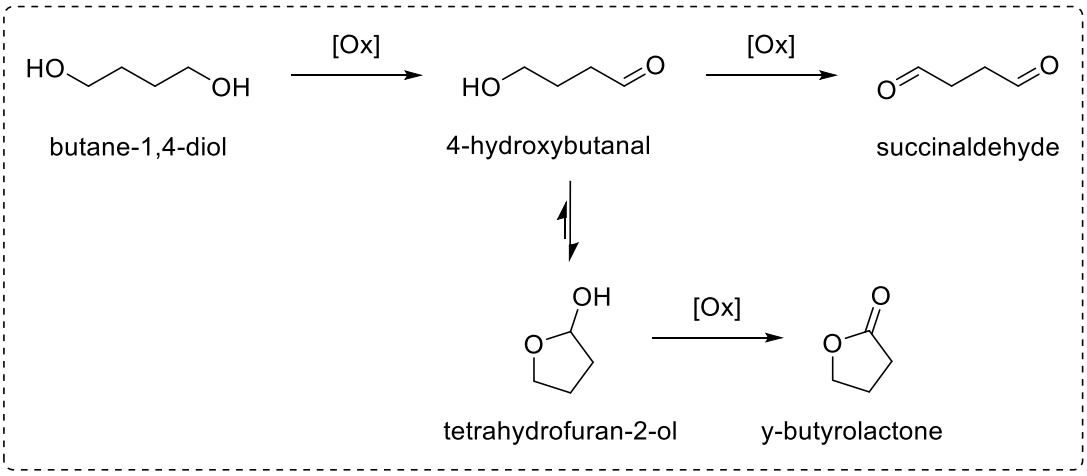

Figure 40. Steps in the oxidation reaction of BDO.

5.4 Oxidation reactions in 3D printed reactors

5.4.1 Fixed bed reactor with PVC-click-TEMPO

A column measuring 10.3 cm in length and 2.5 cm in width is utilized for the use of PVC-click-TEMPO catalysts in continuous flow (**Figure 41**). The column is filled with 27 catalyst pellets, which are prepared by CuAAC. A syringe pump is employed with flow rate of 1.5 mL·min^{-1} or 1.95 mL·min^{-1}, respectively, for a residence time of 30 min and 20 min.

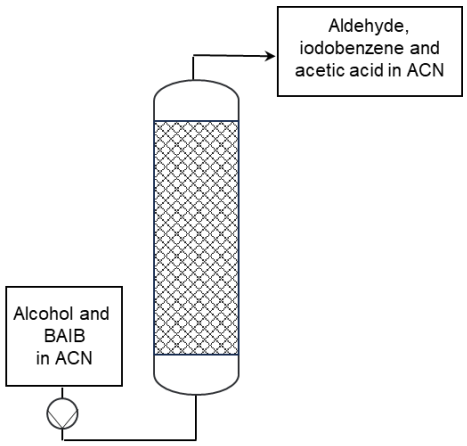

Figure 41. Continuous process with a packed bed reactor using PVC-click-TEMPO catalysts.

The catalyst pellets have a width of 1 cm, a length of 1.2 cm and a wall thickness of 1.0 mm. The total surface area of the pellets is 1.3 cm^2 and their total mass is 12.5 g. A TEMPO loading of 2 mmol·g^{-1} results in a total amount of catalyst of approximately 25 mmol. BAIB is used as the co-oxidizing agent for TEMPOL. The ratio of benzyl alcohol to BAIB was 1.00:1.04. TBAB was not used in this series of experiments, as it predated the corresponding batch studies; the earlier presentation of the results is apparent from the chapter structure. Samples are taken to allow a monitoring of the process.

The PVC-click-TEMPO catalysts demonstrate insufficient activity to achieve complete conversions in the continuous set-up. A decrease in conversion is observed with each reduced residence time. A steady state is not attained. The residence time has more or less no influence on the activity: a maximum conversion of 48 % (20 min) and 43 %

(30 min; **Figure 42**) was obtained. The maximum conversions are attained just after the second reduced residence time and decline from there onwards. This behavior is related to leaching of the TEMPO entities from the pellets, like was already mentioned and which is validated here.

The catalysts show a weight reduction of 25% and visibly altering. EDX measurements show an increase in chlorine content and confirm catalyst leaching from the surface (**Figure 43**,**Table 6**). The shape of the pellets remained the same before and after catalysis, despite the loss in weight.

PVC-click-TEMPO is unsuitable for use in 3D printed reactors because of low conversions and poor stability.

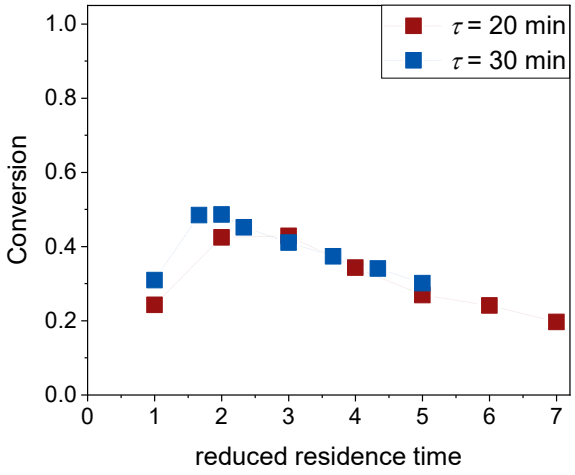

Figure 42. Conversions of benzyl alcohol to benzaldehyde versus reduced residence time in continuous oxidation with PVC-click-TEMPO as catalysts at a residence time of 20 min (red) and 30 min (blue).

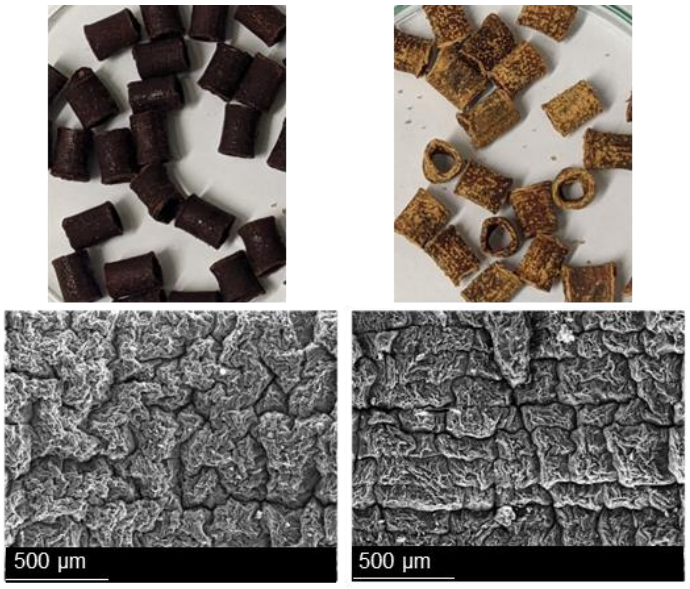

Figure 43. Images (visual/EDX) of pellets before reaction (left) and after catalysis (right)

Table 6. Atomic fractions by EDX mapping of catalytic PVC-click-pellets.

sample*	C%	Cl%	O%	N%
virgin	49	20	7	3
20 min	52	24	6	2
30 min	51	24	6	3

*: min refer to the hydrodynamic residence time, use of 1.5 h

5.4.2 Fixed bed reactor with PVC-TEMPO

PVC-TEMPO catalyst pellets prepared via the Williamson ether synthesis, were tested in continuous oxidation using three types of geometries (**Table 7**). The column mentioned in Section 5.4.1 was packed with pellets to a comparable height. The total surface area was calculated by multiplying the surface area of one catalyst pellet with the number of pellets in the tube. The oxidation of benzyl alcohol by PVC-TEMPO/BAIB served as test reaction. The conversion of benzyl alcohol was similar for all reactor configurations and decreased after some residence times (**Figure 44**).

Table 7. Catalyst geometries and process conditions for benzyl alcohol oxidation.

Parameter	small	grid	large
Geometry			
Total surface area / cm^2	537	567	245
Free volume / mL	29.5	31.5	39.5
Flow rate / $\mu L \cdot min^{-1}$	984	700	867
Temperature / °C	50	35	35
Residence time / min	30	45	45

The first oxidation reaction used small catalyst pellets with an active surface area of 537 cm^2, a reaction temperature of 50 °C, and a residence time of 30 min. Conversion initially increased, similar to PVC-click-TEMPO catalysts. Steady state was achieved up to the third residence time with a maximum conversion of 63 %, indicating higher reactivity of PVC-TEMPO catalysts with minimized steric hindrance compared to PVC-click-TEMPO catalysts. Conversion then decreased to 31 % after the third residence time. This decline likely resulted from TEMPO leaching. As described above, excessive temperature could be the cause of this.

The reaction temperature using large and grid pellets was reduced to 35 °C to enhance stability, based on the results obtained from batch trials. The residence time was increased to 45 min to maintain high conversion. The active surface area of the grid pellets was slightly enlarged, measuring 567 cm^2. The reaction with grid pellets was carried out twice, using newly functionalized pellets in both cases. The curve followed the trend of small pellets, with slightly higher conversion because of longer reaction times. A longer steady state from the second to the fourth residence time was achieved, after which conversion decreased again.

The large pellets had a reduced surface area of 245 cm^2. Conversion curves as a function of time matched those of the other two reactions up to the third residence

time. After this point, conversion sharply dropped to 18 % at six residence times. The sharp drop in conversion compared to grid pellets could imply that catalyst leaching is reliant on the catalyst's active surface area. Insufficient catalyst at the beginning of the reaction enhances leaching, causing a more pronounced decrease in conversion.

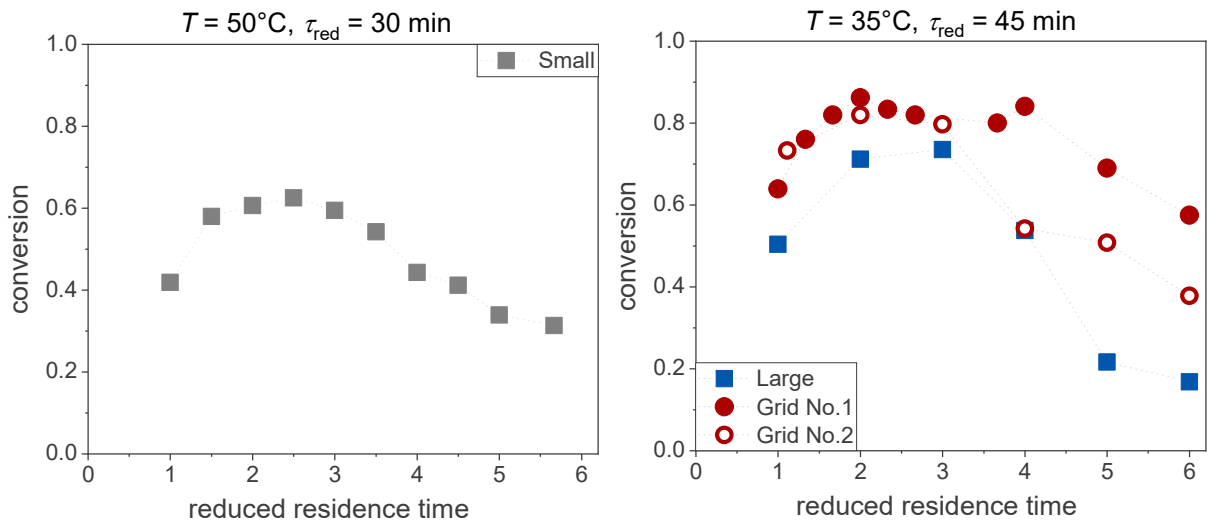

Figure 44. Benzyl alcohol conversion in continuous oxidation by BAIB with small pellets at 50 °C and τ of 30 min (left) and with grid pellets (red) and large pellets (blue) at 35 °C and τ of 45 min (right).

5.4.3 Printed catalytic reactor

The final development is the making of a PVC-based catalytic reactor by 3D printing and functionalization. A first reactor is 16.6 cm long and 2 cm wide. Its reaction chamber is 15 cm long and 1.5 cm wide. SMX mixers of 4 mm width are added to increase surface area (**Figure 45**). The total surface area dedicated to functionalization is 180 cm^2. The free volume (15 mL) was measured by means of water. The 3D-printed reactor exhibits high print quality with no signs of warping, stringing, or other printing artifacts.

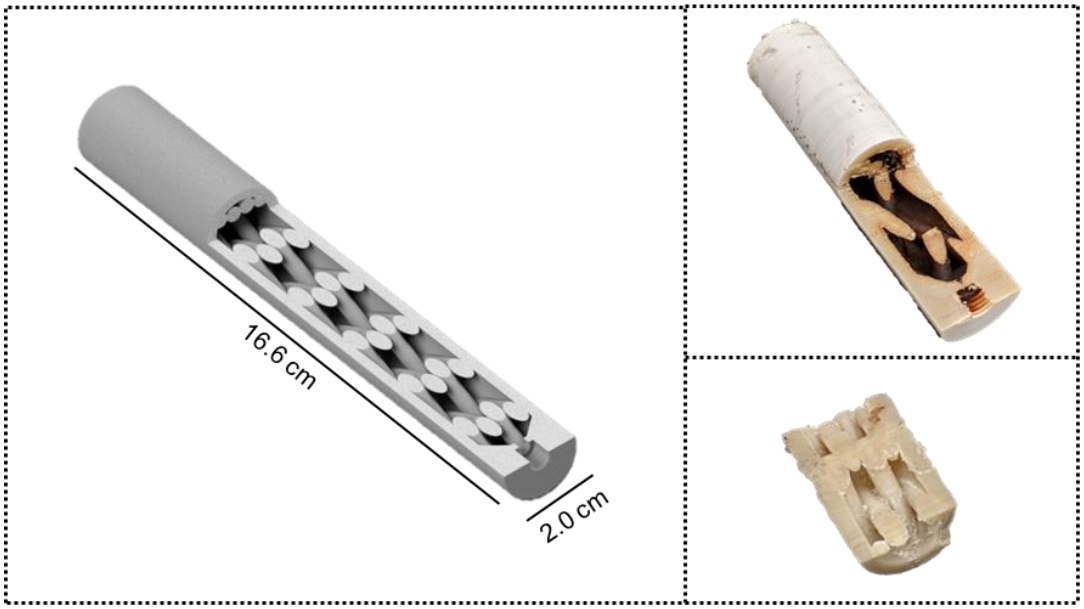

Figure 45. CAD design of the round, small reactor (left) and reactors pieces before (right, bottom) and after functionalization with TEMPOL and oxidation catalysis (right, top).

The inner surface of the reactor is functionalized with TEMPOL by the Williamson ether synthesis procedure with NaH as base and in DMSO/H_2O 17:3 (*v*/*v*) as solvent. The temperature is set to 65 °C. The functionalization was carried out by pumping the mixture of reagents through the reactor in a loop using a peristaltic pump. The surface is uniformly functionalized as taken from the color change. After functionalization, the surface has a brown color that slightly extends into the underlying printing layers. This is indicated by an orange/brown coloration.

It was also found, that the round reactor tends to leak, in beginning and end of each print layer, which align at one certain positions. This weakness obviously results from the printing process. Attempts to reprogram the printer to position the start and end of each layer differently are unsuccessful.

The second reactor was designed in form of a square reactor with a round core (**Figure 46**). This design places the "seam" in a corner. The corner placement prevents reactor leakage. SMX mixers are also redesigned. The diameters are decreased to 1.8 mm each. This enables expansion of the surface area. The overall length and diameter remain unaltered. The total surface area encompasses 283 cm^2, the free volume is 12 mL.

Printing small structures with high accuracy appears challenging. Unwanted thin fibers form inside the reactor as a result. These could be removed by flushing the inside of the reactor with DCM.

The surface was functionalized with TEMPOL like described for the first reactor. Again the surface appears brown, the coloration of the initial layers is less, possibly the treatment with DMC has led to a tighter bonding between the layers.

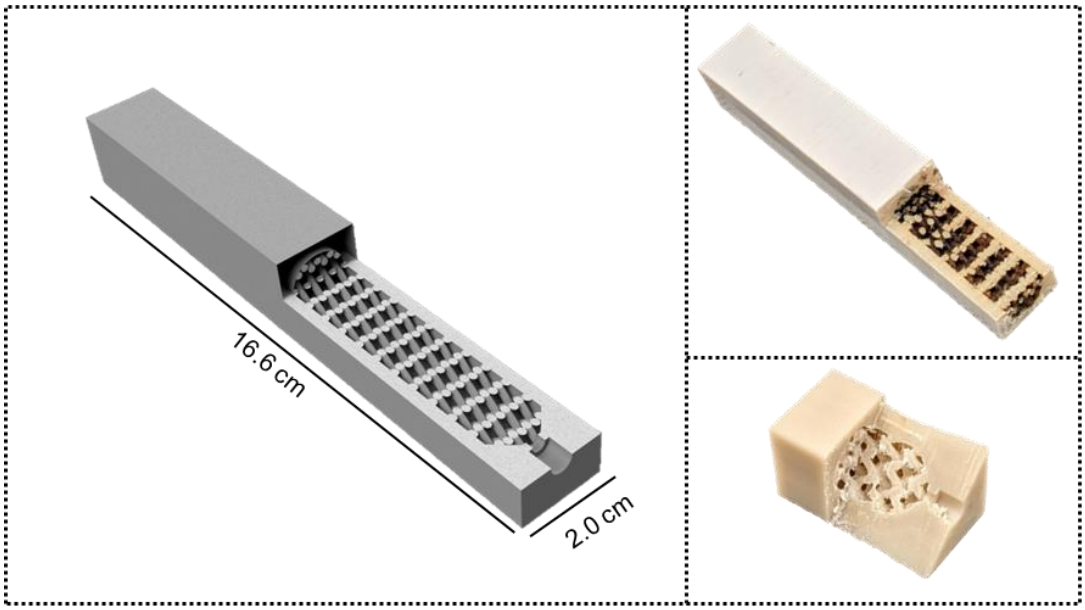

Figure 46. CAD design of the square reactor (left) and reactors pieces before (right, bottom) and after functionalization with TEMPOL and oxidation catalysis (right, top).

The continuous oxidation of benzyl alcohol by TEMPO/BAIB was carried out in the round and the square "catalytic"reactors. Three reactors are connected in series (**Figure 47**). BAIB and benzyl alcohol dissolved in acetonitrile and the mixture is held in a storage vessel. The flow velocity is 1.5 mL/min for round reactors and 1.2 mL/min for square reactors to achieve a residence time of 30 min in both cases.

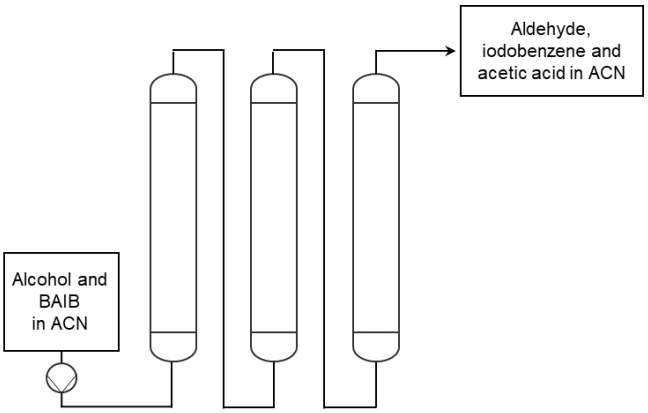

Figure 47. Schematic illustration of continuous process with three functionalized 3D printed reactors using BAIB as co-catalyst.

The benzyl alcohol conversion attains a maximum of approximately 60 %. Round reactors show a better stability at maximum conversion. The conversion decreases significantly after the maximum and reached about 5 %. (**Figure 48**).

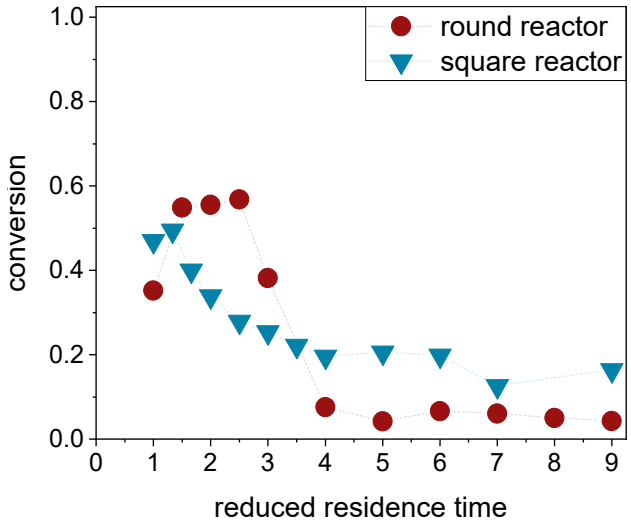

Figure 48. Conversions of benzyl alcohol in continuous oxidation with BAIB in three consecutive round (surface area of 540 cm^2) and square reactors (surface area of 846 cm^2).

It is noted that the printed reactors are catalytically less effective, although they have a larger active surface area. Also, the decrease of conversion with time of operation is more pronounced in the printed reactors.

Next, the benzyl alcohol oxidation was attempted with the combination of TBAB and BAIB, which gave good conversions over a longer time in batch reactions. The mixture of benzyl alcohol, TBAB and BAIB tend to gel at 35 °C. The set-up had to be changed

(**Figure 49**). The square reactors were applied, two in series. Now BAIB is dissolved in ACN at a concentration of 0.26 mol·L^{-1} and held in a separate storage vessel at 35 °C. Benzyl alcohol (188 mmol) and TBAB (5 mol% based on alcohol) are mixed in 9.22 ml ACN and provided in another storage vessel. No oxidation takes place in the storage vessel. A total residence time of 28 min is set by the lower limit of the pumps. Volume flow rate of BAIB solution is at 1.25 mL·min^{-1} and that of alcohol/TBAB solution is 50 μL·min^{-1}.

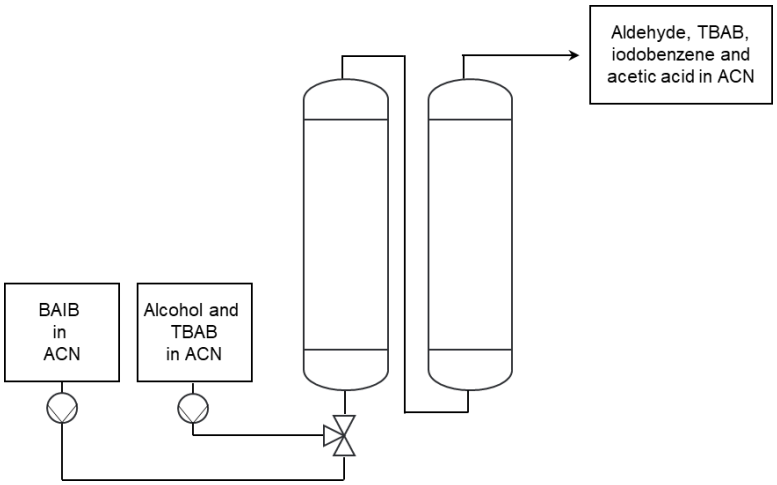

Figure 49. Continuous catalytic oxidation of benzyl alcohol by BAIB/TBAB mixture mediated in two consecutive catalytic 3D printed reactors.

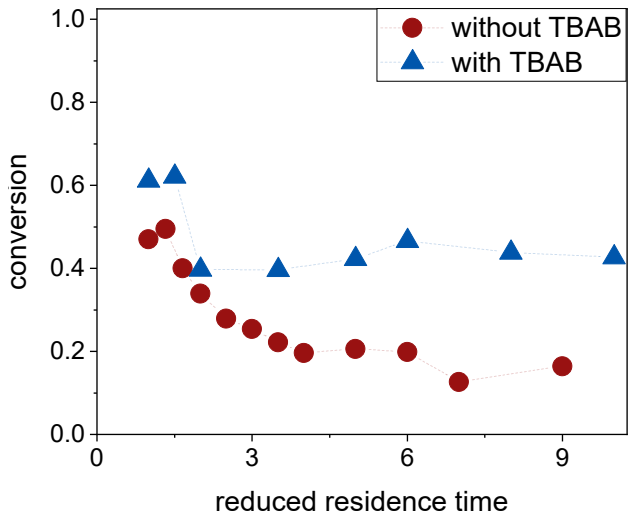

Figure 50. Calculated conversions of benzyl alcohol to benzaldehyde versus reduced residence time in continuous oxidation reactions in three 3D printed reactors with TBAB (blue) and without TBAB (red).

As expected from the experience in batch experiments with TBAB/BAIB, the mixture inflicts a higher rate of benzyl alcohol oxidation (**Figure 50**). The conversion is also stable at a level of just over 40 % for over ten reduced residence times. The conversions are higher after the 6th residence time than in fixed-bed reactors.

The conversion of benzyl alcohol in the configuration of **Figure 49** is apt for improvement. A further reactor was designed, printed and functionalized. The length remains the same. The diameter is increased to 3.5 cm (**Figure 51**), the free volume is 43.5 mL (measured with water). This increase results in a surface area of about 940 cm^2, an increase of surface per reactor of 200%. This larger reactor type replaced the ones in Figure 46. A reactant flow of 2.9 mL·min^{-1} is set to achieve a residence time of 30 min. Volume flow of BAIB mixture is 2.8 mL·L^{-1} and volume flow of alcohol mixture is 112 µL·min^{-1}. Steady state conditions were achieved after three residence times. Conversion of nearly 100 % was obtained. The conversion did not decrease after a long reaction time. The time of activation reaction was shorter.

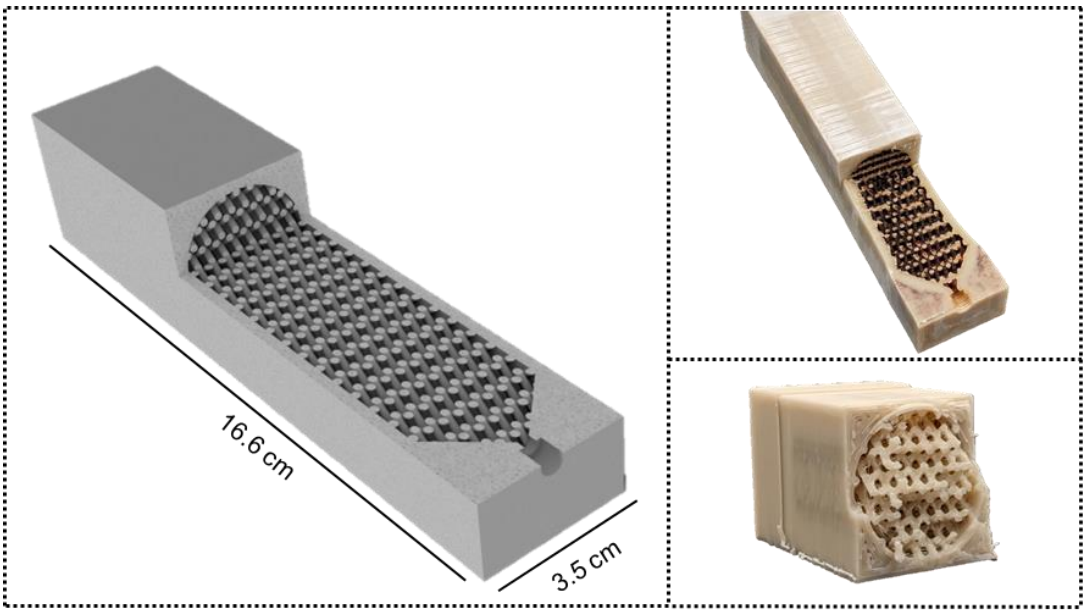

Figure 51. CAD design of the square, tall reactor (left) and reactors pieces before (right, bottom) and after functionalization with TEMPOL and oxidation catalysis (right, top).

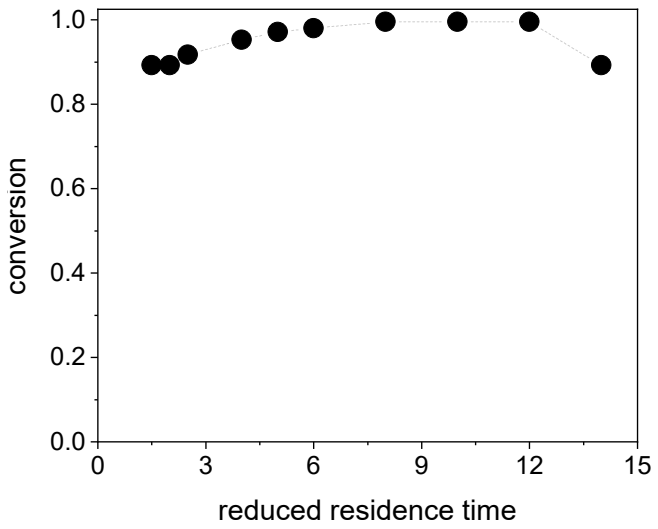

Figure 52. Conversions of benzyl alcohol oxidation with BAIB/TBAB mixtures in two 3D printed square reactors with a volume of 43 mL.

5.4.3.1 Long-term stability

The storage stability of the functionalized reactors was addressed in the next phase of the investigation. Two reactors are functionalized, and continuous oxidation of benzyl alcohol with the BAIB/TBAB mixture are carried out. A first run is carried out three days after functionalization. The reactors are intermediately stored in an exicator with silica orange gel. A second run was carried out after one week and a third one after 12 weeks in the same reactors. They are washed with acetonitrile and water following the catalysis.

The catalytic properties of the reactors after storage of three days or after one week after the functionalization are more or less unchanged (**Figure 53**). The benzyl alcohol conversion after three days reaches 100 % at the 6th residence time. The second run, conducted after one week, does not show a loss in catalyst activity. The initial conversion of benzyl alcohol in the 3rd run and after 12 weeks is at the final level of the 2nd run. Conversion decreases further in the course, down to 62 % after the 13th residence time. Storage of the reactors seems to not change the catalytic properties. It is however, clear that the some wearing takes place, becoming obvious in the configuration after a total of about 20 residence times.

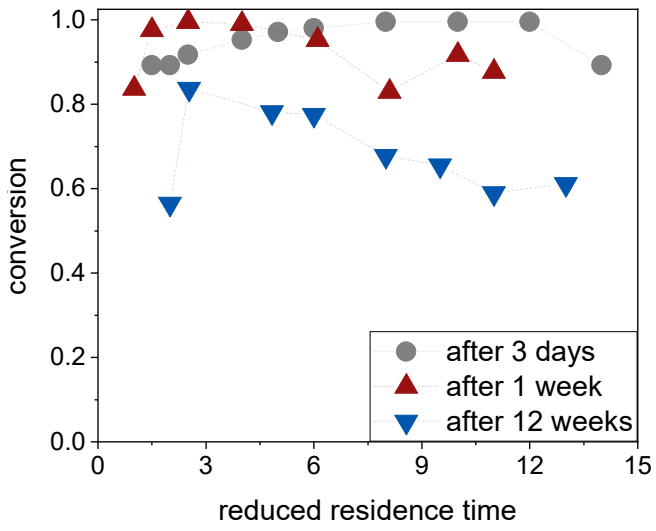

Figure 53. Conversions of benzyl alcohol oxidation by BAIB/TBAB in two 3D printed reactors (square, tall reactor (**Figure 51**)), stored under dry conditions

5.4.3.2 Residence times

The full conversion of benzyl alcohol in the last type of reactors, operated at a residence time of 30 min gives little information on the effectiveness of the reactors. A continuous oxidation reaction of benzyl alcohol is therefore carried out with a reduced residence time of 15 min (volume flow of 5.82 mL·min^{-1}). The conversion decreases with shorter residence times to 87 % (**Figure 54**). The conversion of benzyl alcohol reaches a constant level after three residence times. Some catalyst deactivation occurs over time, which is noticeable in the operation with a residence time of 15 min after 5 h, and for one of 30 minutes after 6 h.

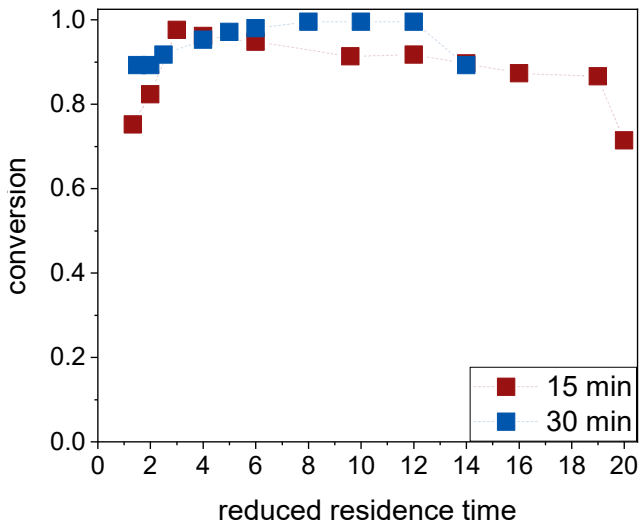

Figure 54. Conversions of benzyl alcohol oxidation by BAIB/TBAB in two 3D printed reactors (square, tall reactor (**Figure 51**)) with different residence times

5.4.3.3 Oxidation of different alcohols

Benzyl alcohol is used in many publications for assessing the feasibility of an oxidation set up. Benzyl alcohol is easily oxidized under the used reaction conditions here too. Further continuous oxidations are performed with butanol and butanediol as substrates, still using the BAIB/TBAB mixture and 35 °C as reaction temperature. Reactions are carried out with a residence time of 30 min.

High conversions of between 91 % and 100 % are achieved, like for benzyl alcohol (**Figure 55**). No decrease in conversion is observed during the entire reaction time. Overoxidation does not occur. Tautomerization takes place when oxidizing BDO, similar to batch reactions. Higher conversion rates of BDO to succinyl aldehyde are observed. Compared to the batch reaction, more of the lactone species than the furan species was formed in the continuous reactions (**Figure 56**). This could be because more catalyst for the oxidation reaction was available in the printed reactor.

Furan species are mainly formed at the beginning of the reaction. The furan is then converted into lactone species. A constant ratio between both species is reached after the 4th reduced residence time. The conversion to the lactone species is 70 %.

This result opens new potential fields of applications. γ-butyrolactone is produced industrially at temperatures between 180 °C and 300 °C using copper as a catalyst.[149] This alternative offered here allows for more efficient production of lactones.

Dialdehydes, which can tautomerize in the intermediate stage, cannot be produced efficiently under these reaction conditions. The intermediate 4-hydroxybutanal is more reactive than the furan species (**Figure 40**). 11 % of the dialdehyde is obtained.

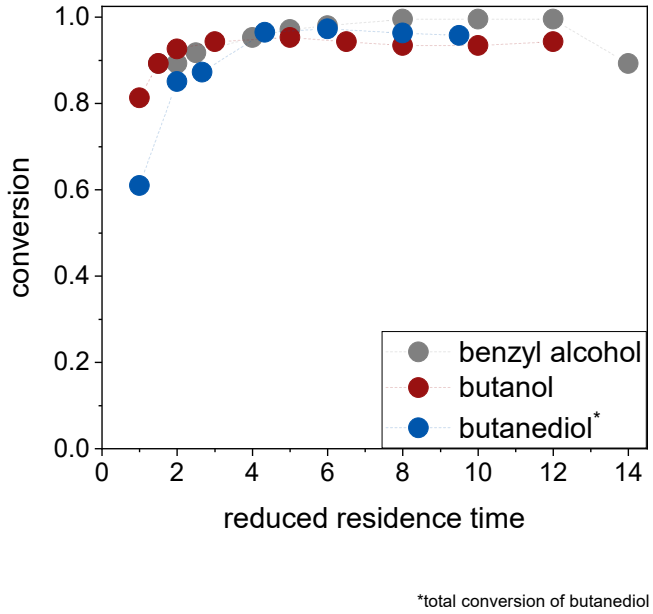

Figure 55. Conversions benzyl alcohol (grey), butanol (red) and butanediol (blue) in two 3D printed (square, tall reactor (**Figure 51**)) reactors.

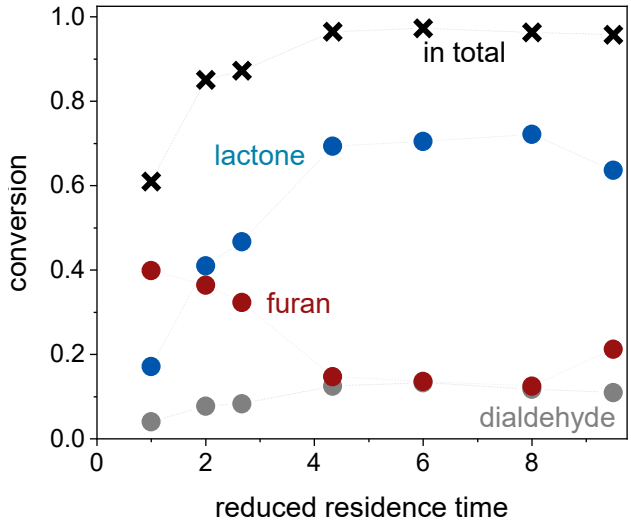

Figure 56. Conversion of butane diol in total (black, crosses), to lactone (blue, dots), to dialdehyde (grey, dots) and to furan species (red, dots).

6. Experimental Part

6.1 Materials

The materials were used as received. 1,4-Benzenedimethanol (TCI, > 99 % purity), Benzyl alcohol (Roth, ≥ 98 % purity), (Diacetoxyiodo)benzol (TCI, > 97 % purity), Butanol (Burdick & Jackson™, 99.8 % purity), copper(I)iodid (Roth, > 98 % purity), 3,4-Dimethoxybenzyl alcohol (Acros Organics, 96 % purity), Dimethylsulfoxide (Fisher scientific, 99.7 % purity), DMSO-d6 (Deutero, 99.8 % purity), N,N-Diisopropylethylamine (Iris Biotech, 100 % purity), Montmorillonite (Aldrich, 100 % purity), N-Methyl-2-pyrrolidone (VWR, > 99.5 % purity), Phenethyl alcohol (Acros Organics, 98 % purity), Propan-2-ol (VWR, 99.7 % purity), Propanol-1-ol (Merck, ≥ 99.5 % purity), Propargyl bromide (Alfa Aesar, 80 % in toluene), Silver oxide (Fluorochem, 99 % purity), Sodium azide (Sigma Aldrich, ≥ 99.5 % purity), Sodium hydride (TCI, 60 % dispersion in Paraffin Liquid), TEMPOL (Evonik, 98 % purity), Tetrabutylammoniumbromid (Sigma Aldrich, ≥ 99.0 % purity), Toluene (Acros Organics, 99.8 % purity)

6.2 Analytics

6.2.1 1H NMR

Oxidation transformations were determined from 1H NMR spectra. The spectra were recorded with a Bruker Avance Ultrashield-400 spectrometer in DMSO-d6 at RT and analyzed using Mestrenova x64. The solvent signal of the reaction solution was suppressed.

6.2.2 FTIR

FTIR spectra were measured on a Thermo Scientific Nicolet iS10 FT-IR spectrometer from 400-4000 cm^{-1} and a resolution of 0.5 cm^{-1}.

6.2.3 Elemental analysis

Elemental analysis of CHNO was performed on a EuroEA Elemental Analyzer with HEKAtech HT oxygen analyzer from EuroVector/Hekatech.

6.2.4 EDX Mapping

For the investigation by EDX mapping, a slice of the catalyst pellets was cut and coated with carbon using the LEICA EM ACE600 sputter coater. Microscopy was conducted with the LEO 1525 scanning electron microscope, with measurements taken for a duration of 328 s at a resolution of 138 eV and a take-off angle of 7.87 °. The software SmartSEM V06.00 was utilized to analyze SEM images and TEAM was used for the EDX measurements.

6.2.5 DSC measurements

DSC measurements utilized a Mettler-Toledo DSC 1 differential calorimeter to determine glass transition of PVC. Initially, the samples were heated to 220 °C at a heating rate of 10 °C/min and maintained at that temperature for 2 min. Subsequently, the samples were cooled to – 20 °C at a rate of 20 °C/min and kept at this temperature for another 2 min. Finally, the samples were reheated at a rate of 10 °C/min to 220 °C and held for 2 minutes. The results indicated that PVC had a glass transition temperature of 78 °C (**Figure 57**).

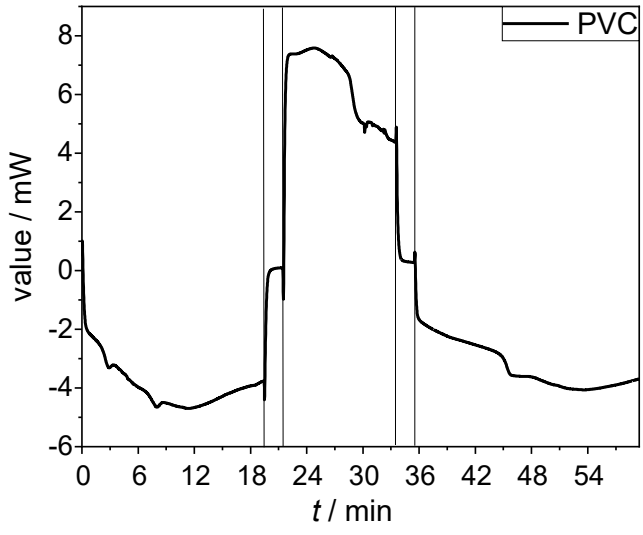

Figure 57. DSC thermogram of PVC.

6.3 Propargyl-TEMPO

In a 250 mL Schlenk flask, 0.84 g (21.0 mmol, 1.2 eq) NaH (60 % in mineral oil) was added. Work was carried out under nitrogen atmosphere. With stirring, 100 mL of dry DMF was added. The suspension was cooled to 0 °C in an ice bath. 3.03 g (17.6 mmol, 1 eq) of TEMPOL was added in portions. The ice bath was removed, and the solution was stirred at RT, during which gas formation occurred. After gas formation ceased (after about 1 h), the reaction mixture was again cooled to 0 °C. Using a dropping funnel, 2.2 mL (19.8 mmol, 1.1 eq) of propargyl bromide was added. The ice bath was removed, and the solution was stirred for 24 h at RT. Subsequently, 100 mL of demineralized water was added for quenching.

For purification, reaction solution was extracted with ethyl acetate was extracted (5x 50 mL), and the combined organic phases were washed with brine and dried over magnesium sulfate. The solvent was removed under reduced pressure. 2.52 g of an orange oil was obtained, which was purified by column filtration (10 % ethyl acetate in hexane). Yield was 45 %.

LRMS (ESI, MH^+): calculated for $C_{12}H_{22}NO_2$: m/z = 212.16451, found: m/z = 212.1649; FTIR: υ [cm^{-1}] = 3230 (≡C-H valence), 2112 (C≡C valence), 1082 (C-O-C valence)

6.4 PVC-N_3

In a 500 mL single-neck flask, 36.23 g (0.56 mol, 2 eq) sodium azide was placed and dissolved in 223 mL solvent (H_2O/DMSO 1:9 *v*/*v*). Subsequently, 17.41 g (0.28 mol, 1 eq) PVC was added. The solution was heated to 65 °C and stirred for 3 d. The PVC-N_3 pellets were filtered and washed with water (5 x 100 mL) to remove all residues. The pellets were stirred in 200 mL H_2O for 30 min and then dried at 40 °C in vacuo. 22.18 g of the PVC-N_3 pellets were obtained.

For the calculation of the azide loading, the pellets were crushed and analyzed by EA. This resulted in an azide loading X_{azide} was calculated by the ratio of nitrogen content

of EA %N to the number of nitrogen atoms in PVC (N(N) = 3) and the molar mass of nitrogen M(N):[80]

$$X_{\text{azide}} = \frac{\%\text{N}}{N(\text{N})M(\text{N})} \tag{1}$$

6.5 PVC-click-TEMPO

For click reaction, 22.18 g (42.36 mmol, with an azide loading of 1.91 mmol·g^{-1}) of PVC-N_3 was suspended in 132.1 mL of solvent (DMSO/H_2O 17:3 *v*/*v*). Then, 13.99 g (66.54 mmol, 1.6 eq.) propargyl-TEMPO, 1.41 g (7.39 mmol, 10 *mol*% based on propargyl-TEMPO) CuI, and 1.22 mL (7.00 mmol, 10 *mol*% based on propargyl-TEMPO) DIPEA were added. The solution was heated to 65 °C and stirred for 24 h. The pellets were filtered and washed 2x with 50 mL each of H_2O and ACN and vacuum dried at 40 °C.

For calculation of TEMPO loading, the pellets were crushed and measured by EA. Unreacted azide groups must be included in the calculation. The nitrogen content originating from the TEMPO molecules $\%N_{TEMPO}$ is calculated from the ratio of the CHN content of the azide to the CHN content from the EA analysis multiplied by the nitrogen content from the EA $\%N_{EA}$:

$$\%\text{N}_{\text{TEMPO}} = \frac{\%\text{N}_{\text{EA}}\left(100 - (\%\text{N}_{\text{azide}} + \%\text{C}_{\text{azide}} + \%\text{H}_{\text{azide}})\right)}{100 - (\%\text{N}_{\text{EA}} + \%\text{C}_{\text{EA}} + \%\text{H}_{\text{EA}})} \tag{2}$$

TEMPO loading is then calculated analogously to azide loading (equation 1), except that the nitrogen atoms already present must be subtracted.

$$X_{\text{TEMPO}} = \frac{\%\text{N}_{\text{TEMPO}} - \%\text{N}_{\text{azide}}}{\text{N}_{\text{add}}(\text{N})M(\text{N})} \tag{3}$$

6.6 PVC-TEMPO

6.6.1 Williamson ether synthesis

In a 100 mL round bottom flask, 3.34 g (83.6 mmol, 1 eq) of sodium hydride (60 % in mineral oil) was placed and 17 mL of technical DMSO was added. Then, 16.00 g (92.9 mmol, 1.1 eq) TEMPOL were added in portions. A strong foaming occurred. When all TEMPOL was added, the mixture was stirred at RT. After 3 h, 3 mL of H_2O and 5.81 g (93.0 mmol, 1.1 eq) of PVC pellets were added. The solution was heated to 65 C and stirred for 24 h - 48 h. The ratio of DMSO/H_2O was varied between DMSO/H_2O 1:0, 1:3, 3:1, and 17:3. In case of Williamson Ether synthesis in toluol, anhydrous toluol was used instead of DMSO/H_2O. The temperature was varied between 20 °C, 35 °C, 50 °C and 65 °C. After reaction, the pellets were washed with H_2O (2 x 50 mL) and ACN (2 x 50 mL) and dried in vacuum at 40 °C.

6.6.2 Williamson ether synthesis with Ag_2O

0.69 g (2.98 mmol, 10 *mol*% based on TEMPOL) Ag_2O, 5.13 g (29.8 mmol, 1.5 eq) TEMPOL and 1.25 g (19.5 mmol, 1 eq) PVC were placed in a 25 mL round bottom flask. To cover all PVC pellets in solvent, 10 mL anhydrous toluol were added. The mixture was stirred at 40 °C for 24 h. The pellets were filtered, washed with H_2O (2 x 50 mL) and ACN (2 x 50 mL) and dried in vacuum at 40 °C

6.6.3 Williamson ether synthesis with Maghnite K+

In a 50 mL round bottom flask, 1.61 g (40.25 mmol, 1 eq) NaH was suspended in 11.5 mL DMSO. Then 9.30 g (54.0 mmol, 1.3 eq) TEMPOL was added in portions. The mixture was stirred at RT. After 30 min, gas formation was complete and 0.84 g Maghnite K+, as well as 2.2 mL H_2O and 3.37 g (53.9 mmol, 1.3 eq) PVC were added. The reaction was stirred for 48 h at 65 °C. To investigate the influence of Maghnite K+, the ratios of Maghnite K+/NaH were varied between 1:0, 1:3, and 3:1.

6.7 Activation of catalyst pellets

Activation of the pellets was performed similarly to Schulze et. al:

Assuming that, as in click chemistry, the pellets had a TEMPO loading of approximately 2 mmol·g^{-1}: 1.34 g (10.1 mmol, 9.2 eq) NCS was dissolved in 16.7 mL ACN and 3.4 mL dioxane, resulting in a concentration of 0.51 mol/L of NCS. 0.75 mL of HCl (0.4 mol·L^{-1}) was added. The solution turned yellow. Then, 0.55 g (1.1 mmol, 1 eq.) PVC-TEMPO was added, and the solution was heated to 40 °C. After 30 min, the reaction was terminated by filtering the pellets and washing with water (3 x 50 mL) and ACN (3 x 50 mL). The pellets were dried in vacuo at 40 °C.

6.8 Oxidation reactions in batch

All oxidation reactions were performed according to the following example:

In a 10 mL rolling round tube, 0.35 g (1.1 mmol, 1.1 eq) BAIB and 17 mg (0.05 mmol, 5 *mol*% based on alcohol) TBAB were dissolved in 4 mL ACN at 35 °C. Subsequently, about 0.55 g (two-four pellets) PVC-TEMPO was added first, followed directly by 1 mmol (1 eq) alcohol. The reaction was terminated after 30 min by removing the catalyst. Conversion was determined by 1H NMR

$$X = \frac{I_{\text{aldehyde}}}{I_{\text{aldehyde}} + I_{\text{alcohol}}} \quad (4)$$

6.8.1 Benzyl alcohol

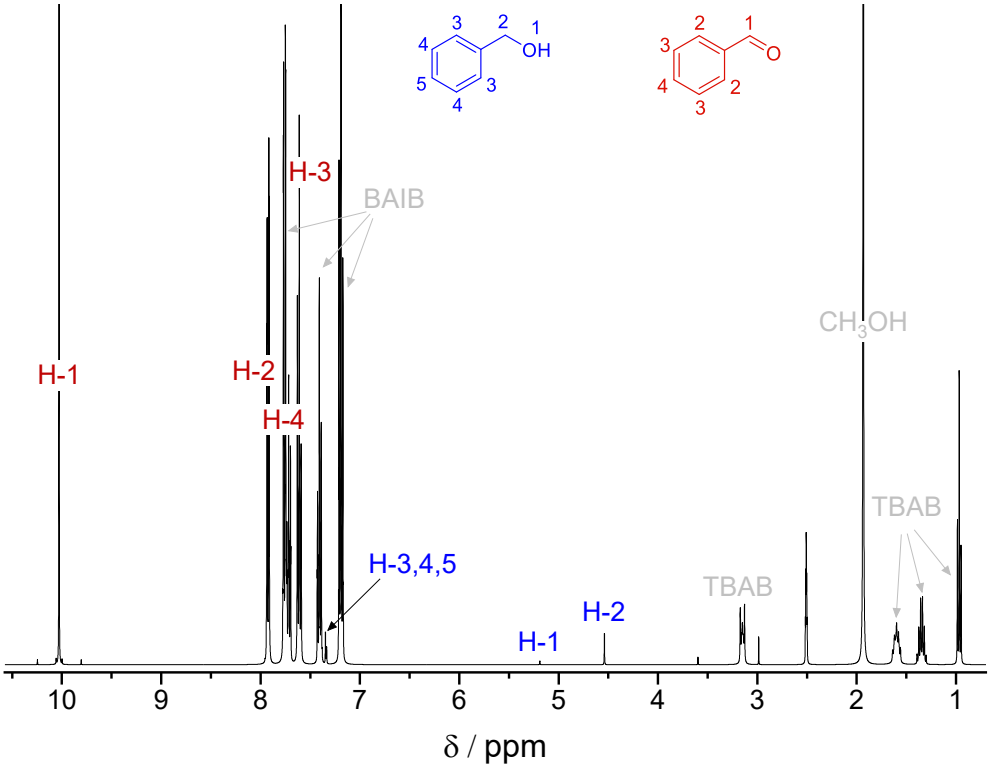

Figure 58. 1H NMR of the reaction solution after the oxidation of benzyl alcohol to benzaldehyde using BAIB/TBAB as co-oxidant system.

^{1}H NMR (500 MHz, DMSO):δ = 10.03 (s), 7.93 (d, *J* = 7.3 Hz), 7.76 (d, *J* = 7.7 Hz), 7.73 (t, *J* = 7.4 Hz), 7.62 (t, *J* = 7.6 Hz), 7.41 (t, *J* = 7.4 Hz), 7.34 (d, *J* = 4.3 Hz), 7.20 (t, *J* = 7.7 Hz), 4.53 (s), 3.59 (s), 3.22 – 3.11 (m), 1.93 (s), 1.64 – 1.54 (m), 1.34 (h, *J* = 7.4 Hz), 0.96 (t, *J* = 7.4 Hz).

6.8.2 (3,4-Dimethoxyphenyl)methanol

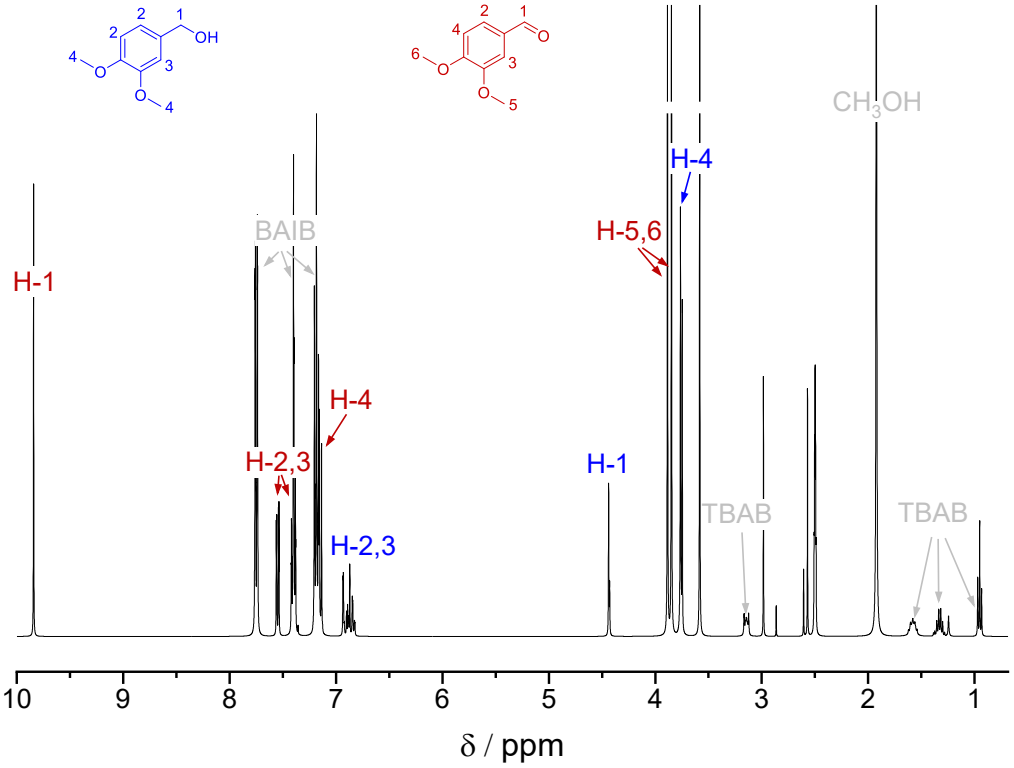

Figure 59. 1H NMR of the reaction solution after the oxidation of (3,4-dimethoxyphenyl)methanol to 3,4-dimethoxybenzaldehyde using BAIB/TBAB as co-oxidant system

^{1}H NMR (400 MHz,):δ = 9.84 (s), 7.79 – 7.71 (m), 7.55 (dd, *J* = 8.2, 1.9 Hz), 7.45 – 7.34 (m), 7.23 – 7.09 (m), 6.96 – 6.80 (m), 4.44 (d, *J* = 4.8 Hz), 3.87 (d, *J* = 14.6 Hz), 3.76 (d, *J* = 6.8 Hz), 3.59 (s), 3.16 – 3.10 (m), 2.98 (s), 1.93 (s), 1.58 (p, *J* = 8.3 Hz), 1.34 (dp, *J* = 14.7, 7.4 Hz), 0.96 (t, *J* = 7.3 Hz).

6.8.3 2-Phenylethanol

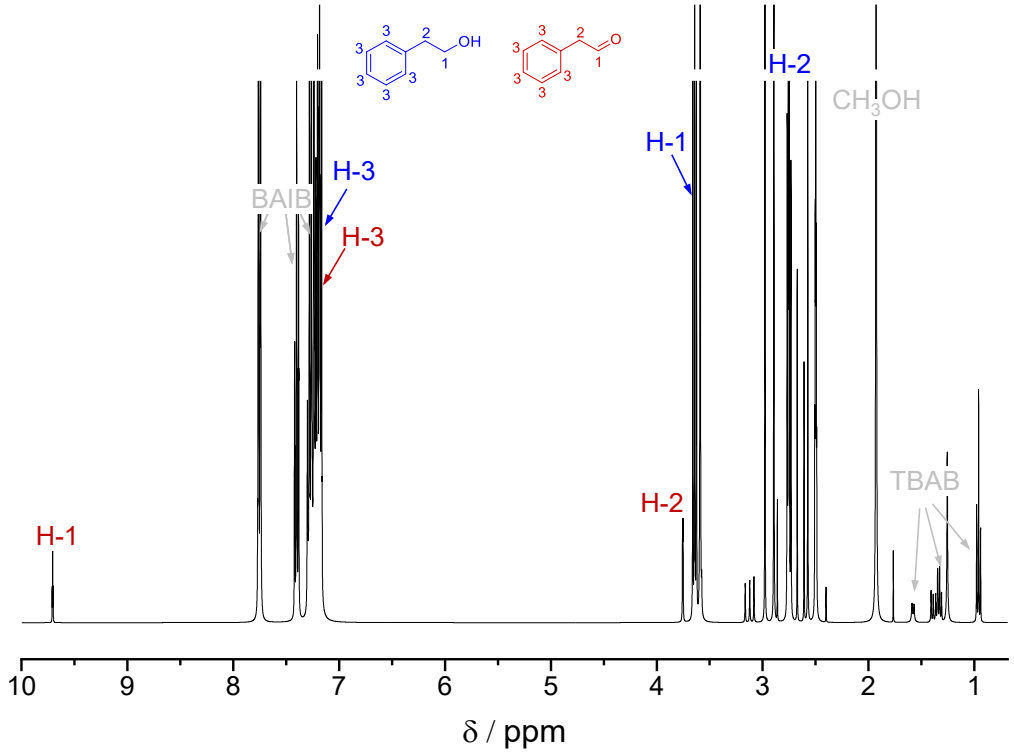

Figure 60. 1H NMR of the reaction solution after the oxidation of 2-phenylethanol to 2-phenylacetaldehyde using BAIB/TBAB as co-oxidant system

1H NMR (300 MHz, DMSO): δ = 9.71 (t, *J* = 1.4 Hz), 7.78 – 7.73 (m), 7.43 – 7.37 (m), 7.31 – 7.21 (m), 7.21 – 7.16 (m), 3.64 (t, *J* = 5.3 Hz), 3.59, 2.98, 2.90, 2.78 – 2.72 (m), 2.57, 1.93, 1.77, 1.65 – 1.48 (m), 1.43 – 1.29 (m), 1.26, 0.96 (t, *J* = 5.4 Hz).

6.8.4 n-Butanol

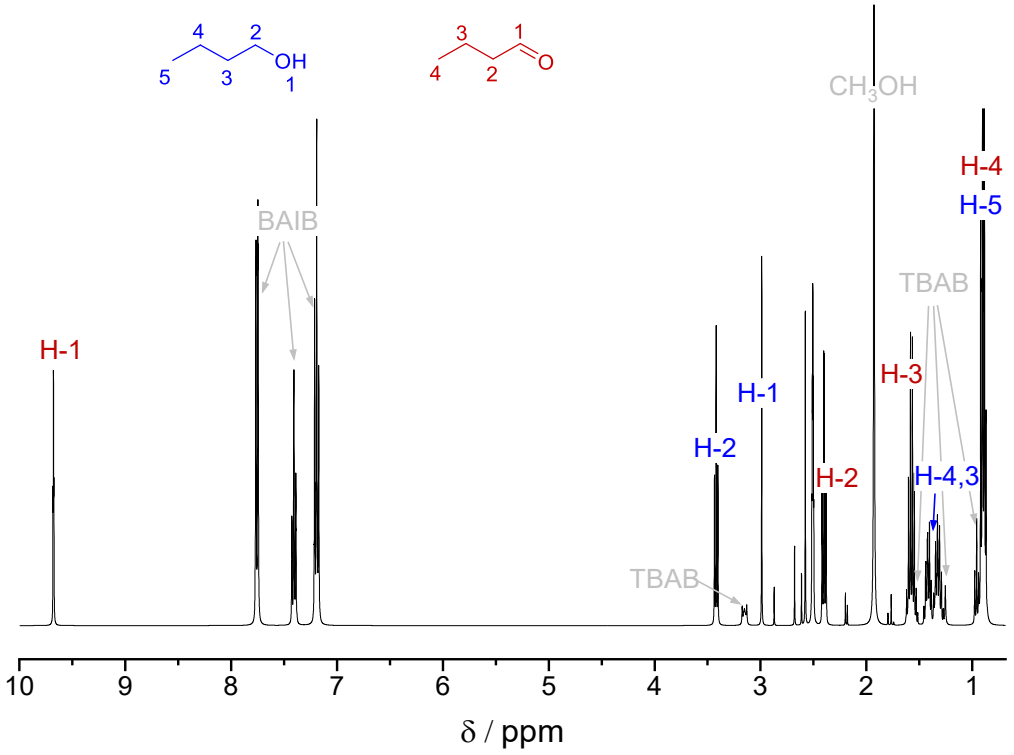

Figure 61. 1H NMR of the reaction solution after the oxidation of n-butanol to butyraldehyde using BAIB/TBAB as co-oxidant system

^{1}H NMR (400 MHz, DMSO): δ= 9.68 (t, *J* = 1.7 Hz), 7.80 – 7.72 (m), 7.45 – 7.36 (m), 7.24 – 7.15 (m), 3.42 (t, *J* = 6.4 Hz), 3.20 – 3.11 (m), 2.99 (s), 2.40 (td, *J* = 7.2, 1.7 Hz), 1.93 (s), 1.58 (h, *J* = 7.3 Hz), 1.48 – 1.23 (m), 0.96 (t, *J* = 7.3 Hz), 0.93 – 0.86 (m).

6.8.5 n-Propanol

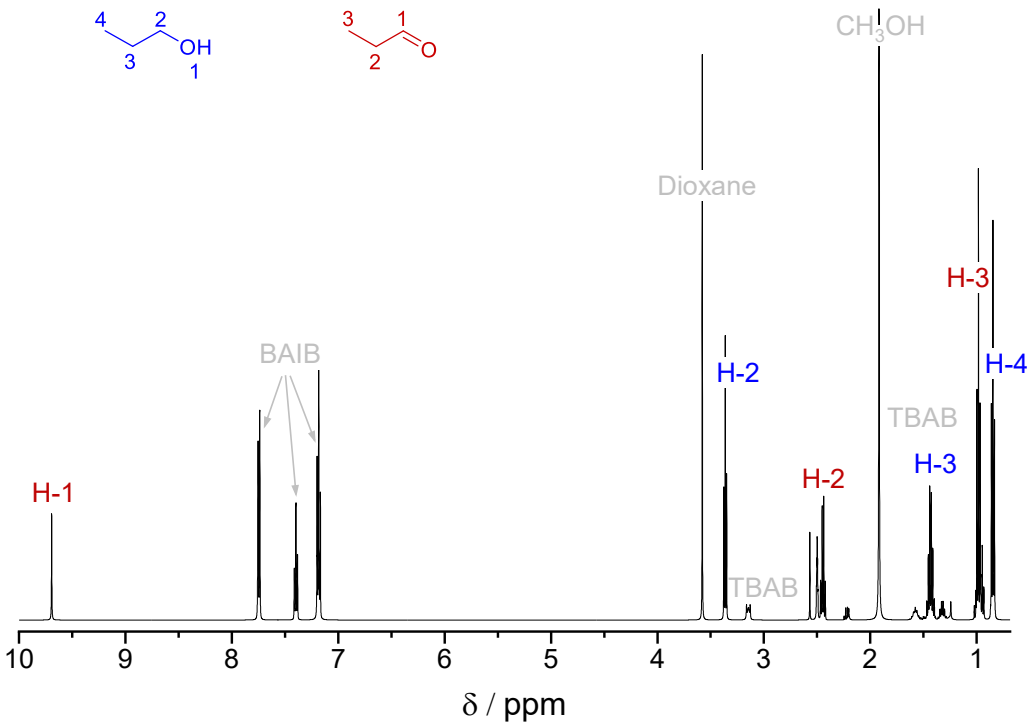

Figure 62. 1H NMR of the reaction solution after the oxidation of n-propanol to propionaldehyde using BAIB/TBAB as co-oxidant system

1H NMR (300 MHz, DMSO) δ = 9.69, 7.75 (dd, *J* = 4.7, 0.8 Hz), 7.42 – 7.37 (m), 7.18 (t, *J* = 4.7 Hz), 3.58, 3.36 (t, *J* = 4.0 Hz), 3.17 – 3.12 (m), 2.57, 2.45 (qd, *J* = 4.5, 0.6 Hz), 1.92, 1.62 – 1.53 (m), 1.43 (h, *J* = 4.3 Hz), 1.32 (h, *J* = 4.5 Hz), 1.03 – 0.93 (m), 0.85 (t, *J* = 4.5 Hz).

6.8.6 Isopropyl alcohol

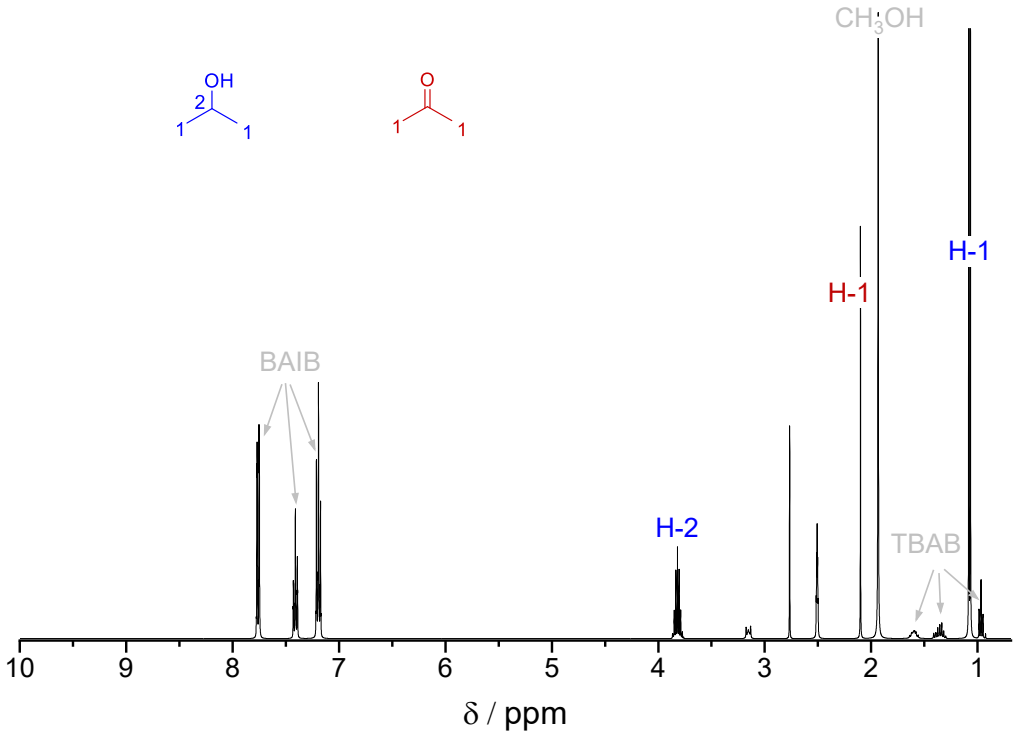

Figure 63. 1H NMR of the reaction solution after the oxidation of isopropyl alcohol to acetone using BAIB/TBAB as co-oxidant system

^{1}H NMR (400 MHz, DMSO): δ = 7.79 – 7.72 (m), 7.45 – 7.36 (m), 7.23 – 7.14 (m), 3.82 (h, *J* = 6.1 Hz), 3.18 – 3.11 (m), 2.09 (s), 1.93 (s), 1.63 – 1.54 (m), 1.07 (d, *J* = 6.1 Hz), 1.00 – 0.95 (m)

6.8.7 1,4-Phenylenedimethanol

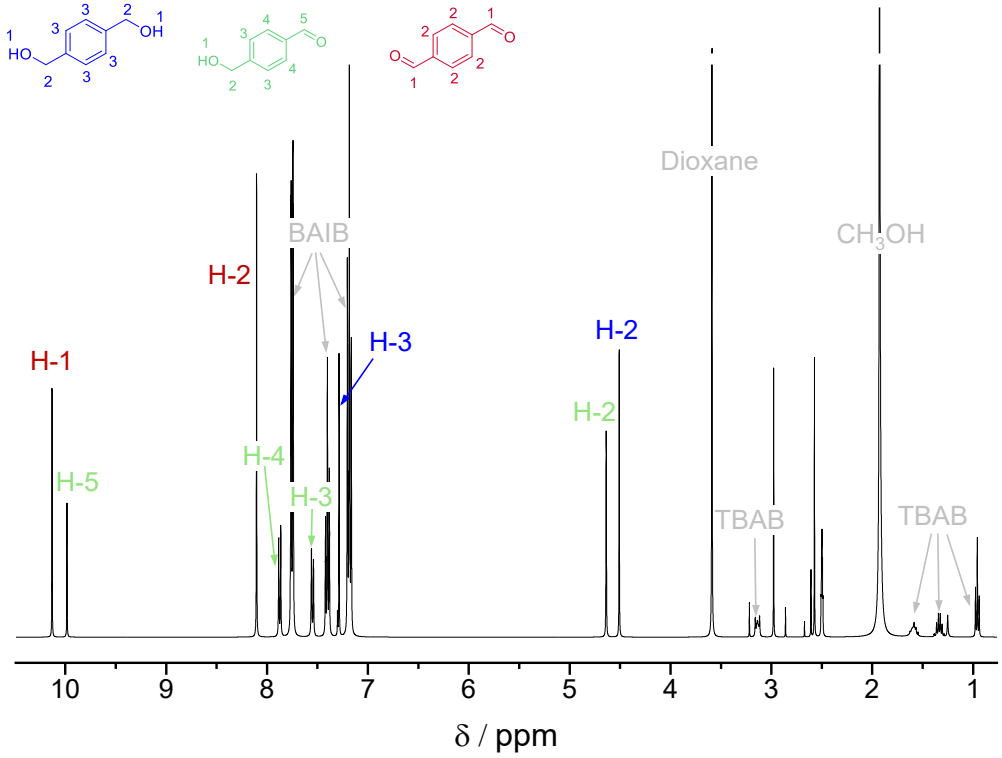

Figure 64. 1H NMR of the reaction solution after the oxidation of 1,4-phenylenedimethanol to terephthalaldehyde using BAIB/TBAB as co-oxidant system

^{1}H NMR (400 MHz, DMSO): δ = 10.13 (s), 9.98 (s), 8.11 (s), 7.88 (d, *J* = 8.2 Hz), 7.80 – 7.71 (m), 7.55 (d, *J* = 7.9 Hz), 7.29 (s), 7.24 – 7.12 (m), 4.64 (s), 4.51 (s), 3.59 (s), 1.93 (s,), 1.65 – 1.52 (m), 1.41 (s), 1.41 – 1.27 (m), 0.96 (t, *J* = 7.3 Hz).

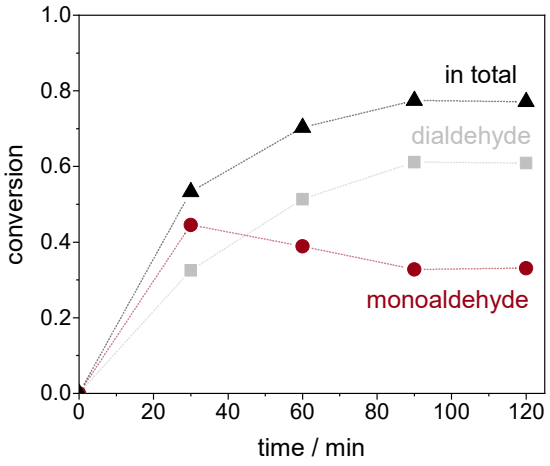

Figure 65. Reaction progress of the oxidation of 1,4-phenylenedimethanol to terephthalaldehyde (grey) and 4-(hydroxymethyl)benzaldehyde (red) as well as total conversion (black) using 1.1 eq. BAIB and 2.5 *mol*% TBAB.

6.8.8 1,4-Butanediol

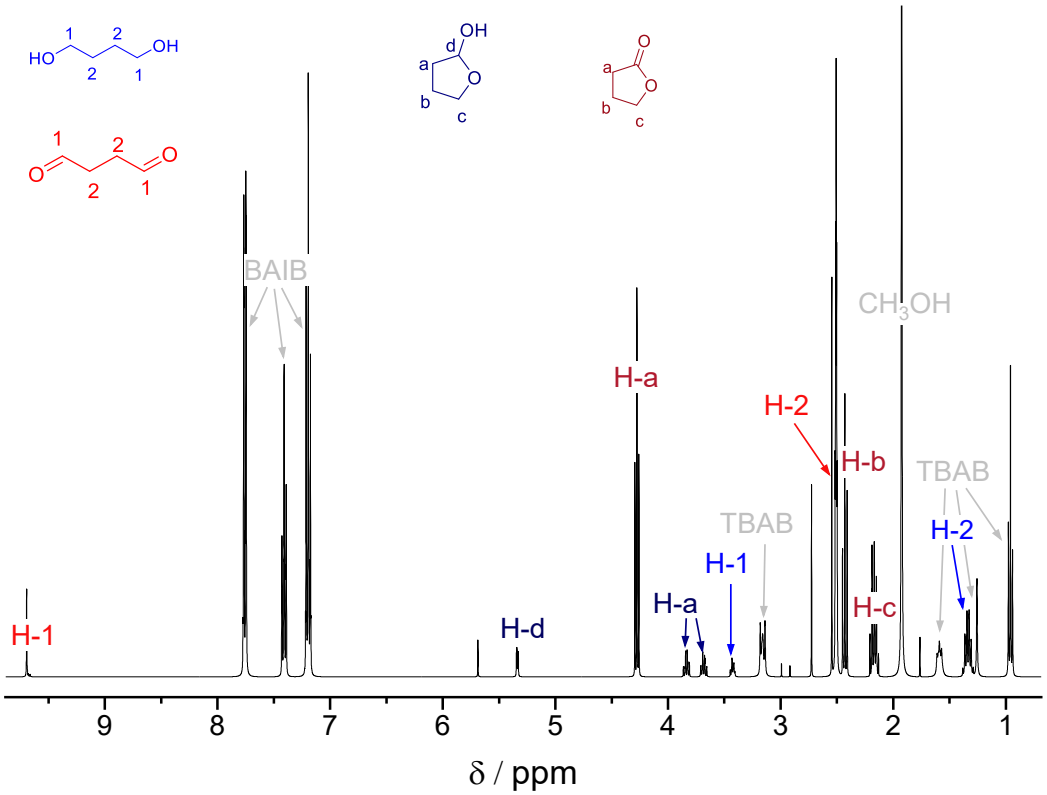

Figure 66. 1H NMR of the reaction solution after the oxidation of 1,4-butanediol to succinaldehyde, tetrahydrofuran-2-ol and γ-butyrolactone using BAIB/TBAB as co-oxidant system

1H NMR (400 MHz, DMSO): δ = 9.70, 7.94 – 7.73 (m), 7.45 – 7.37 (m), 7.25 – 7.15 (m), 5.69, 5.34 (dd, *J* = 3.6, 1.3 Hz), 4.28 (t, *J* = 5.3 Hz), 3.84 (td, *J* = 5.9, 4.2 Hz), 3.68 (td, *J* = 5.6, 4.2 Hz), 3.43 (td, *J* = 4.7, 3.0 Hz), 3.20 – 3.12 (m), 2.43 (dd, *J* = 6.4, 5.8 Hz), 2.23 – 2.11 (m), 1.93, 1.59 (dd, *J* = 7.5, 4.5 Hz), 1.34 (h, *J* = 5.5 Hz), 1.26, 0.96 (t, *J* = 5.5 Hz).

6.9 Functionalization of 3D printed reactors

The functionalization of two reactors was performed according to the following example:

The reactors were rinsed with 25 mL DCM and 25 mL water to remove impurities and small filaments formed during 3D printing. The reactors were then dried for three days in a desiccator under silica gel.

In a pre-storage tank, 20.96 g (0.52 mol, 1.3 eq) NaH (60 *w*t% in mineral oil) was suspended in 269 mL DMSO. With stirring, 111.01 g (0.64 mol, 1.6 eq) TEMPOL was added in portions and stirred for 3 h. Meanwhile, two reactors with a total surface area of 1885 cm^2 were connected in series. Assuming a diffusion depth into the reactor wall of 0.1 mm and a specified material density of 1.35 $g \cdot cm^{-3}$, this corresponds to an amount of about 0.41 mol (1.0 eq). Total volume was 175 mL. The reactors were immersed in a water bath at 65 °C and thus tempered. After 3 h, 33 mL of H_2O was added to the reaction solution and pumped through the reactors in loop using a peristaltic pump (*Ismatec mp-4*) at level 8.5. The reaction time was 24 h.

To clean the reactors, they were rinsed with ACN until the solution was clear (about 30 min). Then, the reactors were rinsed with water and dried using compressed air. The reactors were dried in a desiccator under silica gel for three days before being used for an oxidation reaction.

6.10 Oxidation reactions in continuous flow

6.10.1 Fixed-bed reactor

A 10.3 cm long tube with a diameter of 2.5 cm was filled with as many catalyst pellets as possible. The free volume was measured by means of water. The procedure is described using the example of the PVC-TEMPO grid pellets:

77 catalyst pellets were filled into the tube, resulting in a free volume of 31.5 mL. In a storage vessel, 6.25 mL (60.0 mmol, 1.0 eq) benzyl alcohol was added and filled up to 250 mL with ACN. Then, 20 g (62.1 mmol, 1.04 eq) BAIB was added.

The tube was immersed in a 35 °C temperature water bath. The reaction solution was pumped through the fixed bed reactor using *Asia Syringe Pump* by *syrris* at a flow rate of 0.7$mL \cdot min^{-1}$ to reach a residence time of 45 min.

Conversion was monitored by ^1H NMR. Samples were taken during the reaction for this purpose. No further purification was performed.

After the reaction was complete, the pellets were taken and stirred in ACN for 30 min. Subsequently, they were washed with water three times and dried in vacuo at 40 °C.

6.10.2 3D printed reactor without TBAB

The reaction in 3D printed reactors was performed according to the following example:

Three of the reactors were connected in series and immersed in a 35 °C water bath. The reactors were rinsed with 150 mL of ACN (5 mL·min^{-1}). Meanwhile, 81 g (250 mmol, 1.04 eq) of BAIB was dissolved in 1.0 L of ACN at 35 °C in a storage vessel. Before starting the reaction, 25 mL (240 mmol, 1.0 eq) of benzyl alcohol was added to the reaction solution. Using an *Asia Syringe Pump* by *syrris*, the reaction solution was pumped through the reactors at a flow rate of 1.5 mL·min^{-1} (round reactors) and 1.2 mL·min^{-1} (square reactors), resulting in an average residence time of 30 min.

Conversion was determined using ^{1}H NMR. Therefore, samples were taken during reaction.

After the reaction was completed, the reactors were again rinsed with 150 mL of ACN (5 mL·min^{-1}) and then each was rinsed with 25 mL of water. The reactors were dried under compressed air and stored in a desiccator under organ gel.

6.10.3 3D printed reactor with TBAB

The oxidation reaction of an alcohol with BAIB/TBAB in a 3D printed reactor was performed as follows:

Two functionalized reactors with a total volume of 175 mL were connected in series and immersed in a water bath at a temperature of 35 °C. The reactors were rinsed with 250 mL of ACN (flow rate: 10 mL·min^{-1}).

Meanwhile, in one storage vessel, 47.94 g (0.15 mol, 0.25 mol·L^{-1}) BAIB was dissolved in 593 mL ACN at 35 C with stirring. In a second storage vessel, 39.5 mL (0.38 mol,

6.59 mol·L^{-1}) benzyl alcohol and 6.1 g (0.019 mol, 5 *mol*% based on benzyl alcohol) TBAB were dissolved in 18.68 mL ACN.

After the reactor was purged and everything was completely dissolved, the reaction was started. An *Asia Syringe Pump* by *syrris* was used to pump the BAIB/ACN solution at 2.8 mL·min^{-1}and the alcohol solution at 112 µL·min^{-1}. This resulted in a total flow rate of 2.912 mL·min^{-1}, resulting in a residence time of 30 min.

For conversion tracking, samples were taken for ^{1}H NMR during the reaction. No further purification was performed.

After the reaction was completed (between 4.5 h and 7 h), the reactors were rinsed with 200 mL of ACN (10 mL·min^{-1}). Subsequently, the reactors were each rinsed with 50 mL of water and stored in the desiccator.

7. Safety Data

Substance	GHS pictograms	Hazard Sentences	Precaution Sentences
Acetic acid		226, 314	280, 305+351+338, 310
Acetone		225, 302, 319, 336, 373	210, 235, 260, 305+351+338
Acetonitrile		225, 302, 319, 332	210, 280, 305+351+338
Benzaldehyde		302	264, 270, 301+312, 330, 501
Benzol-1,4-dicarbaldehyd	Not a hazardous substance or mixture according to Regulation (EC) No 1272/2008.		
1,4-Benzenedimethanol	Not a hazardous substance or mixture according to Regulation (EC) No 1272/2008.		
Benzyl alcohol		302+332, 319	301+312+330, 304+340+312, 305+351+338
(Diacetoxyiodo) benzol	Not a hazardous substance or mixture according to Regulation (EC) No 1272/2008.		
Butanal		225, 319	210, 233, 240, 241, 242, 305+351+338
Butanol		226, 302, 315, 318, 335, 336	210, 233, 280, 301+312, 303+361+353, 305+351+338

copper iodid		302, 315, 317, 318, 410	273, 280, 301+312+330, 302+352, 305+351+338+310
3,4-Dimethoxybenzyl alcohol		302	264, 301+312
Dimethylsulfoxide	Not a hazardous substance or mixture according to Regulation (EC) No 1272/2008.		
N,N-Diisopropylethylamine		225, 301, 314, 412	210, 273, 280, 301+310, 305+351+338, 310
Iodobenzen		302, 319	305+351+338
Montmorillonite	Not a hazardous substance or mixture according to Regulation (EC) No 1272/2008.		
N-Methyl-2-pyrrolidone		315, 319, 335, 360D	201, 302+352, 305+351+338, 308+313
Phenethyl alcohol		302, 319	264, 270, 280, 301+312, 305+351+338, 337+313
Phenylacetaldehyde		302, 314, 317, 412	261, 273, 280, 301+312, 303+361+353, 305+351+338
Propan-2-ol		225, 319, 336	210, 240, 305+351+338, 403+233
Propanol-1-ol		225, 318, 336	210, 240, 280, 305+351+338, 313, 403+233
Propargyl bromide	 	225, 301, 304, 314, 335, 336, 361d, 373	210, 280, 301+330+331, 303+361+353, 304+340+310, 305+351+338

Propionaldehyde		225, 302+332, 315, 318, 335	210, 280, 301+312, 303+361+353, 304+340+312, 305+351+338, 403+235
Silver oxide		271, 318, 410	210, 220, 280, 283, 305+351+338
Sodium azide		300+310+330, 373, 410, EUH032	262, 273, 280, 301+310+330, 302+352+310, 304+340+310
Sodium hydride		228, 260, 314	210, 231+232, 260, 280, 303+361+353, 305+351+338+310
TEMPOL		302, 318, 373	280, 305+351+338, 310
Tetrabutylammoniumbromid		302, 315, 319, 361fd, 412	202, 273, 301+312, 302+352, 305+351+338, 308+313
Toluol		225, 304, 315, 336, 361d, 373	210, 240, 301+310+330, 302+352, 314, 403+233

8. Literature

[1] Z. Guo, B. Liu, Q. Zhang, W. Deng, Y. Wang, Y. Yang, *Chemical Society reviews* **2014**, *43*, 3480.

[2] W. Köhler, R. Ansorg, H. Brandis (Eds.) *Medizinische Mikrobiologie ; 197 Tabellen*, Urban & Fischer, München, **2001**.

[3] S. Hauptmann, *Organische Chemie*, Dt. Verl. für Grundstoffindustrie; Wiley-VCH, Leipzig, Weinheim, **2001**.

[4] D. J. Rowe, *Chemistry and technology of flavors and fragrances*, Blackwell, Oxford, **2006**.

[5] W. Sweeny, *J. Appl. Polym. Sci.* **1963**, *7*, 1983.

[6] A. M. P. Koskinen, A. O. Kataja in *Organic reactions*, Wiley Online Library, [Hoboken, N.J.], **2003-**, pp. 105–410.

[7] G. Tojo, M. Fernández, *Oxidation of alcohols to aldehydes and ketones*. *A guide to current common practice*.

[8] J.-E. Bckvall, *Modern Oxidation Methods*, Wiley-VCH [Imprint]; John Wiley & Sons, Incorporated, Hoboken, **2011**.

[9] E. Fritz-Langhals, *Org. Process Res. Dev.* **2005**, *9*, 577.

[10] D. Duprez, F. Cavani, *Handbook of Advanced Methods and Processes in Oxidation Catalysis*, Imperial College Press, Singapore, **2014**.

[11] L. Tebben, A. Studer, *Angew. Chem.* **2011**, *123*, 5138.

[12] K. M. Zentel, M. Fassbender, W. Pauer, G. A. Luinstra in *Advances in Chemical Engineering*, Elsevier, **2020**, pp. 97–137.

[13] A. E. C. Collis, I. T. Horváth, *Catal. Sci. Technol.* **2011**, *1*, 912.

[14] a) L. F. Fieser, M. Fieser, T.-L. Ho, *Reagents for organic synthesis*, Wiley, New York, **1967]-**; b) M. Hudlicky, *Oxidations in organic chemistry*, Amer. Chem. Soc, Washington, **1990**.

[15] G. I. Poos, G. E. Arth, R. E. Beyler, L. H. Sarett, *Journal of the American Chemical Society* **1953**, *75*, 422.

[16] J. C. Collins, W. W. Hess, F. J. Frank, *Tetrahedron Letters* **1968**, *9*, 3363.

[17] E. J. Corey, J. Suggs, *Tetrahedron Letters* **1975**, *16*, 2647.

[18] E. J. Corey, G. Schmidt, *Tetrahedron Letters* **1979**, *20*, 399.

[19] G. B. Shul'pin, G. Süss-Fink, L. S. Shul'pina, *Journal of Molecular Catalysis A: Chemical* **2001**, *170*, 17.

[20] I. E. Markó, P. R. Giles, M. Tsukazaki, I. Chellé-Regnaut, C. J. Urch, S. M. Brown, *Journal of the American Chemical Society* **1997**, *119*, 12661.

[21] D. B. Dess, J. C. Martin, *Journal of the American Chemical Society* **1991**, *113*, 7277.

[22] a) A. J. Mancuso, D. Swern, *Synthesis* **1981**, *1981*, 165; b) T. T. Tidwell, *Synthesis* **1990**, *1990*, 857.

[23] S. E. Davis, M. S. Ide, R. J. Davis, *Green Chem* **2013**, *15*, 17.

[24] O. Piloty, B. G. Schwerin, *Ber. Dtsch. Chem. Ges.* **1901**, *34*, 2354.

[25] H. A. Beejapur, Q. Zhang, K. Hu, L. Zhu, J. Wang, Z. Ye, *ACS Catal.* **2019**, *9*, 2777.

[26] F. Montanari, S. Quici, H. Henry-Riyad, T. T. Tidwell, A. Studer, T. Vogler, Y. Rao, C. Zhang, Y. Zong in *Encyclopedia of Reagents for Organic Synthesis*, John Wiley & Sons, Ltd, Chichester, UK, **2001**, pp. 1–12.

[27] E. Megiel, *Advances in colloid and interface science* **2017**, *250*, 158.

[28] *Encyclopedia of Reagents for Organic Synthesis*, John Wiley & Sons, Ltd, Chichester, UK, **2001**.

[29] E. G. ROZANTSEV, V. D. SHOLLE, *Synthesis* **1971**, *1971*, 401.

[30] J. F. W. Keana, *Chem. Rev.* **1978**, *78*, 37.

[31] M. Dagonneau, E. S. Kagan, V. I. Mikhailov, E. G. Rozantsev, v. d. Sholle, *Synthesis* **1984**, *1984*, 895.

[32] D. F. Bowman, T. Gillan, K. U. Ingold, *Journal of the American Chemical Society* **1971**, *93*, 6555.

[33] E. G. Rozantsev, (translated by Hazzard, B. J), *Free Nitroxyl Radicals*, Springer US, Boston, MA, **1970**.

[34] G. I. Likhtenshtein, *Nitroxides. Brief History, Fundamentals, and Recent Developments*, Springer International Publishing, Cham, **2020**.

[35] a) H. Schlude, *Tetrahedron* **1973**, *29*, 4007; b) E. J. Rauckman, G. M. Rosen, M. B. Abou-Donia, *The Journal of organic chemistry* **1976**, *41*, 564; c) H. M. McConnell, C. L. Hamilton, *Proceedings of the National Academy of Sciences of the United States of America* **1968**, *60*, 776; d) G. C. Roberts, J. Hannah, O. Jardetzky, *Science (New York, N.Y.)* **1969**, *165*, 504; e) C. M. Paleos, P. Dais, *J. Chem. Soc., Chem. Commun.* **1977**, 345.

[36] P. L. Bragd, H. van Bekkum, A. C. Besemer, *Topics in Catalysis* **2004**, *27*, 49.

[37] M. G. Banwell, V. S. Bridges, J. R. Dupuche, S. L. Richards, J. M. Walter, *The Journal of organic chemistry* **1994**, *59*, 6338.

[38] a) M. J. Perkins in *Advances in Physical Organic Chemistry*, Elsevier, **1980**, pp. 1–64; b) A. L. J. Beckwith, V. W. Bowry, K. U. Ingold, *Journal of the American Chemical Society* **1992**, *114*, 4983.

[39] T. Vogler, A. Studer, *Synthesis* **2008**, *2008*, 1979.

[40] a) J. Nicolas, Y. Guillaneuf, C. Lefay, D. Bertin, D. Gigmes, B. Charleux, *Progress in Polymer Science* **2013**, *38*, 63; b) D. Yang, C. Feng, J. Hu, *Polym. Chem.* **2013**, *4*, 2384.

[41] A. E. J. de Nooy, A. C. Besemer, H. van Bekkum, *Synthesis* **1996**, *1996*, 1153.

[42] a) Q. Cao, L. M. Dornan, L. Rogan, N. L. Hughes, M. J. Muldoon, *Chem. Commun.* **2014**, *50*, 4524; b) R. A. Sheldon, *Catalysis Today* **2015**, *247*, 4.

[43] R. A. Sheldon, I. W. C. E. Arends, *Adv. Synth. Catal.* **2004**, *346*, 1051.

[44] V. A. Golubev, G. Rozantsev, M. B. Neiman, *Russ Chem Bull* **1965**, *14*, 1898.

[45] J. M. Bobbitt, C. L. Flores, *HETEROCYCLES* **1988**, *27*, 509.

[46] V. A. Golubev, v. d. Sen', I. V. Kulyk, A. L. Aleksandrov, *Russ Chem Bull* **1975**, *24*, 2119.

[47] B. Ganem, *The Journal of organic chemistry* **1975**, *40*, 1998.

[48] J. A. Cella, J. A. Kelley, E. F. Kenehan, *The Journal of organic chemistry* **1975**, *40*, 1860.

[49] Z. Ma, J. M. Bobbitt, *The Journal of organic chemistry* **1991**, *56*, 6110.

[50] V. A. Golubev, V. N. Borislavskii, A. L. Aleksandrov, *Russ Chem Bull* **1977**, *26*, 1874.

[51] M. F. Semmelhack, C. S. Chou, D. A. Cortes, *Journal of the American Chemical Society* **1983**, *105*, 4492.

[52] M. F. Semmelhack, C. R. Schmid, D. A. Cortes, C. S. Chou, *Journal of the American Chemical Society* **1984**, *106*, 3374.

[53] D. H. Hunter, D. Barton, W. J. Motherwell, *Tetrahedron Letters* **1984**, *25*, 603.

[54] M. Zhao, J. Li, E. Mano, Z. Song, D. M. Tschaen, E. J. J. Grabowski, P. J. Reider, *The Journal of organic chemistry* **1999**, *64*, 2564.

[55] C. Bolm, A. S. Magnus, J. P. Hildebrand, *Organic letters* **2000**, *2*, 1173.

[56] S. S. Kim, K. Nehru, S. S. Kim, D. W. Kim, H. C. Jung, *Synthesis* **2002**, 2484.

[57] M. F. Semmelhack, C. R. Schmid, D. A. Cortés, *Tetrahedron Letters* **1986**, *27*, 1119.

[58] A. E. de Nooy, A. C. Besemer, H. van Bekkum, *Tetrahedron* **1995**, *51*, 8023.

[59] A. C. Besemer, A. E. J. de Nooy, WO001995007303A1, **1995**.

[60] G. H. Knaus, J. Paust, DE3705785A1, **1988**.

[61] T. Kükenhöhner, N. Goetz, DE000004007923A1, **1990**.

[62] P. Lucio Anelli, C. Biffi, F. Montanari, S. Quici, *The Journal of organic chemistry* **1987**, *52*, 2559.

[63] J. Einhorn, C. Einhorn, F. Ratajczak, J.-L. Pierre, *The Journal of organic chemistry* **1996**, *61*, 7452.

[64] P. L. Anelli, S. Banfi, F. Montanari, S. Quici, *The Journal of organic chemistry* **1989**, *54*, 2970.

[65] a) M. Frigerio, M. Santagostino, S. Sputore, G. Palmisano, *The Journal of organic chemistry* **1995**, *60*, 7272; b) E. Corey, A. Palani, *Tetrahedron Letters* **1995**, *36*, 3485; c) T. Wirth, *Angew. Chem. Int. Ed.* **2001**, *40*, 2812.

[66] A. de Mico, R. Margarita, L. Parlanti, A. Vescovi, G. Piancatelli, *The Journal of organic chemistry* **1997**, *62*, 6974.

[67] a) H. Tohma, T. Maegawa, S. Takizawa, Y. Kita, *Adv. Synth. Catal.* **2002**, *344*, 328; b) X. Ma, Z. Li, F. Liu, S. Cao, H. Rao, *Adv. Synth. Catal.* **2014**, *356*, 1741.

[68] Z. Li, Z. H. Tang, X. X. Hu, C. G. Xia, *Chemistry (Weinheim an der Bergstrasse, Germany)* **2005**, *11*, 1210.

[69] a) M. Brünjes, G. Sourkouni-Argirusi, A. Kirschning, *Adv. Synth. Catal.* **2003**, *345*, 635; b) J. J. Reilly, D. J. Duncan, T. P. Wunz, R. A. Patsiga, *The Journal of organic chemistry* **1974**, *39*, 3291.

[70] A. Salvo, V. Campisciano, H. Beejapur, F. Giacalone, M. Gruttadauria, *Synlett* **2015**, *26*, 1179.

[71] T. Miyazawa, T. Endo, S. Shiihashi, M. Okawara, *The Journal of organic chemistry* **1985**, *50*, 1332.

[72] T. Miyazawa, T. Endo, *Journal of Molecular Catalysis* **1985**, *31*, 217.

[73] W. Sümmermann, U. Deffner, *Tetrahedron* **1975**, *31*, 593.

[74] Z.-L. Lu, E. Lindner, H. A. Mayer, *Chem. Rev.* **2002**, *102*, 3543.

[75] a) R. A. Sheldon, *Chem. Commun.* **2008**, 3352; b) R. A. Sheldon, *Journal of environmental monitoring : JEM* **2008**, *10*, 406.

[76] G. Ertl (Ed.) *Handbook of heterogeneous catalysis*. *8 volumes*, Wiley-VCH-Verl., Weinheim.

[77] J. M. Thomas, W. J. Thomas, *Principles and practice of heterogeneous catalysis*, VCH, Weinheim [etc.], **op. 1997**.

[78] M. Benaglia, *Recoverable and recyclable catalysts*, Wiley, Hoboken, N.J, **2010**.

[79] a) N. Tsubokawa, T. Kimoto, T. Endo, *Journal of Molecular Catalysis A: Chemical* **1995**, *101*, 45; b) C. Bolm, T. Fey, *Chem. Commun.* **1999**, 1795; c) T. Fey, H. Fischer, S. Bachmann, K. Albert, C. Bolm, *The Journal of organic chemistry* **2001**, *66*, 8154; d) A. J. Shakir, C. Paraschivescu, M. Matache, M. Tudose, A. Mischie, F. Spafiu, P. Ionita, *Tetrahedron Letters* **2015**, *56*, 6878; e) R. Ciriminna, C. Bolm, T. Fey, M. Pagliaro, *Adv. Synth. Catal.* **2002**, *344*, 159; f) M. L. Testa, R. Ciriminna, C. Hajji, E. Zaballos Garcia, M. Ciclosi, J. Sepulveda Arques, M. Pagliaro, *Adv. Synth. Catal.* **2004**, *346*, 655; g) D. Brunel, F. Fajula, J. Nagy, B. Deroide, M. Verhoef, L. Veum, J. Peters, H. van Bekkum, *Applied Catalysis A: General* **2001**, *213*, 73; h) A. Machado, M. H. Casimiro, L. M. Ferreira, J. E. Castanheiro, A. M. Ramos, I. M. Fonseca, J. Vital, *Microporous and Mesoporous Materials* **2015**, *203*, 63; i) B. Karimi, E. Badreh, *Organic & biomolecular chemistry* **2011**, *9*, 4194; j) B. Karimi, A. Biglari, J. H. Clark, V. Budarin, *Angew. Chem. Int. Ed.* **2007**, *46*, 7210; k) B. Karimi, E. Farhangi, H. Vali, S. Vahdati, *ChemSusChem* **2014**, *7*, 2735; l) A. E. Fernandes, O. Riant, K. F. Jensen, A. M. Jonas, *Angew. Chem.* **2016**, *128*, 11210; m) A. E. Fernandes, O. Riant, A. M. Jonas, K. F. Jensen, *RSC Adv.* **2016**, *6*, 36602.

[80] J. S. Schulze, J. Migenda, M. Becker, S. M. M. Schuler, R. C. Wende, P. R. Schreiner, B. M. Smarsly, *J. Mater. Chem. A* **2020**, *8*, 4107.

[81] a) A. Gheorghe, A. Matsuno, O. Reiser, *Adv. Synth. Catal.* **2006**, *348*, 1016; b) T. Miyazawa, T. Endo, *J. Polym. Sci. Polym. Chem. Ed.* **1985**, *23*, 2487; c) D. Li, X. Shen, L. Chen, H. Jiang, J. Wang, *e-Polymers* **2014**, *0*; d) Z. Zheng, J. Wang, H. Chen, L. Feng, R. Jing, M. Lu, B. Hu, J. Ji, *ChemCatChem* **2014**, *6*, 1626.

[82] M. A. Subhani, M. Beigi, P. Eilbracht, *Adv. Synth. Catal.* **2008**, *350*, 2903.

[83] S. J. Liu, Q. Q. Hu, F. Q. Zhao, X. M. Chu, P. X. Li, E. J. Tang, *Express Polym. Lett.* **2014**, *8*, 862.

[84] a) Y. Shi, Y. Nabae, T. Hayakawa, M. Kakimoto, *RSC Adv.* **2015**, *5*, 1923; b) L. Chen, J. Tang, Q. Zhang, J. Wang, *Reactive and Functional Polymers* **2016**, *105*, 134.

[85] A. Dijksman, I. W. C. E. Arends, R. A. Sheldon, *Chem. Commun.* **2000**, 271.

[86] B. C. Anderson, G. D. Andrews, P. Arthur, H. W. Jacobson, L. R. Melby, A. J. Playtis, W. H. Sharkey, *Macromolecules* **1981**, *14*, 1599.

[87] K. A. Günay, P. Theato, H.-A. Klok, *J. Polym. Sci. A Polym. Chem.* **2013**, *51*, 1.

[88] M. A. Gauthier, M. I. Gibson, H.-A. Klok, *Angew. Chem. Int. Ed.* **2009**, *48*, 48.

[89] a) H. Staudinger, J. Fritschi, *HCA* **1922**, *5*, 785; b) H. Staudinger, E. Geiger, E. Huber, *Ber. dtsch. Chem. Ges. A/B* **1929**, *62*, 263.

[90] W. H. Starnes, *J. Polym. Sci. A Polym. Chem.* **2005**, *43*, 2451.

[91] K. Endo, *Progress in Polymer Science* **2002**, *27*, 2021.

[92] S. Moulay, *Progress in Polymer Science* **2010**, *35*, 303.

[93] A. A.Hasan, M. H. Al-Mashhadani, W. H. Al-Dahhan, R. M.Yusop, E. A. Yousif, *ANJS* **2022**, *25*, 8.

[94] T. Kameda, M. Ono, G. Grause, T. Mizoguchi, T. Yoshioka, *Polymer Degradation and Stability* **2009**, *94*, 107.

[95] H. Mekki, M. Belbachir, *Express Polym. Lett.* **2007**, *1*, 495.

[96] M. Belbachir, A. Bensaoula, US 7,094823 B2, **2006**.

[97] P. Jia, L. Hu, G. Feng, C. Bo, M. Zhang, Y. Zhou, *Materials Chemistry and Physics* **2017**, *190*, 25.

[98] V. V. Rostovtsev, L. G. Green, V. V. Fokin, K. B. Sharpless, *Angew. Chem.* **2002**, *114*, 2708.

[99] C. W. Tornøe, C. Christensen, M. Meldal, *The Journal of organic chemistry* **2002**, *67*, 3057.

[100] M. P. Doyle, M. A. McKervey, T. Ye, *Modern catalytic methods for organic synthesis with diazo compounds*. *From cyclopropanes to ylides*, Wiley, New York, **1998**.

[101] A. Earla, R. Braslau, *Macromol. Rapid Commun.* **2014**, *35*, 666.

[102] H. Feuer, J. Hooz in *The Ether Linkage (1967)* (Ed.: S. Patai), John Wiley & Sons, Ltd, Chichester, UK, **1967**, pp. 445–498.

[103] A. W. Williamson, *Q. J. Chem. Soc.* **1852**, *4*, 229.

[104] D. Campbell, L. R. Dix, P. Rostron, *European Polymer Journal* **1993**, *29*, 249.

[105] S. Hallmann, M. J. Fink, B. S. Mitchell, *Journal of Experimental Nanoscience* **2015**, *10*, 588.

[106] R. G. Smith, A. Vanterpool, H. J. Kulak, *Can. J. Chem.* **1969**, *47*, 2015.

[107] a) T. W. Phillips, I. G. Lignos, R. M. Maceiczyk, A. J. deMello, J. C. deMello, *Lab on a chip* **2014**, *14*, 3172; b) N. C. Neyt, D. L. Riley, *React. Chem. Eng.* **2021**, *6*, 1295.

[108] A. Behr, D. W. Agar, J. Jörissen, A. J. Vorholt, *Einführung in die Technische Chemie*, Springer Spektrum, Berlin, Heidelberg, **2016**.

[109] R. GTTEL, *CHEMISCHE REAKTIONSTECHNIK*, Springer, [S.l.], **2021**.

[110] a) G. F. Froment, K. B. Bischoff, *Chemical reactor analysis and design*, Wiley, New York, **1979**; b) B. Nauman, *Handbook of Chemical Reactor Design, Optimization, and Scaleup*, McGraw-Hill Professional Publishing; McGraw-Hill Companies, The [distributor], New York, Blacklick, **2001**.

[111] a) I. R. Baxendale, J. Deeley, C. M. Griffiths-Jones, S. V. Ley, S. Saaby, G. K. Tranmer, *Chem. Commun.* **2006**, 2566; b) K. F. Jensen, *Chemical Engineering Science* **2001**, *56*, 293; c) N. G. Anderson, *Org. Process Res. Dev.* **2012**, *16*, 852.

[112] M. Guidi, P. H. Seeberger, K. Gilmore, *Chemical Society reviews* **2020**, *49*, 8910.

[113] a) K. F. Jensen, B. J. Reizman, S. G. Newman, *Lab on a chip* **2014**, *14*, 3206; b) W. Reschetilowski (Ed.) *Microreactors in Preparative Chemistry*, Wiley-VCH Verlag GmbH & Co. KGaA, Weinheim, Germany, **2013**; c) T. Wirth, *Microreactors in organic chemistry and catalysis*, Wiley-VCH, Weinheim, Germany, **2013**; d) V. Hessel, *Chem. Eng. Technol.* **2009**, *32*, 1655; e) R. L. Hartman, J. P. McMullen, K. F. Jensen, *Angew. Chem. Int. Ed.* **2011**, *50*, 7502; f) J. Wegner, S. Ceylan, A. Kirschning, *Chem. Commun.* **2011**, *47*, 4583; g) C. Wiles, P. Watts, *Green Chem* **2012**, *14*, 38.

[114] a) A. Goršek, P. Glavič, *Chemical Engineering Research and Design* **1997**, *75*, 709; b) H. Löwe, W. Ehrfeld, *Electrochimica Acta* **1999**, *44*, 3679; c) H. Kim, K.-I. Min, K. Inoue, D. J. Im, D.-P. Kim, J. Yoshida, *Science (New York, N.Y.)* **2016**, *352*, 691.

[115] T. Tsubogo, H. Oyamada, S. Kobayashi, *Nature* **2015**, *520*, 329.

[116] P. T. Anastas, J. C. Warner, *Green chemistry. Theory and practice*, Oxford University Press, Oxford, **2014], 2000**.

[117] a) A. Kirschning, C. Altwicker, G. Dräger, J. Harders, N. Hoffmann, U. Hoffmann, H. Schönfeld, W. Solodenko, U. Kunz, *Angew. Chem.* **2001**, *113*, 4118; b) M. Baumann, I. R. Baxendale, S. V. Ley, *Molecular diversity* **2011**, *15*, 613; c) E. Riva, A. Rencurosi, S. Gagliardi, D. Passarella, M. Martinelli, *Chemistry (Weinheim an der Bergstrasse, Germany)* **2011**, *17*, 6221; d) D. Webb, T. F. Jamison, *Chem. Sci.* **2010**, *1*, 675; e) K. Jähnisch, V. Hessel, H. Löwe, M. Baerns, *Angew. Chem. Int. Ed.* **2004**, *43*, 406; f) P. Hodge, *Ind. Eng. Chem. Res.*

2005, *44*, 8542; g) P. H. Seeberger, *Nature chemistry* **2009**, *1*, 258; h) C. F. Carter, I. R. Baxendale, J. B. J. Pavey, S. V. Ley, *Organic & biomolecular chemistry* **2010**, *8*, 1588.

[118] R. Greco, W. Goessler, D. Cantillo, C. O. Kappe, *ACS Catal.* **2015**, *5*, 1303.

[119] V. Dragone, V. Sans, M. H. Rosnes, P. J. Kitson, L. Cronin, *Beilstein journal of organic chemistry* **2013**, *9*, 951.

[120] P. Fastermann, *3D-Druck/Rapid Prototyping. Eine Zukunftstechnologie - kompakt erklärt*, Springer Berlin, Berlin, **2012**.

[121] a) R. V. Rao, V. D. Kalyankar, *Int J Adv Manuf Technol* **2014**, *73*, 1159; b) S. T., S. P., A. M.S., *RPJ* **2020**, *26*, 669; c) B. T. Wittbrodt, A. G. Glover, J. Laureto, G. C. Anzalone, D. Oppliger, J. L. Irwin, J. M. Pearce, *Mechatronics* **2013**, *23*, 713.

[122] A. Przybytek, I. Gubańska, J. Kucińska-Lipka, H. Janik, *Fibres and Textiles in Eastern Europe* **2018**, *26*, 120.

[123] M. P. Groover, E. W. Zimmers, *CAD/CAM. Computer-aided design and manufacturing*, Prentice-Hall International, Englewood Cliffs, New Jersey, **1984**.

[124] M. Hofmann, *ACS Macro Lett.* **2014**, *3*, 382.

[125] a) A. J. Capel, R. P. Rimington, M. P. Lewis, S. D. R. Christie, *Nat Rev Chem* **2018**, *2*, 422; b) F. Guba, Ü. Tastan, K. Gugeler, M. Buntrock, T. Rommel, D. Ziegenbalg, *Chemie Ingenieur Technik* **2018**; c) W. Schierholz, G. Lauschke, S. Ott, U. Schmidt, P. Hein, EP0996498B1, **2000**; d) H. Taheri, Y. Sarin, B. Ozero, US000009340470B2, **2016**; e) T. Monaghan, M. J. Harding, R. A. Harris, R. J. Friel, S. D. R. Christie, *Lab on a chip* **2016**, *16*, 3362.

[126] C. Parra-Cabrera, C. Achille, S. Kuhn, R. Ameloot, *Chemical Society reviews* **2018**, *47*, 209.

[127] S. Rossi, R. Porta, D. Brenna, A. Puglisi, M. Benaglia, *Angew. Chem. Int. Ed.* **2017**, *56*, 4290.

[128] X. Zhou, C. Liu, *Adv. Funct. Mater.* **2017**, *27*, 1701134.

[129] T. Baden, A. M. Chagas, G. J. Gage, T. C. Marzullo, L. L. Prieto-Godino, T. Euler, *PLoS biology* **2015**, *13*, e1002086.

[130] a) M. C. Maier, R. Lebl, P. Sulzer, J. Lechner, T. Mayr, M. Zadravec, E. Slama, S. Pfanner, C. Schmölzer, P. Pöchlauer et al., *React. Chem. Eng.* **2019**, *4*, 393; b) A. J. Capel, S.

Edmondson, S. D. R. Christie, R. D. Goodridge, R. J. Bibb, M. Thurstans, *Lab on a chip* **2013**, *13*, 4583.

[131] S. C. Ligon, R. Liska, J. Stampfl, M. Gurr, R. Mülhaupt, *Chem. Rev.* **2017**, *117*, 10212.

[132] X. Hao, J. Kaschta, X. Liu, Y. Pan, D. W. Schubert, *Polymer* **2015**, *80*, 38.

[133] a) A. Wypych, G. Wypych, *Databook of Solvents*, Elsevier Science & Technology Books, San Diego, **2015**; b) G. Akovali in *Toxicity of Building Materials*, Elsevier, **2012**, pp. 23–53.

[134] a) J. J. Peña, A. Santamaria, G. M. Guzmán, *European Polymer Journal* **1984**, *20*, 49; b) O. P. Obande, M. Gilbert, *J. Appl. Polym. Sci.* **1989**, *37*, 1713; c) G. Pezzin, *Pure and Applied Chemistry* **1971**, *26*, 241.

[135] J. Azuaje, C. R. Tubío, L. Escalante, M. Gómez, F. Guitián, A. Coelho, O. Caamaño, A. Gil, E. Sotelo, *Applied Catalysis A: General* **2017**, *530*, 203.

[136] C. R. Tubío, J. Azuaje, L. Escalante, A. Coelho, F. Guitián, E. Sotelo, A. Gil, *Journal of Catalysis* **2016**, *334*, 110.

[137] A. S. Díaz-Marta, C. R. Tubío, C. Carbajales, C. Fernández, L. Escalante, E. Sotelo, F. Guitián, V. L. Barrio, A. Gil, A. Coelho, *ACS Catal.* **2018**, *8*, 392.

[138] M. Skorski, J. Esenther, Z. Ahmed, A. E. Miller, M. R. Hartings, *Science and technology of advanced materials* **2016**, *17*, 89.

[139] X. Wang, Q. Guo, X. Cai, S. Zhou, B. Kobe, J. Yang, *ACS applied materials & interfaces* **2014**, *6*, 2583.

[140] a) C. Zhu, Z. Qi, V. A. Beck, M. Luneau, J. Lattimer, W. Chen, M. A. Worsley, J. Ye, E. B. Duoss, C. M. Spadaccini et al., *Science advances* **2018**, *4*, eaas9459; b) P. Michorczyk, E. Hędrzak, A. Węgrzyniak, *J. Mater. Chem. A* **2016**, *4*, 18753.

[141] a) P. J. Kitson, S. Glatzel, W. Chen, C.-G. Lin, Y.-F. Song, L. Cronin, *Nature protocols* **2016**, *11*, 920; b) G. Chisholm, P. J. Kitson, N. D. Kirkaldy, L. G. Bloor, L. Cronin, *Energy Environ. Sci.* **2014**, *7*, 3026.

[142] a) M. Konarova, W. Aslam, L. Ge, Q. Ma, F. Tang, V. Rudolph, J. N. Beltramini, *ChemCatChem* **2017**, *9*, 4132; b) N. Kashani-Shirazi, Wloka, V., Gerlinger, W., A. Schmidt, K. Heinen, W. Kollenberg, US020100222209A1, **2010**; c) A. Avril, C. H. Hornung, A. Urban, D. Fraser, M. Horne, J.-P. Veder, J. Tsanaktsidis, T. Rodopoulos, C. Henry, D. R. Gunasegaram, *React. Chem. Eng.* **2017**, *2*, 180.

[143] L. Guo, G. Shi, Y. Liang, *Polymer* **2001**, *42*, 5581.

[144] H. G. O. Becker, *Organikum*. *Organish-chemisches Grundpraktikum*, Wiley-VCH, Weinheim … [etc.], **2001**.

[145] A. Gaudel-Siri, C. Marchal, V. Ledentu, D. Gigmes, D. Siri, L. Charles, *European journal of mass spectrometry (Chichester, England)* **2019**, *25*, 229.

[146] R. Ciriminna, M. Ghahremani, B. Karimi, M. Pagliaro, *ChemistryOpen* **2017**, *6*, 5.

[147] M. Rafiee, B. Karimi, S. Alizadeh, *CHEMELECTROCHEM* **2014**, *1*, 455.

[148] M. Shibuya, M. Tomizawa, Y. Iwabuchi, *The Journal of organic chemistry* **2008**, *73*, 4750.

[149] W. Schwarz, J. Schossig, R. Rossbacher, R. Pinkos, H. Höke in *Ullmann's Encyclopedia of Industrial Chemistry*, Wiley, **2000**, pp. 1–7.

Hiermit versichere ich an Eides statt, die vorliegende Dissertationsschrift selbst verfasst und keine anderen als die angegebenen Quellen und Hilfsmittel benutzt zu haben. Sofern im Zuge der Erstellung der vorliegenden Dissertationsschrift generative Künstliche Intelligenz (gKI) basierte elektronische Hilfsmittel verwendet wurden, versichere ich, dass meine eigene Leistung im Vordergrund stand und dass eine vollständige Dokumentation aller verwendeten Hilfsmittel gemäß der Guten wissenschaftlichen Praxis vorliegt. Ich trage die Verantwortung für eventuell durch die gKI generierte fehlerhafte oder verzerrte Inhalte, fehlerhafte Referenzen, Verstöße gegen das Datenschutz- und Urheberrecht oder Plagiate.

_____

(Datum, Unterschrift)

Danksagung

An dieser Stelle möchte ich mich bei all den Menschen bedanken, die mich auf meinem Weg zur Dissertation begleitet und unterstützt haben.

Zunächst gilt mein Dank Prof. Dr. Luinstra, der mich in seinem Arbeitskreis herzlichen aufgenommen und mir die Möglichkeit gegeben hat, in seinem Arbeitskreis meine Dissertation anzufertigen. Ebenso möchte ich mich bei Dr. Kristina Zentel bedanken – nicht nur für die Übernahme des Zweitgutachtens, sondern auch für ihre Unterstützung bei der Bewerbung um das Stipendium und dafür, dass sie mir geholfen hat, mein Vertrauen in mich selbst nicht zu verlieren.

Ein großer Dank gilt dem gesamten Arbeitskreis Luinstra/Pauer: für die tollen Seminarfahrten, unseren „Klassenfahrten“, die unzähligen Abende in der Teeküche und die kleinen und großen Denkanstöße. Ganz besonders möchte ich die hervorheben, die mittlerweile Freunde fürs Leben geworden sind: für all die Reisen, Hochzeiten, Schaumweinseminare oder Schanzenabende. Ihr habt diese Zeit einzigartig gemacht.

Mein Dank gilt auch meinen fleißigen Praktikant:innen, ohne deren Unterstützung vieles nicht möglich gewesen wäre.

Ein ebenso großes Dankeschön geht an meine Freunde, die das Leben einfach schöner machen. Insbesondere meiner „Schnattergruppe“ und Annika danke ich von Herzen: für euren Glauben an mich, euren Zuspruch und dafür, dass ihr einfach immer da seid, wann immer man euch braucht.

Zum Schluss möchte ich mich bei meiner Mutter und meinen Schwestern bedanken. Auch wenn ihr vielleicht nicht immer alles verstanden habt, habt ihr es zumindest versucht – und vor allem nie gefragt, wie lange ich denn noch studieren möchte. Ihr wart immer da, habt mir Mut zugesprochen und dafür gesorgt, dass Aufgeben für mich keine Option war.